

Function of two redox sensing kinases  
from the methanogenic archaeon  
*Methanosarcina acetivorans*

dem Fachbereich Biologie der Technischen Universität Kaiserslautern zur  
Erlangung des akademischen Grades „Doktor der Naturwissenschaften“  
genehmigte Dissertation

angefertigt im  
**Fachbereich Biologie**  
Abteilung Mikrobiologie

vorgelegt von  
**Kerstin Fiege**

Wissenschaftliche Aussprache: Kaiserslautern, 28.03.2019

**Referent:** Prof. Dr. Nicole Frankenberg-Dinkel  
**Korreferent:** Prof. Dr. Johannes Herrmann  
**Vorsitz:** Prof. Dr. Matthias Hahn

# Eidesstattliche Erklärung

Ich erkläre hiermit an Eides statt, dass ich die vorliegende Dissertation selbständig und ohne Benutzung anderer als angegebenen Hilfsmittel angefertigt habe. Die aus fremden Quellen übernommenen Gedanken sind ausnahmslos als solche kenntlich gemacht. Die Promotionsordnung des Fachbereichs Biologie der TU Kaiserslautern ist mir in der derzeit gültigen Fassung bekannt. Die Ergebnisse anderer Mitarbeiter sowie anderer Autoren wurden klar gekennzeichnet. Die Dissertation oder Teile daraus wurden in keinem anderen Fachbereich oder keiner anderen Fakultät als Prüfungsarbeit eingereicht. Ich habe zu keinem früheren Zeitpunkt an einer anderen Universität ein Promotionsverfahren beantragt.

Kaiserslautern, den 30.01.2019

Kerstin Fiege

# Danksagung

Zu Beginn möchte ich mich besonders bei meiner Doktormutter Prof. Dr. Nicole Frankenberg-Dinkel für die Vergabe dieses interessanten und sehr vielseitigen Themas bedanken. Vielen Dank nicht nur für die Möglichkeit meine Doktorarbeit in ihrer Arbeitsgruppe anfertigen zu können, sondern auch für ihre immer vorhandene Unterstützung und Diskussionsbereitschaft. Zudem danke ich für die Ermöglichung der Teilnahme an mehreren interessanten internationalen und nationalen Konferenzen.

Bei Herrn Prof. Dr. Johannes Herrmann möchte ich mich für die freundliche Übernahme des Korreferats bedanken. Herrn Prof. Dr. Matthias Hahn danke ich für die Bereitschaft den Vorsitz der Promotionskommission zu übernehmen.

Bedanken möchte ich mich auch bei allen Kooperationspartnern: Bei Christine Joy Querebillo und Prof. Dr. Peter Hildebrandt von der TU Berlin für die Resonanz Raman Spektroskopie Messungen. Bei ihnen möchte ich mich für die hilfreichen Diskussionen meiner spektroskopischen Ergebnisse bedanken. Prof. Dr. Antonio Pierik von der TU Kaiserslautern möchte ich für die mehrfache Diskussionsbereitschaft und Möglichkeit am Anaeroben Zelt zu arbeiten bedanken. Ihm und Dominique Bechtel danke ich ebenso für die Messung der EPR-Spektroskopie. Christian Schöne und Prof. Dr. Michael Rother von der TU Dresden danke ich für die anfängliche Bereitstellung von genomischer *M. acetivorans* DNA, die zur Verfügung gestellten *M. acetivorans* Stämme und für die Hilfe bei der Etablierung der anaeroben Anzucht. Des Weiteren möchte ich Prof. Dr. Michael Rother für die interessanten und hilfreichen Diskussionen und Tipps zu meinem Thema während der VAAM Jahrestagungen danken. Bei Christoph Laurich und Prof. Dr. Wolfgang Lubitz vom Max-Planck-Institut für chemische Energiekonversion in Mühlheim a. d. Ruhr möchte ich mich für die Redox-Potential Messungen bedanken. Auch danke ich Dr. Claus Scholz und Dr. Konrad Förstner von der Core Unit Systemmedizin der Universität Würzburg für die RNAseq Analysen und die Hilfe bei der Auswertung dieser Daten. Ebenso danke ich von der TU Kaiserslautern Dr. Frederik Sommer für die Messung der Massen-Spektrometrie und Florian Mahler für die CD-Spektroskopie.

Den FKBlern sowohl zunächst an der Ruhr-Universität Bochum als auch an der TU Kaiserslautern danke ich für die tolle Zeit im Labor. Vielen Dank an die Bochumer Krissy, Sabrina, Julia und besonders Christian für die Einarbeitung und Hilfe am Anfang meiner Arbeit in Bochum. Ebenso möchte ich mich bei der gesamten Mikrobiologie Gruppe an der TU Kaiserslautern bedanken. Ganz besonders bei meinen Laborkollegen und Freunden Natascha, Katrin, Lorian, Anne, Bin, Martina, Benni und Marco für die immer lockere

Arbeitsatmosphäre und vielen gemeinsamen Freizeitaktivitäten. Danke auch an Christine für die Unterstützung im Labor. Bei dem Team Methano bedanke ich mich für die Unterstützung und Diskussionen zu unseren Arbeiten und danke Anne für die immer wieder neuen Ohrwürmer. Des Weiteren möchte ich mich bei meinen ehemaligen Bachelor- und Masterstudenten für die Unterstützung in meinem Projekt bedanken.

Mein allergrößter Dank geht an meine Familie, ohne deren Unterstützung während meines Studiums und meiner Arbeit ich jetzt nicht da wäre wo ich bin. Danke Mama, Papa und Sabrina!



# Contents

Danksagung	iii
Abbreviations	1
<b>1 Introduction</b>	<b>3</b>
1.1 Signal transduction	3
1.1.1 Two-component systems	3
1.1.2 Heme-based sensors	4
1.1.3 Thiol/disulfide switch dependent redox sensing	6
1.1.4 Signal transduction in Archaea	7
1.1.5 Protein phosphorylation in archaeal signal transduction	8
1.1.6 Pyrrolysine, the 22 <sup>nd</sup> proteinogenic amino acid	8
1.2 The model organism <i>Methanosarcina acetivorans</i>	9
1.2.1 Methanogenesis in <i>M. acetivorans</i>	10
1.3 Objectives of this work	12
<b>2 Materials and methods</b>	<b>13</b>
2.1 Materials and chemicals	13
2.1.1 Equipment	13
2.1.2 Special material, chemicals, enzymes and kits	14
2.1.3 Bacterial and archaeal strains	15
2.2 Microbiological techniques	16
2.2.1 Culture media and supplements for <i>E. coli</i> cultures	16
2.2.2 Storage of <i>E. coli</i> cultures	16
2.2.3 Cultivation of <i>E. coli</i> cells	16
2.2.4 Cultivation media for <i>M. acetivorans</i> cells	16
2.2.5 Storage of <i>M. acetivorans</i> cultures	18
2.2.6 Cultivation of <i>M. acetivorans</i> cells	18
2.2.7 Determination of cell density	18
2.3 Molecular biological techniques	18
2.3.1 Production of chemically competent <i>E. coli</i> cells	18
2.3.2 Transformation of chemically competent <i>E. coli</i> cells	18
2.3.3 Electroporation of <i>E. coli</i> cells	19
2.3.4 Preparation of plasmid-DNA	19
2.3.5 Preparation of genomic DNA from <i>M. acetivorans</i>	20
2.3.6 Preparation of RNA from <i>M. acetivorans</i>	20
2.3.7 Polymerase chain reaction	20
2.3.8 Determination of DNA and RNA concentration in aqueous solution	21
2.3.9 Agarose gel electrophoresis	21
2.3.10 Purification of PCR products	21
2.3.11 Restriction of DNA	21
2.3.12 Gel extraction of DNA fragments	21
2.3.13 Dephosphorylation of DNA	22
2.3.14 Ligation of DNA	22
2.3.15 Construction of expression and coexpression vectors	22

2.3.16	Site-directed Mutagenesis . . . . .	22
2.3.17	Construction of an <i>E. coli</i> Nissle 1917 strain for T7-dependent protein production . . . . .	23
2.3.18	Sequencing of DNA . . . . .	23
2.3.19	RNAseq analysis . . . . .	24
2.3.20	Analysis of protein-protein interactions by bacterial two-hybrid system . . . . .	25
2.4	Protein biochemical and biophysical techniques . . . . .	27
2.4.1	Production of recombinant proteins in <i>E. coli</i> BL21(DE3) . . . . .	27
2.4.2	Production of recombinant proteins with incorporation of pyrrolysine . . . . .	27
2.4.3	Production of recombinant proteins in <i>E. coli</i> Nissle 1917 . . . . .	27
2.4.4	Production of recombinant proteins in <i>E. coli</i> RP523 . . . . .	28
2.4.5	Cell disruption of <i>E. coli</i> cells . . . . .	28
2.4.6	Purification of recombinant produced <i>StrepII</i> -tagged proteins . . . . .	28
2.4.7	SDS-polyacrylamide gel electrophoresis . . . . .	29
2.4.8	Immuno-detection of immobilized proteins (Western blot) . . . . .	30
2.4.9	Determination of protein concentration . . . . .	30
2.4.10	Size exclusion chromatography . . . . .	31
2.4.11	Optical absorption spectroscopy (UV/vis) . . . . .	32
2.4.12	Electron paramagnetic resonance spectroscopy . . . . .	32
2.4.13	Circular dichroism spectroscopy . . . . .	32
2.4.14	Mass spectrometry . . . . .	33
2.4.15	Acidified butanone extraction . . . . .	33
2.4.16	Catalase activity assay . . . . .	33
2.4.17	Protein kinase assay . . . . .	33
2.4.18	Acid-base treatment of phosphorylated proteins . . . . .	34
2.4.19	Thin layer chromatography of phosphorylated proteins . . . . .	34
2.4.20	Pyridine hemochrome assay . . . . .	34
2.4.21	Redox titration . . . . .	34
2.4.22	Resonance Raman spectroscopy . . . . .	35
2.4.23	Determination of disulfide bonds . . . . .	35

<b>3</b>	<b>Results Part 1 - Improved method for heme protein production in <i>Escherichia coli</i></b>	<b>37</b>
3.1	Introduction . . . . .	37
3.2	Used plasmids and oligonucleotides . . . . .	38
3.3	Results and Discussion . . . . .	39
3.3.1	Protein heme saturation by <i>E. coli</i> strain Nissle 1917 . . . . .	39
3.3.2	UV/vis spectroscopy of MsmS_sGAF2 produced with different heme incorporation methods . . . . .	41
3.3.3	Resonance Raman spectroscopy of MsmS_sGAF2 produced by different methods . . . . .	42
3.3.4	Production of MsmS from Nissle 1917, Resonance Raman, and autophosphorylation activity . . . . .	43
3.3.5	<i>E. coli</i> Nissle 1917 is a general suitable host for the expression of heme proteins . . . . .	46
3.3.6	Construction of an EcN strain for T7-RNA polymerase dependent gene expression . . . . .	49

<b>4</b>	<b>Results part 2 - The sensor kinase MsmS</b>	<b>50</b>
4.1	Introduction . . . . .	50
4.2	Used plasmids and oligonucleotides . . . . .	52
4.3	Characterization of the sensor kinase MsmS . . . . .	55
4.3.1	Mutational analysis of heme binding ligands in MsmS_sGAF2 . . . . .	55
4.3.2	No impact of pH value on heme coordination in MsmS_sGAF2 . . . . .	58
4.3.3	Redox potential of MsmS_sGAF2_C656A . . . . .	60
4.3.4	Full-length domain structure influences heme iron coordination . . . . .	61
4.3.5	UV/vis spectroscopy of MsmS full-length variants . . . . .	62
4.3.6	Analyzing the autophosphorylation activity of MsmS . . . . .	64
4.3.7	Coenzyme M influences autophosphorylation activity but not heme coordination . . . . .	65
4.3.8	Oligomerization state of MsmS is independent of redox state . . . . .	66
4.3.9	Protein-protein interaction studies of MsmS with Msr regulator proteins . . . . .	67
4.3.10	RNAseq analysis of wild-type <i>M. acetivorans</i> vs. <i>msmS</i> deletion strain . . . . .	70
<b>5</b>	<b>Results part 3 - The putative sensor kinase MA0863</b>	<b>71</b>
5.1	Introduction . . . . .	71
5.2	Used plasmids and oligonucleotides . . . . .	72
5.3	Characterization of the putative sensor kinase MA0863 . . . . .	75
5.3.1	Covalent binding of heme cofactor is mediated by Cys620 . . . . .	77
5.3.2	Mutational analysis of heme binding ligands in MA0863_sGAF2 produced by heme reconstitution . . . . .	78
5.3.3	Mutational analysis of heme binding ligands in MA0863_sGAF2 produced in <i>E. coli</i> Nissle 1917 . . . . .	79
5.3.4	Mutational analysis of heme iron ligands in MA0863_O216K full-length protein . . . . .	80
5.3.5	Resonance Raman spectroscopy for determination of heme coordination . . . . .	82
5.3.6	Autophosphorylation activity of MA0863_O216K is redox dependent . . . . .	83
5.3.7	MA0863_O216K is no typical histidine sensor kinase . . . . .	84
5.3.8	Production of wild-type MA0863 with pyrrolysine in <i>E. coli</i> . . . . .	85
5.3.9	CoM-SH influences the autophosphorylation activity of MA0863_O216K . . . . .	87
5.3.10	Heme cofactor is not essential for redox dependent autophosphorylation activity . . . . .	88
5.3.11	MA0863_O216K contains putative redox active disulfide bonds . . . . .	89
5.3.12	Oligomerization state of MA0863_O216K is independent on redox condition and disulfide bonds . . . . .	90
5.3.13	First analysis of cysteine variants reveal no differences . . . . .	91
5.3.14	Protein-protein interaction analysis of MA0863_O216K and Msr-regulators . . . . .	92
<b>6</b>	<b>Discussion</b>	<b>94</b>
6.1	Establishment of an improved method for heme protein production in <i>E. coli</i> . . . . .	94
6.2	MsmS and MA0863 - two structural similar proteins . . . . .	94
6.3	MsmS and MA0863 contain a covalent bound heme cofactor - effecting the redox potential . . . . .	95
6.4	Configuration of the heme cofactor in MsmS and MA0863 is most likely a HS species . . . . .	97
6.5	Putative heme coordinating ligands in MsmS . . . . .	97
6.6	Putative heme coordinating ligands in MA0863 . . . . .	99

6.7	MA0863 is a redox sensor similar to MsmS . . . . .	100
6.8	Redox sensing is probably mediated by thiol/disulfide switch . . . . .	100
6.9	Heme cofactor might integrate a second signal . . . . .	102
6.10	Incorporation of pyrrolysine into RdmS in <i>E. coli</i> . . . . .	102
6.11	Role of pyrrolysine in RdmS . . . . .	104
6.12	Signaltransduction by MsmS and RdmS - no typical two-component system .	104
6.13	MsmS and RdmS belong to the methylsulfide metabolism of <i>M. acetivorans</i> . .	106
<b>7</b>	<b>Summary</b>	<b>108</b>
<b>8</b>	<b>Zusammenfassung</b>	<b>109</b>
	<b>References</b>	<b>110</b>
	<b>Appendix</b>	<b>125</b>
	<b>Lebenslauf</b>	<b>127</b>
	<b>Publications</b>	<b>128</b>
	<b>Conference contributions</b>	<b>129</b>

# Abbreviations

$\epsilon$ .....	molar extinction coefficient
2D .....	two-dimensional
aa .....	amino acid
ALA .....	5-aminolevulinic acid
AU .....	absorbance unit
BACTH .....	bacterial adenylate cyclase two-hybrid system
BCIP .....	5-bromo-4-chloro-3-indolyl phosphate
bp .....	base pair
CoM .....	Coenzyme M; 2-mercaptoethanesulfonate
CV .....	column volume
DHp .....	dimerization domain
DMS .....	dimethyl sulfide
DMSO .....	dimethyl sulfoxide
DNA .....	deoxyribonucleic acid
DTH .....	sodium dithionite
DTNB .....	5,5'-dithiobis-(2-nitrobenzoic acid)
DTT .....	dithiothreitol
EPR .....	electron paramagnetic resonance
Fe(II) .....	Fe(II) heme complex, or hemin
Fe(III) .....	Fe(III) heme complex, or hemin
GAF .....	domain conserved in cyclic GMP-specific and stimulated phosphodiesterases, adenylate cyclases and <i>E. coli</i> formate hydrogen lyase transcriptional activator
GRX .....	glutaredoxin
h .....	hour
H <sub>4</sub> SPT .....	tetrahydrosarcinopterin
H_ATPase .....	histidine kinase-like ATPase domain
HAMP .....	present in histidine kinases, adenyl cyclases, methyl-accepting proteins and phosphatases
HPEX .....	heme protein expression
HPt .....	histidine phosphotransfer
HTH .....	helix-turn-helix
IPTG .....	isopropyl- $\beta$ -thiogalactosidase
LB .....	lysogeny broth
LMW .....	low molecular weight
MCD .....	magnetic circular dichroism
MeSH .....	methanethiol
MMPA .....	methylmercaptopropionate
MW .....	molecular weight
MWCO .....	molecular weight cut off
NBT .....	nitro blue tetrazolium chloride
NHE .....	normal hydrogen electrode
OCS .....	one-component system
ORF .....	open reading frame
PAC .....	PAS-associated C-terminal motif

## Abbreviations

---

PAS	Per ( <i>Drosophila</i> period clock protein)/Arnt (vertebrate aryl hydrocarbon receptor nuclear translocator)/Sim ( <i>Drosophila</i> single-minded protein)
PBS	phosphate buffered saline
PCR	polymerase chain reaction
PVDF	polyvinylidene fluoride
R	regulator protein
REC	receiver domain
ResReg	response regulator
RNA	ribonucleic acid
ROS	reactive oxygen species
rpm	revolutions per minute
RR	resonance raman
RT	room temperature
SDS	sodium dodecyl sulfate
SDS-PAGE	sodium dodecyl sulfate-polyacrylamide gel electrophoresis
SEC	size exclusion chromatography
SHK	sensor histidine kinase
SK	sensor kinase
TCA	trichloroacetic acid
TCEP	tris(2-carboxyethyl)phosphine
TCS	two-component system
TEMED	N,N,N',N'-tetramethylethane-1,2-diamine
TES	2-[Tris(hydroxymethyl)-methylamino]-ethanesulfonic acid
TRX	thioredoxin
UV/vis	Ultraviolet/visible
v/v	volume per volume
w/	with
w/o	without
w/v	weight per volume
wt	wild-type
ZWS	Zwei-Komponenten System

# 1 Introduction

## 1.1 Signal transduction

The ability to rapidly respond to changes in the environment or inside the cell is essential for survival of organisms. A variety of mechanisms evolved to monitor critical parameters like e.g. temperature, oxygen, pH or nutrients. The signal is sensed by the cell and transduced to modulate cellular functions in order to respond to the new condition, thereby ensuring survival. These responses are mainly mediated by chemosensory signalling pathways consisting of one- and two-component systems [110, 111, 141].

### 1.1.1 Two-component systems

Two-component systems (TCS) are widely distributed in the domain of *Bacteria* and *Archaea* [68, 140]. TCSs are also found in some eukaryotic organisms [128]. A typical bacterial TCS consists of a sensor histidine kinase (SHK) and a response regulator (ResReg). Most SHKs are multi domain proteins with one or more sensor domains and a kinase domain. The sensor domain detects a certain signal, which results in autophosphorylation of a conserved histidine residue (H-box) in the kinase domain [64]. The phosphoryl group is then transferred to a conserved aspartate residue of the ResReg receiver domain (REC) leading to activation of the ResReg effector domain (Fig. 1.1). The most common type of SHK has an extracytosolic sensor domain, linked by a HAMP (histidine kinases, adenyl cyclases, methyl-accepting proteins and phosphatases) sensor domain to a cytosolic kinase domain (Fig. 1.1 a) like the osmosensor EnvZ from *Escherichia coli* [140]. Alternatively, the sensor domain can be embedded inside the membrane or even be completely located in the cytoplasm (Fig. 1.1 b,c). In order to sense a variety of signals, several different types of sensor domains for extracytosolic and cytosolic sensing evolved [17]. Most systems use a linear phosphotransfer between one SHK and one ResReg, but also cross-regulation between two systems or multiple phosphorylated components (e.g. during sporulation) can be found [16, 57]. Such a complex system is the phosphorelay system. It consists of a membrane spanning SHK with an additional receiver domain, in which the phosphoryl group is first transferred intramolecularly from the H-box to the bound REC domain. The phosphoryl group is then transferred to a histidine phosphotransfer protein (HPt) and subsequently transferred to the REC domain of the ResReg (Fig. 1.1 d) [53].

A SHK typically binds ATP to autophosphorylate a conserved substrate histidine residue (H-box) on the partner subunit within a dimer [36]. Autophosphorylation of the conserved histidine residue results in the formation of a high-energy phospho-amidate, optimal for the phosphotransfer [140]. The substrate domain often also functions as a dimerization domain

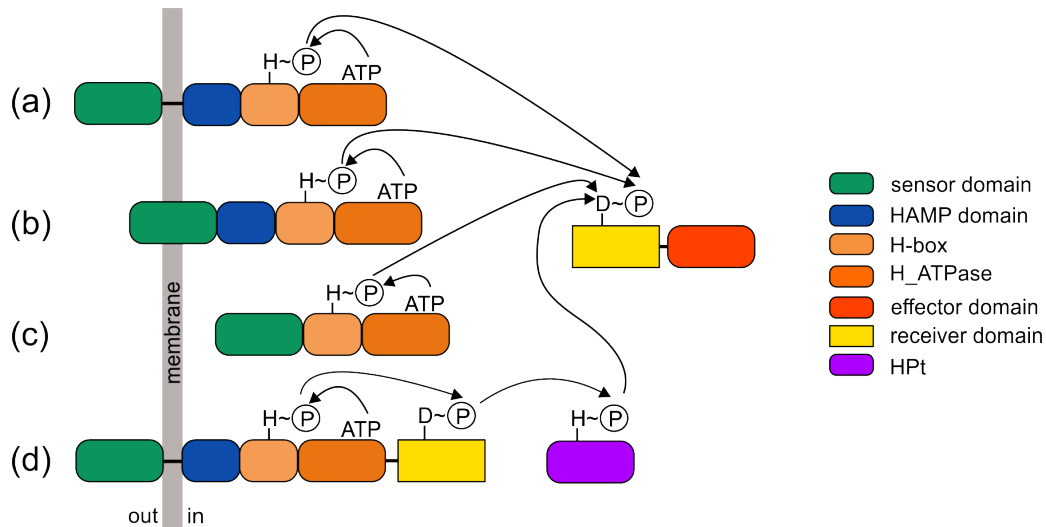


**Figure 1.1 Schematic overview of two-component signal transduction.** In a typical bacterial two-component system (a) a membrane bound SHK has a extracytoplasmic sensor domain which is often linked by a HAMP sensor domain to the cytosolic part. Upon sensing the signal the H\_ATPase domain binds and hydrolyzes ATP and autophosphorylates a conserved histidine residue in the H-box. The phosphoryl group is subsequently transferred to a conserved aspartate residue in the receiver domain (REC) of the response regulator (ResReg), activating the effector domain. Another type of SHK (b) has a sensor domain located in the membrane or (c) is entirely cytoplasmatic. Moreover, (d) in a phosphorelay system a hybrid kinase gets phosphorylated and transfers a phosphoryl group intramolecularly from an H-box to a bound receiver domain. A histidine phosphotransfer (HPt) shuttles the phosphoryl group to the REC domain of a ResReg, activating the effector domain. (modified from [58])

(DHp). The H-box is one of several conserved motifs within the kinase domain involved in ATP-binding and hydrolysis [115, 140]. These motifs are part of the catalytic core and are distinct from Ser/Thr/Tyr kinases (see 1.1.5). Some HKs possess also phosphatase activity for fine-tuning of the ResReg phosphorylation [36, 115]. After autophosphorylation of the kinase the phosphoryl group is transferred to the REC domain of the ResReg, forming a high-energy acyl phosphate. The phosphotransfer leads to a conformational change within the ResReg and activates the effector domain [115]. The effector domain can be involved in DNA-binding, RNA-binding, ligand-binding, protein-binding, or enzymatic activity [34, 36].

### 1.1.2 Heme-based sensors

Heme proteins are involved in a variety of biological processes, like oxygen binding and transport (hemoglobin, myoglobin) [10], cell respiration (cytochromes) [99], production and sensing of nitric oxide (NO synthase, heme/nitric oxide/oxygen (H-NOX) proteins) [48, 116], electron transfer (cytochromes) [15] and signal transduction (FixL and CooA) [41, 96, 130]. The heme molecule is typically bound via a PAS (*Drosophila* periodic clock (PER), vertebrate aryl hydrocarbon receptor nuclear translator (ARNT) [119], and *Drosophila* single-minded protein (SIM)) or GAF (cGMP-specific phosphodiesterases, adenylyl cyclases, and



transcriptional activator *FhlA*) domain to the protein [18, 40]. Within proteins PAS domains are able to monitor changes in light, redox potential, oxygen, small ligands, and overall energy level inside the cytosol but can also be involved in protein-protein interactions [40, 52, 56, 113, 146]. For these functions they bind cofactors like heme in FixL [40], FAD (flavin adenine dinucleotide) in NifL [52] or a 4-hydroxycinnamyl chromophore in PYP (photoactive yellow protein) [113]. PAS domains are often found together with PAC (PAS-associated C-terminal motif) domains. GAF domains are structurally related to PAS domains. One of the largest protein groups containing GAF domains are phytochromes [126] but they are also found in heme-containing redox sensors like DosS and DosT from *Mycobacterium tuberculosis* [18, 133]. In Archaea two heme containing sensors are described: the aerotaxis inducer *Hs-HemAT* from *Halobacterium salinarium* and the redox sensor MsmS from *Methanosarcina acetivorans* [54, 95].

### The heme cofactor

A heme cofactor is a prosthetic group consisting of a circular tetrapyrrole molecule with a central iron atom. The heme iron is coordinated by four nitrogens of the tetrapyrrole molecule, leaving two binding sites free for additional ligands at the distal and proximal side (Fig. 1.2). For the heme-based redox sensor MsmS from *M. acetivorans* it was shown that the heme cofactor can be coordinated by molecules like CO, dimethyl sulfide (DMS) or imidazole [95]. Moreover, the iron atom is able to change between the ferrous (Fe(II)) and ferric (Fe(III)) state, an important characteristic for heme-based redox sensors. Binding of ligands induces changes in the protein structure and therefore influences the protein activity [50, 72]. Most heme-based sensors contain non-covalently bound b-type heme, however, sensors with c-type heme (like in cytochrome c), e.g., the chemotaxis signal-transducing

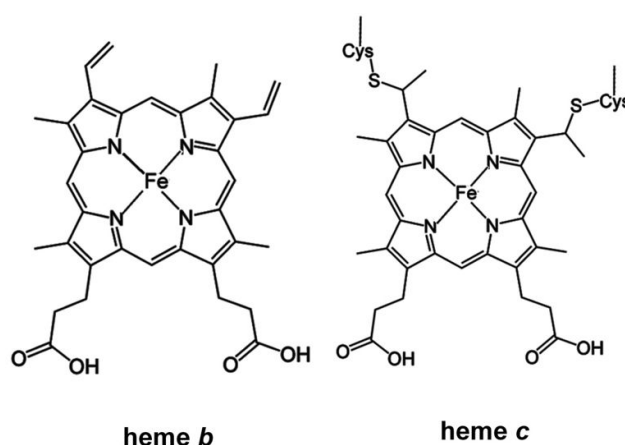


**Figure 1.2 Chemical structures of b-type and c-type hemes.** B-type and c-type hemes consist of a circular tetrapyrrole molecule with a central iron atom. The iron atom is coordinated by the nitrogen atoms of the tetrapyrrole molecule. B-type hemes are non-covalently bound, whereas c-type hemes are covalently bound via the two vinyl side groups to cysteine residues of the protein [81].

protein DcrA from *Desulfovibrio vulgaris* [164], two methyl-accepting chemotaxis proteins GU582 and GU935 from *Geobacter sulfurreducens* [117] and the redox sensor MsmS from *M. acetivorans* [95], have been reported. The heme cofactor of the heme protein MsmS is no typical c-type heme as it is covalently bound via only one cysteine residue [95]. A characteristic of c-type containing sensors is their low redoxpotential between -85 and -250 mV [95, 164]. It is suggested that this property results in a more stable Fe(II) complex than the Fe(III) complex and that a redox-dependent ligand switching leads in a conformational change inside the heme-binding site [131].

### 1.1.3 Thiol/disulfide switch dependent redox sensing

Redox changes in the external environment or inside the cell can have a huge impact on the cell and its metabolism. Therefore, several mechanisms, like iron-sulfur-clusters, heme-based sensors or thiol/disulfide switches evolved to monitor redox changes [59, 65, 130]. Cysteine residues are very sensitive to oxidative modifications and can play a role on the structure, function or regulation of a protein. This versatility is due to the reactive cysteine thiol group, which can be deprotonated to a thiolate anion [125]. Due to the reducing environment inside cells, protein disulfide bonds are very rarely present under normal conditions. Oxidation of cysteine thiol groups happens when oxidative species, like reactive oxygen species (ROS), are present. This interaction leads to the formation of the unstable oxidation intermediate sulfenic acid (RSOH) which can interact with a nearby cysteine to form a disulfide bond [125]. The disulfide bond is formed intramolecularly between two cysteine residues of one protein molecule, intermolecularly between two protein molecules, or between a protein and low molecular weight (LMW) thiol (Fig. 1.3 A). Common LMW thiols are glutathione and cysteine whereas also organism-specific LMW thiols exist, e.g. Coenzyme M (CoM-SH) and Coenzyme B (CoB-SH) in methanogenic Archaea (Fig. 1.3 B) [120]. In Bacteria, two main LMW thiol systems maintain the redox state of the cell: the glutaredoxin (GRX) and the thioredoxin (TRX) system.

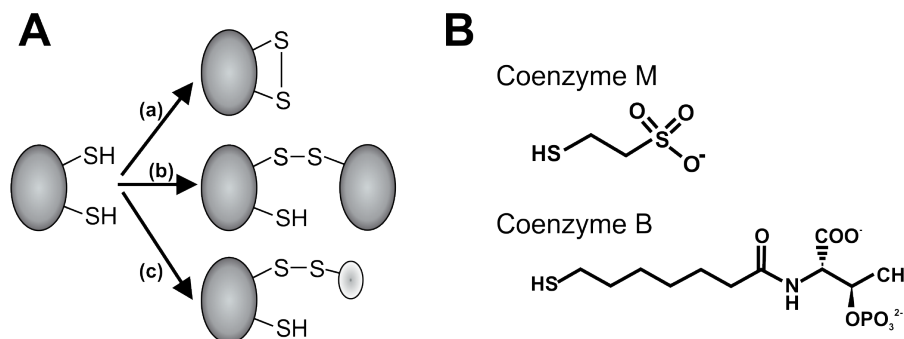


**Figure 1.3 Thiol/disulfide switches and low molecular weight thiols.** (A) Formation of (a) intramolecular disulfide bond, (b) intermolecular disulfide bond and (c) disulfide bond between a protein molecule and a low molecular weight thiol. (B) Specific low molecular weight thiols present in methanogenic Archaea.

The transcriptional regulator OxyR from *E. coli*, for example, monitors the concentration of H<sub>2</sub>O<sub>2</sub>. Cysteine thiols in OxyR are oxidized by H<sub>2</sub>O<sub>2</sub> which then activates the expression of H<sub>2</sub>O<sub>2</sub> defense proteins by OxyR. When the concentration of H<sub>2</sub>O<sub>2</sub> decreases, the disulfide bonds of OxyR are reduced by glutaredoxin [6, 166]. In contrast to Bacteria, methanogenic Archaea lack glutathione but the majority contain TRXs, like *M. acetivorans* [28, 88, 145].

### 1.1.4 Signal transduction in Archaea

In contrast to Bacteria, archaeal signal transduction is dominated by one-component systems (OCS) [149]. An OCS consists of a protein with fused input and output domain. Transcription of prokaryotic operons like the *lac* operon are typically regulated by single-molecule repressors which are able to bind a ligand and DNA [78, 114]. Genes for two-component systems were not found in the genomes of *Cren-*, *Kor-* or *Nanoarchaeota*, however, the low number of sequenced genomes of the latter two phyla has to be taken into consideration [5, 35]. Most genes for TCSs were found in *Thaumarchaeota* and *Euryarchaeota*. Therefore, it is assumed that TCSs originated in Bacteria and were acquired by Archaea through multiple events of horizontal gene transfer [68]. In *Euryarchaeota* TCSs were most abundant in methanomicrobia and halobacteria typically encoding for 10 or more TCSs [35, 69]. Whereas in Bacteria SHK and ResRegs are present almost in an 1:1 ratio, in Archaea and especially in methanogens the ratio varies more and in some genomes SHKs outnumbered the ResReg genes [35]. This suggests that archaeal TCSs do not work as strict pairs, but that one ResReg is phosphorylated by multiple SHKs. Furthermore, it was found that, in Bacteria, 73-88% of SHKs possess transmembrane domains and that the evolution of TCSs from OCSs is due to the advantage to sense signals in the extracytoplasmic space [19, 33, 35, 149]. In Archaea, however, 62% of SHKs lack transmembrane regions [35], indicating a cytosolic location, suggesting that the role of archaeal SHKs is rather sensing cytosolic signals than compared to bacterial SHKs. The domain structure of archaeal SHKs also supports this hypothesis as it was reported that 72% of archaeal SHKs contain a PAS and/or GAF domain, which are typical cytosolic sensor domains [35, 146]. Moreover, most REC domains in Archaea are stand-alone domains and the number of archaeal ResRegs with DNA-binding helix-turn-helix (HTH) domains is very small in comparison to those found in Bacteria [35]. Therefore, it is assumed that transcriptional regulation is not the major role of archaeal TCSs. Currently only very few archaeal TCSs are described in the literature and only two TCSs are biochemically characterized: 1) The FilI/FilRs system from *Methanosaeta harundinaceae*, involved in regulation of acetoclastic methanogenesis [79] and 2) the temperature-responsive TCS LtrK/LtrR from *Methanococcoides burtonii* [101]. Both systems consist of a membrane-bound SHK which phosphorylates one or two ResReg(s).

### 1.1.5 Protein phosphorylation in archaeal signal transduction

Reversible protein phosphorylation is one of the most important post-transcriptional modifications in all three domains of life. It is important for signal transduction systems and is involved in almost all processes inside a cell. Protein kinases catalyze the phosphorylation of another protein using ATP, whereas phosphatases remove the covalently linked phosphoryl group. The first genome wide approach of an archaeal phosphoproteome was carried out in *Halobacterium salinarium* with a Ser/Thr/Tyr phosphorylation distribution of 86/12/1% [1]. A second phosphoproteome of *Sulfolobus solfataricus* revealed a Ser/Thr/Tyr distribution of 26/21/56% [27]. Both phosphoproteomes showed that the protein phosphorylation plays an important role in Archaea as it was already shown for Bacteria and Eukaryotes. Sequence information revealed that Archaea contain abundant protein kinases (PK) phosphorylated at serine, threonine and tyrosine residues. In bacterial TCSs, His and Asp phosphorylation plays an important role and was also found in the two archaeal TCSs FilI/FilRs and LtrK/LtrR [79, 101]. The mode of action of HK and ResRegs distinguishes the HK family from the larger Ser/Thr/Tyr kinase family, which directly transfers the phosphoryl group from ATP to a substrate. In contrast to Bacteria, phosphorylation-based signal transduction in Eukaryotes is dominated by Ser/Thr/Tyr phosphorylation [46, 66]. They form phosphoesters instead of phosphoramidates, which are more stable under acidic conditions.

Eukaryotic PKs, called Hanks-type kinases (ePK), can be mainly divided into Ser/Thr- and Tyr-specific kinases, but share a catalytic core structure with 12 conserved sequence motifs [47]. Several ORFs encoding putative eukaryotic-like protein kinases have been identified in Archaea, based on bioinformatic prediction [75, 134]. One example is the eukaryotic-like serine/threonine kinase ST1565 from *Sulfolobus tokodaii*. It possesses an autophosphorylation activity and is able to phosphorylate a forkhead-associated-domain-containing protein [154]. Furthermore, the histidine kinase-like redox sensor MsmS from *M. acetivorans* was also found to have an autophosphorylation activity and autophosphorylation most likely occurs at serine and/or tyrosine residues [94, 95].

### 1.1.6 Pyrrolysine, the 22<sup>nd</sup> proteinogenic amino acid

Most organisms share a genetic code containing 20 amino acids, whereas some have an expanded genetic code with 21 or even 22 amino acids, using selenocysteine and/or pyrrolysine (Pyl) [3]. Pyrrolysine is synthesized by the *pyl* genes: the *pylT* gene encodes for tRNA<sup>Pyl</sup>, *pylS* for pyrrolysyl-tRNA synthetase and *pylBCD* for the biosynthetic machinery of pyrrolysine (Fig. 1.4) [84]. In Archaea, pyrrolysine, encoded by the amber codon UAG, is to date only known to be present in the members of *Methanosarcinaceae* [121]. However, a new order, the Methanomassiliicoccales, was shown to encode the amber codon and the necessary genetic machinery for Pyl synthesis [12]. In *Methanosarcina* species, Pyl was discovered by studying methane formation from monomethylamine, dimethylamine and trimethylamine

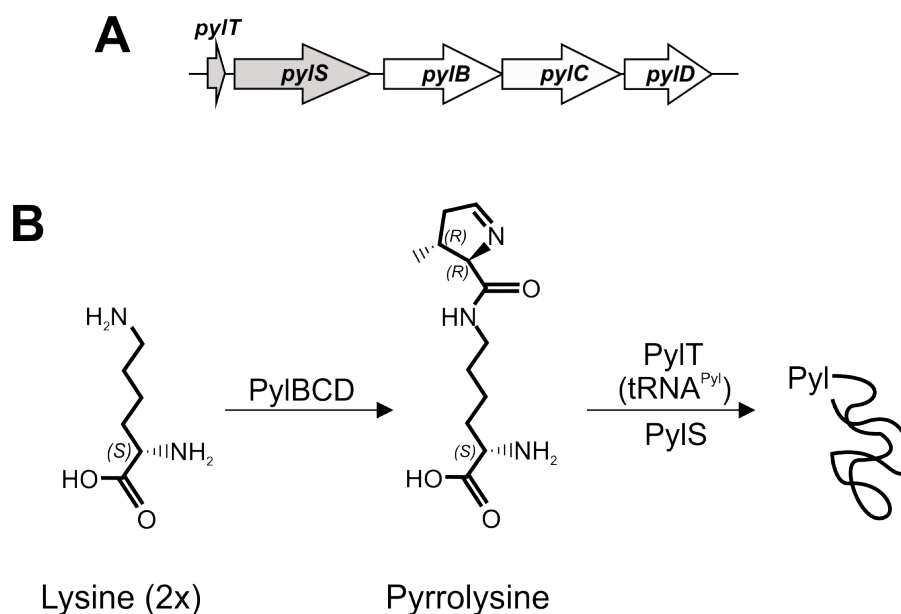


**Figure 1.4 Schematic synthesis and incorporation of pyrrolysine in *Methanosarcina* sp.. (A)** Genetic organisation of genes for biosynthesis and incorporation of Pyl. **(B)** Biosynthesis and incorporation of pyrrolysine from two molecules of lysine. (modified from [37])

[112] as these substrates are recognized by methyltransferases containing Pyl in their active centers [70]. In the methyltransferase MtmB from *Methanosarcina barkeri*, Pyl mediates the methylation of the methyltransferase MtmC by the C-2 atom of the pyrrolysine ring [70]. The amber codon for Pyl is found in all known homologs of methylamine methyltransferases, where it plays a role for activity [25, 32]. In addition, Pyl incorporation was shown for a tRNA<sup>His</sup> guanylyltransferase (Thg1) as a common amino acid without a specific function [51]. Genome analysis of *M. acetivorans* revealed 267 ORFs with one or more in-frame UAG codon(s) but, for most of them, it is not known if they are expressed or if the resulting proteins contain Pyl [106]. Reduction of the genetic code of *M. acetivorans* by deleting *pylT* revealed two more proteins in which Pyl is required for read-through of an in-frame UAG codon (MA0864 and MA3625). Both proteins are hypothetical proteins which are linked by Pyl to C-terminal proteins with known functions: MA0864 with the SHK MA0863 and MA3625 with MA3624, a tRNA splicing endonuclease [106]. The function of Pyl in these two proteins remains to be characterized.

## 1.2 The model organism *Methanosarcina acetivorans*

*Methanosarcina acetivorans* was first isolated from marine sediments in 1984. It is an obligate anaerobic methanogenic organism [139] and belongs to the *Archaea* which is the third domain of life beneath the *Bacteria* and *Eukarya* [156]. All methanogenic *Archaea* are part of the phylum *Euryarchaeota*. They can be divided into five orders: the *Methanobacteriales*, the *Methanococcales*, the *Methanomicrobiales*, the *Methanopyrrales* and the *Methanosarcinales*. *M. acetivorans* is classified to the last order and therein to the family *Methanosarcinaceae*.

*M. acetivorans* can be present as single cells or multicellular complexes depending on the prevailing environmental conditions [139]. During the exponential growth phase, in the presence of acetate, single cells dominate, whereas in the stationary phase, more multicellular aggregates are present [139]. The genome of *M. acetivorans* is completely sequenced. It is the largest known archaeal genome with ~5.7 Mbp and about 4500 ORFs arranged on a single circular chromosome [32]. Sophisticated systems for genetic manipulation are available for *M. acetivorans* and other *Methanosarcina* species [67], like plasmid shuttle vectors and transformation protocols [26, 89], directed mutagenesis of specific genes [165], markerless genetic exchange methods [123], selectable markers [11], reporter gene fusions [23, 45], chromosomal integration of genes [103], tight regulation of genes [45] and anaerobic incubators for growth on solid media [90]. Due to the availability of these tools, together with the metabolic diversity, *M. acetivorans* is used as a model organism to study methanogenesis and energy conversion [74, 167]. The genome of *M. acetivorans* encodes for 50 representatives of sensory histidine kinases, forming the third largest multigene family in *M. acetivorans*. However, only 18 response regulator receiver domains were found [32]. Therefore, the genome reveals a different approach to signal transduction than bacterial genomes, which have a one-to-one ratio of HKs and ResRegs. Seven of the found ResReg domains are part of hybrid kinases, ten are small proteins with a single domain and only one protein with a ResReg domain is long enough for a bacterial-like effector domain. This leads to the suggestion that two-component systems in *M. acetivorans* function differently than their bacterial counterparts. One possibility is that the kinases also phosphorylate other substrates than receiver domains [32].

### 1.2.1 Methanogenesis in *M. acetivorans*

Methanogenic Archaea use methanogenesis to gain energy by producing methane from different substrates. Based on these substrates, four major methanogenesis pathways can be distinguished: the hydrogenotrophic pathway is using H<sub>2</sub> to reduce CO<sub>2</sub>, the methylotrophic pathway utilizes methylated compounds, the acetoclastic pathway is using acetate as a substrate, and the carboxidotrophic pathway utilizes CO to reduce CO<sub>2</sub> [20, 24, 107]. Most methanogenic Archaea only possess one of the four methanogenic pathways and utilize not more than two substrates [167]. In this group of species, the *Methanosarcinaceae* are the most versatile, in that they are the only methanogenic Archaea which possess all four known pathways of methanogenesis. In contrast to most *Methanosarcina* species, *M. acetivorans* is not capable of growing methanogenically using H<sub>2</sub> to reduce CO<sub>2</sub> [139], presumably due to lack of two important hydrogenases. Neither the *fre* operon for the F<sub>420</sub>-reducing hydrogenase [151] nor the *ech* operon for the energy-conserving ferredoxin-dependent hydrogenase [71] are encoded in the genome. Therefore, *M. acetivorans* is able to utilize methylated compounds, like methanol or dimethylsulfide, acetate and CO (Fig. 1.5) [107, 139]. Interestingly, when growing on CO, methane is not the only product which is synthesized, but also

formate, acetate, methanethiol (MeSH) or DMS occur [97, 127]. It is currently not known how the formation of these compounds is connected with energy conservation mechanisms. Three corrinoid/methyltransferase fusion proteins (MtsH/D/F) were found to play a role

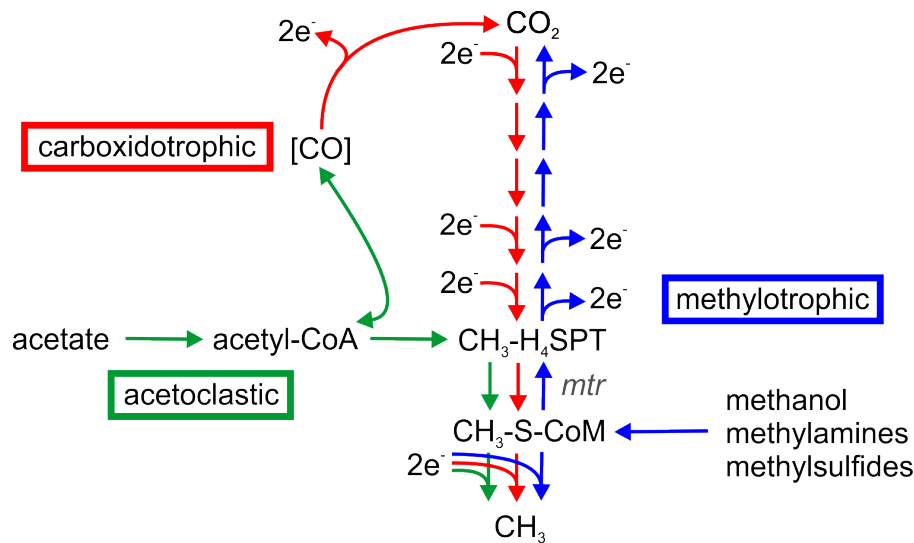


**Figure 1.5 Schematic representation of the methanogenesis pathways in *M. acetivorans*.** *M. acetivorans* is able to use three different pathways to produce methane: the acetoclastic (green), the methylotrophic (blue) and the carboxidotrophic (red) pathway. The electrons which are required for the reduction of the methylated compounds are generated by an oxidation of methyl-groups to  $\text{CO}_2$ .

either in methylsulfide metabolism [108] or bypass of the *mtr*-encoded  $\text{CH}_3\text{-H}_4\text{SPT}:\text{CoM}$  methyltransferase complex during methanogenesis (Fig. 1.5) [77, 152]. They contain a corrinoid-binding domain at the N-terminus and an uroporphyrinogen decarboxylase/methyltransferase domain at the C-terminus [14]. This type of methyltransferase is unique to *M. acetivorans*. Upstream of the *mts* genes, regulatory proteins belonging to the Msr family are encoded in the direct vicinity (*MsrG/F/C*) (Fig. 1.6). In order to test the influence of these regulator proteins, deletion strains of the *msr* genes were constructed. Deletion resulted in a significant decrease in levels of mRNA of the *mts* genes, indicating an activating effect of the Msr regulator proteins on the expression of the *mts* genes [14]. In the genome of *M. acetivorans*, genes for SHKs are located directly upstream of *msrG* and *msrF*: *msmS* and MA0863, respectively (Fig. 1.6 A). Comparison of the wild type strain with a deletion strain of *msmS* showed an impact of MsmS on the biosynthesis of MtsF (Fig. 1.6 B) [95]. As *mtsF* is regulated by MsrC, MsmS has to interact with this regulator to have an impact on MtsF biosynthesis. This result, together with the genomic location, led to the assumption that the SKs MsmS and MA0863 form TCSs with the Msr regulator proteins and that a cross-regulation between the single systems exist. A more detailed introduction about the two sensor kinases (Ch. 4.1 & Ch. 5.1) can be found before the result chapters of MsmS and MA0863.

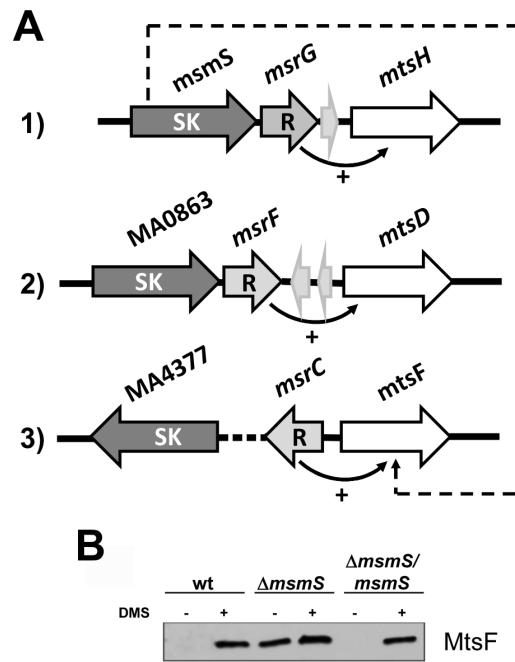


**Figure 1.6 Three putative two-component systems in *M. acetivorans*.** (A) Each system consists of a sensor kinase (SK), a regulator protein (R) and a corrinoid/methyltransferase fusion protein (*mtsH/D/F*). The regulator protein activates the expression of the *mtsH/D/F* genes. (B) Immuno-detection of MtsF: wild-type strain (wt),  $\Delta$ *msmS* and  $\Delta$ *msmS/msmS* grown with and without DMS. (modified from [13, 95])

### 1.3 Objectives of this work

For the domain *Archaea* only very little is known about signal transduction. In some cases their cellular processes are similar to known eukaryotic or bacterial signalling models, but it is thought that many functions work different and still have to be discovered. In a former study the protein MsmS was initially characterized and identified as a heme-based redox sensor kinase. It was shown that the kinase has an autophosphorylation activity dependent on the redox state of a covalently bound heme cofactor [95].

The objective of this work was the biochemical and biophysical characterization of the kinase MsmS and its homolog MA0863. In order to investigate the role of the heme cofactor, different variants of the full-length and truncated proteins should be tested for their heme iron coordination. Furthermore, it was aimed to identify the signal which is sensed by the kinases and how the the signal is transduced inside the cell. Therefore, it should be analyzed whether the kinases interact with the corresponding regulator proteins MsrG/F/C, forming a putative two-component signal transduction system.



## 2 Materials and methods

### 2.1 Materials and chemicals

All chemicals used were ACS grade or better and were purchased from AppliChem (Darmstadt), Carl Roth (Karlsruhe), Merck (Darmstadt) and Sigma-Aldrich (Munich) unless stated otherwise. All solutions for microbial cultivation were autoclaved or filter sterilized prior to use. The glass ware was sterilized by dry heat. For all solutions, buffers and growth media ultra-pure water was used at a resistance of 18 MΩ.

#### 2.1.1 Equipment

**Table 2.1** Instruments

Type of instrument	Name	Manufacturer
Anaerobic Chamber	Type B/ Type C (N <sub>2</sub> with 5% H <sub>2</sub> )	Coy Lab
Autoclave	VX 150	Systec
Blotting equipment	Semidry-Blot Trans-Blot <sup>®</sup> SD	BioRad
Cell disruption	LM 10	Microfluidics
Centrifuges and rotors	Centrifuge 5415D	Eppendorf
	Rotor F-45-24-11	
	5418R	Eppendorf
	Rotor FA-45-18-11	
	5810R	Eppendorf
	Rotor A-4-62	
	5430R	Eppendorf
	Rotors FA-45-30-11, F-35-6-30	
	Z32HK	HERMLE
	Rotor 12/002	
Sorvall LYNX 6000	Thermo Fisher	
Rotors T29, F9		
CD spectroscopy	Chirascan Plus Spectropolarimeter	Applied Photophysics
Electroporation	MicroPulser	BioRad
EPR spectrometer	Elexsys E580	Bruker
	Pulsed Microwave Bridge	
	E580-1010	
	Cavity 4122SHQE-W1/1017	
FPLC	ÄktaPure	GE Healthcare
FPLC columns	Superdex <sup>TM</sup> 200 Increase 10/300 GL	GE Healthcare
	Superose <sup>TM</sup> 6 Increase 10/300 GL	
Gel electrophoresis	Com Phor L Mini/Midi	Biozym
Gel documentation	GeliX20 Imager	Intas
Incubator	Innova 44 Incubator Shaker Series	New Brunswick Scientific
	Polymax 1040	Heidolph
	SM 30 CONTROL	Edmund Buehler
Mass spectrometer	TripleTOF <sup>®</sup> 6600	SCIEX

- Continuation on next page -

	coupled to ekspert nanoLC 425	
pH meter	Basic pH Meter P-11	Sartorius
PhosphoImager	Cyclone Typhoon FLA 7000	Perkin Elmer GE Healthcare
Photometers	8453 UV visible System Nanodrop <sup>TM</sup> Lite Novaspec III	Agilent Thermo Fisher Amersham Bioscience
Power supplies	PowerPac <sup>TM</sup> Basic PowerPac <sup>TM</sup> 300 PowerPac <sup>TM</sup> HC	BioRad  BioRad
Scales	Research Acculab	Sartorius
SDS-PAGE	Mini-PROTEAN <sup>®</sup> II System Mini-PROTEAN <sup>®</sup> Tetra cell System	BioRad
Sonifier	UW 2200 with tip KE 76	Bandelin
Thermoblock	ThermoStat plus	Eppendorf
Thermocycler	T-Personal T-Gradient	Biometra
Ultra-pure water system	MilliQ <sup>®</sup> Integral Water Purification System	Merck Millipore
Vacuum pump	Laboport	KNF
Water bath	MP	Julabo

## 2.1.2 Special material, chemicals, enzymes and kits

**Table 2.2** Chemicals and materials.

Type of material	Name	Manufacturer
Anaerobic Atmosphere Generation System	AnaeroGen <sup>TM</sup> sachet	Thermo Fisher
Column material for affinity chromatography	<i>Strep</i> -tactin <sup>®</sup> Sepharose <sup>®</sup> TALON <sup>®</sup> Metal affinity resin	IBA GmbH Clontech
Centrifugal concentrators	Vivaspin 6 10,000 MWCO Amicon Ultra-4 MWCO 10,000 Amicon Ultra-15 MWCO 50,000 Amicon Ultra-15 MWCO 100,000	Satorius Merck Millipore Merck Millipore Merck Millipore
Dialysis tubing	Visking MWCO 10,000	Carl Roth
DNA loading dye	DNA Gel Loading Dye Purple (6x)	New England Biolabs
DNA size standard	GeneRuler <sup>TM</sup> DNA Ladder Mix	Thermo Fisher
DNA stain	GelRed <sup>TM</sup>	Biotium
Filter	PTFE, 0.45 $\mu\text{m}$ $\varnothing$	Phenex
PD MiniTrap <sup>TM</sup> G-25	Sephadex <sup>TM</sup> G-25 Medium	GE Healthcare
Protein size standard	PageRuler <sup>TM</sup> prestained protein ladder	Thermo Fisher
PVDF membrane	Roti <sup>®</sup> -PVDF-Membrane	Carl Roth
Sterile filter	Rotilabo <sup>®</sup> RC, 0.2 $\mu\text{m}$ $\varnothing$ 33 mm Rotilabo <sup>®</sup> RC, 0.45 $\mu\text{m}$ $\varnothing$ 15 mm PVDF, 0.45 $\mu\text{m}$ $\varnothing$ 25 mm	Carl Roth  Diagonal

**Table 2.3** Enzymes and kits.

Type of material	Name	Manufacturer
Cloning kit	NEBuilder <sup>®</sup> HiFi DNA Assembly Master Mix (2x)	New England Biolabs
DNA Ligase	T4-DNA-Ligase	Thermo Fisher
DNA Poylmerase	Phusion <sup>®</sup> HF DNA Polymerase PRECISOR HF Polymerase DreamTaq Green PCR Mastermix (2x)	Thermo Fisher BioCat Thermo Fisher
PCR clean-up kit	NucleoSpin <sup>®</sup> Gel and PCR Clean-up	Macherey-Nagel
Phosphatase	Fast-Alkaline Phosphatase	Thermo Scientific
Plasmid DNA Miniprep kit	NucleoSpin <sup>®</sup> Plasmid EasyPure	Macherey-Nagel
Restriction endonuclease	FastDigest line	Thermo Fisher New England Biolabs
RNA isolation kit	Quick-RNA <sup>TM</sup> Miniprep kit	Zymo Research

### 2.1.3 Bacterial and archaeal strains

**Table 2.4** *E. coli* and *M. acetivorans* strains

Strain	Genotype	Reference
<i>Escherichia coli</i>		
JM83	<i>Ara</i> , $\Delta$ <i>lac-pro</i> , <i>strA</i> , <i>thi</i> , 80 <i>lacZ</i> $\Delta$ M15	[153]
DH5 $\alpha$	F <sup>-</sup> 1 <sup>-</sup> <i>supE44D</i> ( <i>argF-lac</i> ) U169 <i>j80dlacZ</i> $\Delta$ M15 <i>hsdR17 recA1 endA1 gyrA96 thi-1 relA1</i>	[42]
DH10B	F <sup>-</sup> <i>mcrA</i> $\Delta$ ( <i>mrr-hsdRMS-mcrBC</i> ) $\Phi$ 80 <i>lacZ</i> $\Delta$ M15 <i>lacX74 recA1 endA1 araD139</i> $\Delta$ ( <i>ara leu</i> ) 7697 <i>galU galK rpsL nupG</i> $\lambda$ <sup>-</sup>	Invitrogen
BL21( $\lambda$ DE3)	<i>fhuA2</i> [ <i>lon ompT gal</i> ( $\lambda$ DE3) [ <i>dcm</i> ] $\Delta$ <i>hsdS</i> $\lambda$ DE3 = $\lambda$ <i>sBamHIo</i> $\Delta$ EcoRI-B <i>int::(lacI::</i> <i>PlacUV5::T7 gene1) i21</i> $\Delta$ <i>nin</i>	[143]
Nissle 1917	serotype O6:K5:H1	[43]
BTH101	F <sup>-</sup> , <i>cya-99</i> , <i>araD139</i> , <i>galE15</i> , <i>rpsL1</i> ( <i>Str</i> <sup>r</sup> ), <i>hsdR2</i> , <i>mcrA1</i> , <i>mcrB1</i>	[60]
JM109	<i>endA1</i> , <i>recA1</i> , <i>gyrA96</i> , <i>thi</i> , <i>hsdR17</i> ( <i>r<sub>k</sub></i> <sup>-</sup> , <i>m<sub>k</sub></i> <sup>+</sup> ), <i>relA1</i> , <i>supE44</i> , $\Delta$ ( <i>lac-proAB</i> ), [ <i>F'</i> <i>traD36</i> , <i>proAB</i> , <i>laqI</i> <sup>q</sup> Z $\Delta$ M15]	[162]
RP523	F <sup>-</sup> , <i>thr-1</i> , <i>leuB6</i> (Am), <i>fhuA21</i> , <i>lacY1</i> , <i>hemB220</i> , <i>glnX44</i> (AS), <i>e14-</i> , <i>rfbC1</i> , <i>glpR200</i> ( <i>glpc</i> ), <i>thiE1</i>	[80]
<i>Methanosarcina acetivorans</i>		
WWM73	$\Delta$ <i>hpt::PmcrB-tetR-ΦC31-int-attP</i>	[45]
$\Delta$ 4561	WWM1, $\Delta$ <i>ma4561</i>	[95]

## 2.2 Microbiological techniques

### 2.2.1 Culture media and supplements for *E. coli* cultures

For *E. coli* cultivations Luria Bertani (LB) medium or LB high salt medium was used with appropriate antibiotics and supplements. Agar plates contain additionally 1.5% (w/v) Agar-Agar. For anaerobic cultivation TB medium was used.

LB medium			LB high salt medium			TB medium		
5.0	g/l	yeast extract	5.0	g/l	yeast extract	24.0	g/l	yeast extract
5.0	g/l	tryptone	5.0	g/l	tryptone	12.0	g/l	tryptone
10.0	g/l	NaCl	24.22	g/l	NaCl	4	ml/l	glycerol
						17	mM	KH <sub>2</sub> PO <sub>4</sub>
						72	mM	K <sub>2</sub> HPO <sub>4</sub>

**Table 2.5** Media supplements for *E. coli*

Supplement	Stock concentration	Final concentration
Ampicillin (Amp)	100 mg/ml	100 µg/ml
Anhydrotetracyclin (AHT)	2 mg/ml	200 µg/l
Chloramphenicol (Cmp)	34 mg/ml	34 µg/ml
Hemin	100 mM	10 µM
Isopropyl-β-D-thiogalactopyranoside(IPTG)	1 M	0.5-1 mM
Kanamycin (Kan)	50 mg/ml	50 µg/ml
Spectinomycin (Spc)	50 mg/ml	50 µg/ml

### 2.2.2 Storage of *E. coli* cultures

For longterm storage of *E. coli* an overnight culture was diluted with sterile 80% (v/v) glycerol to an final glycerol concentration of 20%. All stocks were stored at -80 °C. For short term storage of *E. coli* cells were streaked out on LB agar plates and stored at 4 °C.

### 2.2.3 Cultivation of *E. coli* cells

Pre-cultures of *E. coli* were grown in LB medium overnight at 37 °C with shaking at 180 rpm (SM 30 CONTROL, Edmund Buehler). For selection conditions the appropriate antibiotics were added (2.5). On the next day, the main culture was inoculated with 1:100 of the pre-culture in LB or LB high salt medium. Growth cultures were incubated at 37 °C and 100 rpm. For anaerobic conditions, 1 l serum bottles were used and inoculated with 1:100 of the pre-culture in LB high salt or TB medium. Agar plates containing the appropriate antibiotics were incubated at 37 °C overnight with the exception of *E. coli* strain Nissle 1917, which was incubated on plate at 30 °C overnight.

### 2.2.4 Cultivation media for *M. acetivorans* cells

For cultivation of *M. acetivorans* cells anaerobic high salt (HS) medium was used. All components (with exception of the salts) were mixed together and filled up to 1 l with A. dest in

a 3 l round bottom flask. The solution was boiled for 10 min under a N<sub>2</sub>/CO<sub>2</sub> (80/20 [v/v]) gas flow (water vaporized). The medium was cooled down on ice under gas flow and afterwards inserted into the anaerobic chamber. Inside the chamber the salts were added to reduce the medium. When the solution became pale 125 mM anaerobic methanol was added and the volume was filled up again to 1 l with anaerobic A.dest. The medium was filled into Balch tubes, hungate tubes or serum bottles and closed. After getting out the medium of the anaerobic chamber, the gas phase was adjusted to 40 kPa N<sub>2</sub>/CO<sub>2</sub> (80/20 [v/v]). Before use 1:100 sterile anaerobic 0.5 M KH<sub>2</sub>PO<sub>4</sub> was added.

10x Mix A			10x Mix B		
Component	Stock conc.	Final conc. per l medium	Component	Stock conc.	Final conc. per l medium
NaCl	4 M	0.4 M	MgCl <sub>2</sub> × 6 H <sub>2</sub> O	540 mM	54 mM
KCl	130 mM	13 mM	CaCl <sub>2</sub> × 2 H <sub>2</sub> O	20 mM	2 mM

**1000x trace elements**

Component	Stock conc.	Final conc. per l medium
Nitrilotriacetic acid	58 mM	58 μM
FeSO <sub>4</sub> × 7 H <sub>2</sub> O	20 mM	20 μM
Na <sub>2</sub> SeO <sub>3</sub> × 5 H <sub>2</sub> O	11 mM	11 μM
CoCl <sub>2</sub> × 6 H <sub>2</sub> O	4 mM	4 μM
MnSO <sub>4</sub> × H <sub>2</sub> O	6 mM	6 μM
Na <sub>2</sub> MoO <sub>4</sub> × H <sub>2</sub> O	4 mM	4 μM
Na <sub>2</sub> WO <sub>4</sub> × 2 H <sub>2</sub> O	3 mM	3 μM
ZnSO <sub>4</sub> × H <sub>2</sub> O	3 mM	3 μM
NiCl <sub>2</sub> × 6 H <sub>2</sub> O	12 mM	12 μM
H <sub>3</sub> BO <sub>3</sub>	1.6 mM	1.6 μM
CuSO <sub>4</sub>	0.4 mM	0.4 μM

1000x concentrated in 100 ml A.dest,  
pH 6.5 with KOH adjusted, autoclaved

**500x vitamin solution**

Component	Stock concentration	Final concentration
<i>p</i> -Aminobenzoic acid	364.5 μM	729 nM
Nicotinic acid	406 μM	812 nM
Ca-Pantothenate	209.5 μM	419 nM
Pyridoxine-HCl	243 μM	486 nM
Riboflavin	133 μM	266 nM
Thiamine-HCl	148 μM	296 nM
Biotin	102 μM	204 nM
Folic acid	56.5 μM	113 nM
α-Lipoic acid	121 μM	242 nM
Vitamine B <sub>12</sub>	18.5 μM	37 nM

500x concentrated in 200 ml A.dest, filter sterilized

Final composition of anaerobic HS medium			Salts		
100	ml/l	10x MixA	1	g/l	NH <sub>4</sub> Cl
100	ml/l	10x Mix B	0.5	g/l	Cystein-HCl
1	ml/l	0.1% (w/v) resazurin solution	0.05	g/l	Na <sub>2</sub> S x 9 H <sub>2</sub> O
1	ml/l	1000x trace elements			
2	ml/l	500x vitamin solution			
20	mM	MOPS, pH 7.0, NaOH			

### 2.2.5 Storage of *M. acetivorans* cultures

For long term storage of *M. acetivorans* cells, were stored as both glycerol stocks and liquid culture stocks. For glycerol stocks 8 ml of an anaerobic grown culture in a 10 ml serum bottle was mixed with 2 ml 50% sterile anaerobic glycerol to a final glycerol concentration of 10%. The anaerobic stocks were evacuate and shrink-wrapped in a gas-tight film. All glycerol stocks were stored at -80 °C. 1 ml of glycerol stock was used to inoculated 10 ml of anaerobic medium. For liquid culture storage anaerobic grown cultures were stored at RT in Balch tubes.

### 2.2.6 Cultivation of *M. acetivorans* cells

Cultures were inoculated 1:100 from RT stored cultures or fresh pre-cultures. *M. acetivorans* cultures with 125 mM methanol were grown anaerobically in Balch tubes or serum bottles at 37 °C without shaking. For selective conditions the culture was supplemented with the 2 µg/ml puromycine.

### 2.2.7 Determination of cell density

To determine the cell density of liquid culture the optical density at 578 nm (OD<sub>578</sub>) was measured via a photometer. One OD<sub>578</sub> corresponds to 0.1\*10<sup>7</sup> cells per milliliter.

## 2.3 Molecular biological techniques

### 2.3.1 Production of chemically competent *E. coli* cells

To produce chemically competent *E. coli* cells the CaCl<sub>2</sub> heat shock method was used. 100 ml LB medium (with antibiotica) was inoculated 1:100 with an overnight culture. Cells were incubated at 37 °C and 180 rpm to an OD<sub>578</sub> of about 0.5. The culture was centrifuged at 4000 rpm for 10 min at 4 °C (Eppendorf 5810R, rotor A-4-62) and the supernatant was discard. Cells were resuspended in 50 mM CaCl<sub>2</sub> and incubated on ice for 45 min. Afterwards the cells were again centrifuged at 4000 rpm, 4 °C for 10 min (Eppendorf 5810R, rotor A-4-62). The pellet was resuspended in 5 ml 50 mM CaCl<sub>2</sub> with 15% glycerol and aliquoted to 200 µl. The competent cells were stored at -80 °C. Competent cells of *E. coli* Nissle 1917 were not longer stored than 3 month.

### 2.3.2 Transformation of chemically competent *E. coli* cells

To transfer DNA into chemically competent *E. coli* cells, 200 µl of competent cells were thawed on ice. For the transformation 50-100 ng of plasmid DNA was used. For the trans-

formation of ligation reactions 10  $\mu\text{l}$  of the mixture was used. The DNA was gently mixed with the cells and incubated for 15 min on ice. Afterwards the cells were heat-shocked for 2 min at 42 °C and incubated again for 1 min on ice. 700  $\mu\text{l}$  of LB medium was added and the cells were incubated at 37 °C for 1 h at 180 rpm. After incubation the cells were plated on selective agar plates and incubated over night at 37 °C. Transformation cells of *E. coli* strain Nissle 1917 were incubated over night at 30 °C.

### 2.3.3 Electroporation of *E. coli* cells

For electroporation of *E. coli* the cell suspension have to be free of any salts. Therefore, 100 ml LB medium was inoculated 1:100 with an overnight culture. Cells were incubated at 37 °C and 180 rpm until an OD<sub>578</sub> of 0.5 was reached. The culture was centrifuged at 4000 rpm and 4°C for 5 min (Eppendorf 5810R, rotor A-4-62) and the supernatant was discard. The cell pellet was resuspended in 50 ml sterile A. dest, centrifuged and the washing step repeated again. Afterward, cells were resuspended in sterile 10% glycerol and centrifuged again. The supernatant was decanted and cells resuspended in the remaining glycerol. Cells were stored at -80 °C as 50  $\mu\text{l}$  aliquots. For electroporation 0.5-1  $\mu\text{l}$  salt-free DNA was added to 50  $\mu\text{l}$  of *E. coli* cells and transferred to an pre-chilled 0.2 cm electroporation cuvette (BioRad). Upon electroporation cells were diluted in 700  $\mu\text{l}$  LB medium, incubated for 1 h at 37 °C and 180 rpm and plated onto LB agar plates with appropriate antibiotica.

### 2.3.4 Preparation of plasmid-DNA

Preparation of plasmid DNA was performed using an alkaline lysis protocol. 5 ml of LB medium were inoculated with a single colony and incubated over night at 37 °C and 180 rpm (SM 30 CONTROL, Edmund Buehler). To pellet the cells two time 2 ml of the culture were centrifuged at 13,000 rpm for 2 min. The supernatant was discarded and the pellet resuspended in 300  $\mu\text{L}$  GTE-buffer with 100  $\mu\text{g}/\text{ml}$  RNase A. After incubation of 5 min at RT additional 300  $\mu\text{L}$  of buffer P2 was added to the sample, inverted and incubated for 5 min on ice. In the next step 300  $\mu\text{l}$  of buffer P3 was added, inverted and incubated for 5 min on ice. Afterwards the sample was pelleted for 15 min at 13,000 rpm (Z32HK Hermle, rotor 12/002). The supernatant was transferred into a new 2 ml eppendorf tube and 800  $\mu\text{l}$  of 100% EtOH was added. The plasmid-DNA was precipitated for 2 min at RT and sedimented for 15 min at 13,000 rpm (Z32HK Hermle, rotor 12/002). The pellet was washed with 300  $\mu\text{l}$  of 70% EtOH, centrifuged for 5 min at 13,000 rpm (Z32HK Hermle, rotor 12/002) and dried at 37°C. The remaining plasmid DNA was solved in 30  $\mu\text{l}$  A.dest. For plasmid stocks or sequencing the NucleoSpin<sup>®</sup> Plasmid EasyPure Kit (Macherey Nagel) was used according to manufacturer's instructions. The plasmids were controlled by agarose gel electrophoresis (2.3.8) and stored at -20 °C.

P1	50 mM	Tris-HCl pH 8.0
	10 mM	EDTA
	100 $\mu\text{l}/\text{ml}$	RNase A (freshly added)
P2	200 mM	NaOH
	61 % (w/v)	SDS
P3	3 M	sodium acetate pH 5.5

### 2.3.5 Preparation of genomic DNA from *M. acetivorans*

For the isolation of genomic DNA from *M. acetivorans* the CTAB-method was used with some modifications [100]. For this 25 ml of a culture grown with 125 mM MeOH in anaerobic HS-medium to stationary phase at 37 °C was pelleted for 10 min at 4000 rpm in a 50 ml falcon (Eppendorf 5810R, rotor A-4-62). The supernatant was discarded and the cell resuspended in 1.5 ml sucrose buffer and transferred into a 10 ml falcon. 75 µl of 10% SDS, 75 µl of Proteinase K (20 mg/ml) and 15 µl RNase A (10 mg/ml) were added, mixed gently and incubated for 1 h at 37 °C (Julabo water bath). After incubation 250 µl 5 M NaCl and 200 µl CTAB/NaCl solution were added, mixed gently and incubated for 10 min at 65 °C (Julabo water bath). Afterwards one volume of chloroform/isoamylalcohol (24:1) was added and centrifuged for 45 min at 4000 rpm (Eppendorf 5810R, rotor A-4-62). The aqueous phase was transferred into a new tube and mixed with one volume of phenol/chloroform/isoamylalcohol (25:24:1). The sample was centrifuged again at 4000 rpm for 30 min (Eppendorf 5810R, rotor A-4-62) and the upper phase was transferred into a 2 ml Eppendorf tube. 3/4 volume of isopropanol was added to precipitate the DNA and centrifuged for 10 min at 4000 rpm (Z32HK Hermle, rotor 12/002). The step was repeated with 100% EtOH and the sediment washed with iccold 70% EtOH and dried. The pellet was solved in 100 µl A.dest for 1 h at 50 °C or overnight at RT.

### 2.3.6 Preparation of RNA from *M. acetivorans*

To isolate total RNA from *M. acetivorans* 50 ml of a culture grown until the mid-exponential phase was used. The growth was stopped by adding 4 ml of iccold RNA stop solution (5-10% buffered phenol in EtOH) to the anaerobic culture. The serum bottle was opened and the culture was pelleted for 5 min at 4000 rpm and 4 °C (Eppendorf, rotor). The supernatant was discarded and for storage at -80 °C the cell pellet was frozen with liquid nitrogen. For RNA isolation the Quick-RNA<sup>TM</sup> Miniprep Kit (Zymo Research) was used according to manufacturer's instructions. RNA isolation was tested via agarose gel electrophoresis and PCR to verify the DNA-free RNA. Remaining DNA was removed via DNase digestion.

### 2.3.7 Polymerase chain reaction

The polymerase chain reaction (PCR) was used to amplify DNA fragments and specific introduction of restriction sites. For screening PCRs the DreamTaq Green PCR Master Mix (Thermo Fisher) was used according to the manufacturers protocol. For amplification of DNA fragments for cloning the Phusion<sup>®</sup> High-Fidelity DNA Polymerase (Thermo Fisher) was used, as it possesses a 3'-5' exonuclease proofreading activity. As a template 10 ng of plasmid DNA or 100 ng of genomic DNA was used.

PCR reaction mix:

x	µl	template DNA
each 1	µl	Primer [100 pmol/µ]
0,5	µl	Phusion polymerase [2000 U/ml]
10	µl	5x HF-Puffer
5	µl	dNTPs [2,5 mM]
x	µl	A. dest
<hr/>		
50	µl	



PCR program:

98 °C	5 min	Initial denaturation	30 cycles
98 °C	1 min	Denaturation	
X °C	30 sec	Annealing	
72 °C	1 min	Elongation	
72 °C	10 min	Final elongation	
12 °C	Pause	Cooling	

### 2.3.8 Determination of DNA and RNA concentration in aqueous solution

To determine the concentration of liquid DNA and RNA samples the NanoDrop<sup>TM</sup> Lite photometer (Thermo Fisher) and the corresponding software was used. The absorbance was measured at 260 nm. The purity of the samples were determined by the comparison of the absorbance at 260 nm ( $A_{260}$ ) and 280 nm ( $A_{280}$ ). For double-stranded DNA an  $A_{260}/A_{280}$  ratio of  $\sim 1.8$  and for RNA an  $A_{260}/A_{280}$  ratio of  $\sim 2.0$  was accepted as sufficiently pure.

### 2.3.9 Agarose gel electrophoresis

Agarose gel electrophoresis was used to separate and identify DNA and RNA molecules in a horizontal gel electrophoresis chamber. Standard agarose gels were run in 1x TAE buffer with an agarose concentration of 1%. Small gels were run at 90 V and large gels at 140 V until the fragments were separated. For visualization the fragments were stained with a GelRed<sup>TM</sup> 10,000x stock dilution of 1:50,000. The fluorescent labeled DNA was detected by the GelDoc (Intas).

#### 1x TAE buffer

40	mM	Tris/acetate pH 8.0
1	mM	EDTA

### 2.3.10 Purification of PCR products

PCR products were purified by using the NucleoSpin<sup>®</sup> Gel and PCR Clean-up kit (Macherey-Nagel) according to manufacturer's instructions.

### 2.3.11 Restriction of DNA

Restriction of DNA was carried out using FastDigest enzymes (Thermo Fisher) or restriction enzymes from New England Biolabs (NEB) according to manufacturer's instructions. Test restrictions were performed in a total volume of 10  $\mu$ l for 20 min at 37°C. Preparative DNA digestion was achieved in bigger approaches up to a total volume of 50  $\mu$ l with an incubation at 37 °C for 1 h. Digestion was performed stepwise with a thermal inactivation for 5 min at 80 °C in between, when two different enzymes were needed.

### 2.3.12 Gel extraction of DNA fragments

Digested DNA was purified via gel extraction after agarose gel electrophoresis. For the extraction the NucleoSpin<sup>®</sup> Gel and PCR Clean-up kit (Macherey-Nagel) was used according

to manufacturer's instructions.

### 2.3.13 Dephosphorylation of DNA

To avoid self-ligation of vector DNA the ends were dephosphorylated using FastAP Thermo-sensitive Alkaline Phosphatase (Thermo Fisher) according to manufacturer's instructions. Reaction was performed in a total volume of 20  $\mu\text{l}$  for 10 min at 37 °C and stopped at 75 °C for 5 min.

### 2.3.14 Ligation of DNA

Vector DNA and PCR products were ligated by using T4 DNA Ligase (Thermo Fisher) as recommended by manufacturer's instructions. For the ligation reaction 10-100 ng of vector DNA was incubated with a 3-fold molar excess of insert DNA. The reaction was performed in a total volume of 20  $\mu\text{l}$  for 0.5-1 h at RT. The T4 DNA Ligase was inactivated for 10 min at 65 °C prior to the transformation of the ligation product into appropriate chemically competent *E. coli* cells.

### 2.3.15 Construction of expression and coexpression vectors

The coding regions were amplified from genomic or plasmid DNA. The appropriate restriction sites were introduced by PCR using primers listed in Tab. 4.3 & 5.3. The obtained PCR products were cut with the corresponding restriction enzymes and ligated into the similarly cut vector. The ligation product was transformed into either *E. coli* JM83 or DH5 $\alpha$  cells. For vectors pUT18, pUT18C, pKT25 and p25N ligation fragments were transformed into *E. coli* JM109 cells. Cells were plated onto LB agar plates with the appropriate antibiotic. The obtained colonies were used for overnight cultures to isolate the plasmids. Correct plasmids were verified by sequencing. For larger DNA fragments like full-length *msmS* the NEBuilder® HiFi DNA Assembly Master Mix was used according to the manufacturers protocol.

### 2.3.16 Site-directed Mutagenesis

The different variants of wild type proteins were created by site-directed mutagenesis. The specific mutations were introduced by primers harbouring either single or double base exchanges (Tab. 4.1). The corresponding plasmids were obtained by a PCR reaction. 25  $\mu\text{L}$  of the PCR reaction was mixed with 3  $\mu\text{l}$  10x CutSmart buffer and 2  $\mu\text{L}$  DpnI (New England Biolabs) and incubated for 2 h at 37 °C. The plasmids were sequenced prior to use.

PCR reaction mix:

10 - 100 ng	$\mu\text{l}$	template DNA
each 1.25	$\mu\text{l}$	primer [100 pmol/ $\mu\text{l}$ ]
10	$\mu\text{l}$	5x HiFi buffer
2.5	$\mu\text{l}$	dNTPs [2,5 mM]
1	$\mu\text{l}$	PRECISOR-HF Polymerase [2 U/ $\mu\text{l}$ ]
x	$\mu\text{l}$	A.dest
<hr/>		
50	$\mu\text{l}$	

PCR program:

98 °C	1 min	Initial denaturation	30 cycles
98 °C	10 sec	Denaturation	
56 °C	30 sec	Annealing	
72 °C	1 min/kb	Elongation	
72 °C	4 min	Final elongation	

### 2.3.17 Construction of an *E. coli* Nissle 1917 strain for T7-dependent protein production

In order to use T7-dependent expression systems with the newly established method for recombinant heme protein production in *E. coli* Nissle 1917 (EcN), the T7-RNA-polymerase gene should be introduced into the chromosome of EcN. For this a homologous recombination systems based on the *E. coli* specific  $\lambda$  phage was used [2]. The phage is capable of introducing genes into any chromosomal location.

To obtain an IPTG inducible gene expression of the T7-RNA polymerase a *lacUV5* promoter was added via PCR primers with overhanging sequences to the gene. The template for the PCR reaction was genomic DNA of *E. coli* BL21(DE3). As a selection marker a kanamycin resistance cassette flanked with FRT recognition sites was ligated to the 5' end of the T7-RNA-Polymerase gene via a *SalI* restriction site (Fig. 2.1, step 1&2). The appropriate fragment was purified via agarose gel extraction and blunt-end cloned (*SmaI*) into the vector pUC-Sma-only (pYPRUB168) for a interim storage and as template for further PCR reactions. The derived plasmid pUC-T7-FRT-Kan was used as a PCR template to add homologous DNA sequences of the desired recombination positions at both sites of the integration cassette (Fig. 2.1, step 3). The linear integration cassette was then introduced via electroporation in EcN cells carrying the vector pKD46 (Fig. 2.1, step 4). The plasmid pKD46 contains the genes *gam*, *beta* and *exo* from Phage  $\lambda$  which are responsible for the integration event. Expression of these genes are under the control of a pBAD promoter. Therefore, 1 mM L-arabinose was added to the freshly transformed cells. After transformation the cells were incubated at 30 °C and 180 rpm for 12 h. Upon incubation cells were plated onto MacConkey agar plates containing 1% maltose and kanamycin (Fig. 2.1, step 5). Positiv colonies were kanamycin resistant and incapable of utilizing maltose indicated by white colony color. Obtained mutants were then screened via PCR and sequence analysis.

### 2.3.18 Sequencing of DNA

For sequencing plasmids were purified by using the Kit from Macherey & Nagel. The sequencing mixture was composed of 5  $\mu$ l of 50-100 ng/ $\mu$ l DNA and 5  $\mu$ L of primer. For sequencing PCR fragments 5  $\mu$ l of 5-50 ng/ $\mu$ l DNA was mixed with 5  $\mu$ L of the appropriate primer. Sequencing was conducted by GATC Biotech (Konstanz) and Eurofins Genomics (Ebersberg).

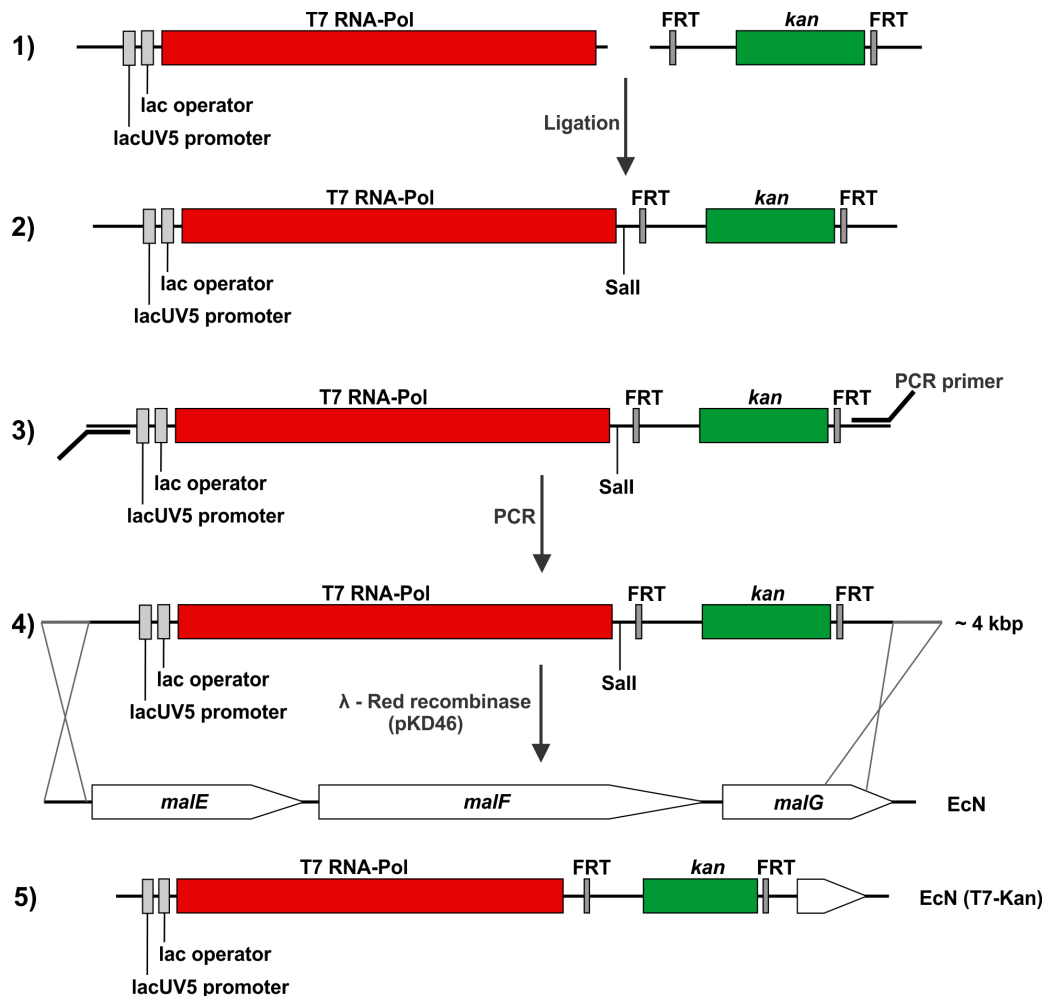


**Figure 2.1 Integration strategy for the introduction of T7-RNA-Polymerase into the chromosome of *E. coli* Nissle 1917.** (1) Amplification and ligation of genes for T7-RNA-polymerase and FRT-flanked Kan<sup>r</sup> cassette. The lac operator and lacUV5 promoter was added by PCR primers. (2) Ligation product containing Sall restriction side between the two genes. The fragment was cloned into pYPRUB168 via blunt-end-cloning. (3) Amplification of the integration cassette with primers containing homologous sequences to the target malEFG operon. (4) λ-red recombination mediated by the additionally transformed plasmid pKD46. (5) Desired EcN mutant strain EcN (T7-Kan). (modified from [2])

### 2.3.19 RNAseq analysis

To identify differentially expressed genes in the wild type and  $\Delta msmS$  strain RNAseq analysis was performed. For this two biological samples for each strain were prepared. The strains were grown in 50 ml high salt medium with methanol as a substrate until the mid-exponential phase with an OD<sub>578</sub> 0.5 - 0.7 was reached. RNA was isolated as described in 2.3.5. For transcriptome analysis 2  $\mu$ g of total RNA was used. RNAseq analysis was conducted by Konrad Förstner and Claus Scholz of the Core Unit Systems Medicine of the University of Würzburg. RNAseq libraries for gene expression profiling were prepared without rRNA depletion. RNA was fragmented, ligated to adapter sequences and subsequently reverse transcribed. Sequencing of the library was performed using a high-output run with  $\sim$ 140-170 M reads. The results were mapped against the *M. acetivorans* C2A reference genome. The differentially expressed genes were identified using the value log<sub>2</sub>FoldChange and adjusted p-value <0.05. A Heatmap of the first 50 differentially expressed genes accord-

ing to the log<sub>2</sub>FoldChange value (adjusted p-value <0.05) was created using the online tool *Heatmapper* (<http://heatmapper.ca/expression/>).

### 2.3.20 Analysis of protein-protein interactions by bacterial two-hybrid system

To test whether two proteins interact with each other or not the bacterial adenylate cyclase two-hybrid (BACTH) system was used. The BACTH system is based on the interaction-mediated activity of adenylate cyclase in *E. coli*. The catalytic domain of adenylate cyclase (CyaA) from *Bordetella pertussis* consists of two complementary fragments, T18 and T25 which are not active when physically separated (Fig. 2.2 A). For protein-protein interaction studies putative interaction partners are fused to one of the fragments, respectively. Only when an interaction occurs functional complementation between T18 and T25 fragment results in an active enzyme. The active enzyme uses ATP to synthesize cAMP which binds to the catabolite activator protein, CAP and the cAMP/CAP complex binds to the promoter of the *lac* and *mal* operons. Therefore, *E. coli*  $\Delta$ *cyaA* cells become able to catabolize maltose and lactose and can be screened on indicator or selective agar plates.

To test whether the proteins interact with each other they were cloned into the vectors pUT18, pUT18C, p25N and pKT25, containing the T18 and T25 fragment, respectively. For each fragment two plasmids are present with different orientated multiple cloning sites to get N- and C-terminal fusions (Fig. 2.2 B). The corresponding plasmids were co-transformed into *E. coli* BTH101 and plated on LB agar plates with ampicillin and kanamycine. To obtain a heterolog mix 10-15 colonies were resuspended in 50  $\mu$ l of LB and 5  $\mu$ l of the cell suspension was dropped onto MacConkey agar plates containing 1% lactose and 3 mM 5-aminolevulinic acid. The plates were incubated at 30 °C for up to 72 h. For anaerobic conditions the plates contained 20 mM sodium nitrate and were incubated in an anaerobic box with an AnaeroGen<sup>TM</sup> sachet (Thermo Fisher). If an interaction occurs the cells become red, whereas cells with no interaction remain colorless.

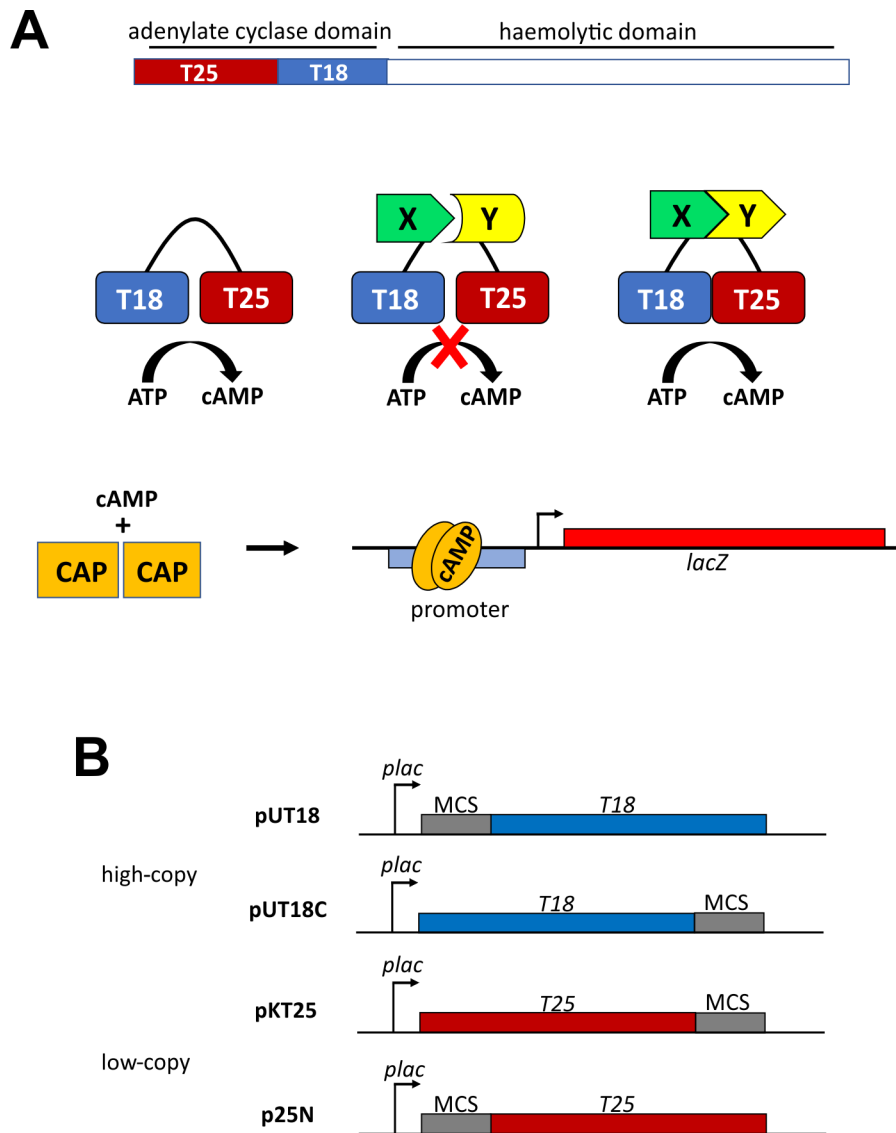


**Figure 2.2 Principle of bacterial two-hybrid system.** (A) The adenylate cyclase of *B. pertussis* consists of two catalytic domains which can be divided into the T25 and T18 fragment. Both fragments together form an active enzyme able to convert ATP to cAMP. Putative interaction partners (X & Y) can be fused to each of the fragments. If these both proteins interact with each other the T25 and T18 fragments can be reconstituted to an active enzyme. The formed cAMP binds together with the catabolite activator protein (CAP) to a promoter activating the expression of the *lacZ* reporter gene, resulting in an active  $\beta$ -galactosidase enzyme. (B) Four different plasmids are available with multiple cloning sites at the 5'- and 3'-end of the T18 and T25 fragments for different fusion combinations. (modified from [60])

## 2.4 Protein biochemical and biophysical techniques

### 2.4.1 Production of recombinant proteins in *E. coli* BL21(DE3)

Recombinant proteins fused to a C-terminal *StrepII*-tag were produced using *tet* promoter-driven expression system (IBA). *E. coli* BL21(DE3) cells containing the appropriate expression plasmid were grown at 37 °C and 100 rpm in LB medium with 100 µg/ml ampicillin. Full-length proteins were produced in LB high salt (LB-HS) medium. When an OD<sub>578</sub> of ~0.5 was reached the cultures were cooled down to 17 °C. Protein production was induced by addition of 200 ng/ml anhydrotetracycline and cells were further incubated at 17 °C and 100 rpm for 18-20 h. Cells were harvested at 9000 rpm and 4 °C for 10 min (Thermo Fisher, Sorvall LYNX 6000, rotor F9) and either frozen at -20 °C or subsequently used for protein purification. For co-expression experiments, the plasmid pHPEX3-Kan was used to express the heme receptor *ChuA*. Co-expression was performed as described before, with the exception that the cultures contain 25 µg/ml kanamycin and 50 µg/ml ampicillin. Expression of *chuA* was induced by addition of 1 mM isopropyl-β-thiogalactosidase (IPTG). Directly after induction 10 µM hemin (freshly made stock in DMSO) was added to the cultures. Co-expression cultures were incubated in the dark.

### 2.4.2 Production of recombinant proteins with incorporation of pyrrolysine

To produce a protein containing an amber UAG codon for pyrrolysine the plasmids pCDF-Duet-*pylST* and pRSF-Duet-*pylDBC* were coexpressed with the expression vector of the gene of interest [102]. For this all three plasmids were cotransformed into BL21(DE3) cells. The protein production was performed in 2YT-high salt medium with 50% of antibiotics. The cells were grown until an OD<sub>578</sub> of 0.5 at 37 °C and 100 rpm. After reaching the correct OD the cells were cooled down to 17 °C *pyl* gene expression was induced with 0.5 M IPTG and shaken for 3 hours at 17 °C. Afterwards the production of the protein of interest was induced with 200 ng/ml anhydrotetracycline and further 0.05 mM IPTG. The cells were incubated at 17 °C and 100 rpm over night for 18 h.

#### 2YT high salt medium

10.0	g/l	yeast extract
16.0	g/l	tryptone
24.22	g/l	NaCl

### 2.4.3 Production of recombinant proteins in *E. coli* Nissle 1917

Expression of heme proteins in *E. coli* Nissle 1917 was performed as described for *E. coli* BL21(DE3), with the exception that the cultures grow until an OD<sub>578</sub> of ~1.2 before cooling down and induction. Directly after induction 10 µM hemin (freshly made stock in DMSO) was added to the growth medium and the cultures were incubated in the dark. Anaerobic production was conducted using 1 l serum bottles with LB-HS medium containing 20 mM sodium nitrate and 20 mM 3-(N-morpholino)propanesulfonic acid (MOPS) buffer (pH 7.0). The cells were harvested via an anaerobic chamber to ensure an oxygen-free environment. After harvesting the cell pellet was evacuated, shrink-wrapped and frozen at -20°C.

#### 2.4.4 Production of recombinant proteins in *E. coli* RP523

For the production of recombinant apo-protein the heme-permeable *hemB* mutant strain RP523 of *E. coli* was used. Under aerobic growth conditions the strain need heme or other porphyrin analogs [160]. To produce apo-protein the cells were cultured under anaerobic conditions in TB medium with 1% glucose using 1 l serum bottles. The cells were grown at 37 °C until an OD<sub>578</sub> of ~0.5. After cooling down the cells to 17 °C expression was induced with 200 ng/ml AHT. Expression cultures were further incubated at 17 °C for 18 - 20 h.

#### 2.4.5 Cell disruption of *E. coli* cells

Prior to cell disruption the cells were thawed overnight on ice. On the next morning they were resuspended in icecold buffer W for cells containing proteins variants sGAF2, GAF2 and G2P2. Cells containing variants G2G1, G2P1 and full-length protein were resuspended in icecold buffer W with additional 10% glycerol and 0.05% Tween-20 for stabilization of large proteins. After addition of a spatula tip of lysozyme, DNase I, 1 mM dithiothreitol (DTT) and 0.25 mM 4-(2-aminoethyl)benzenesulfonyl fluoride hydrochloride (AEBSF) the cells were incubated on ice for 30 min. The cells were lysed using a microfluidizer or sonifier. Cell disruption with microfluidizer was performed for three rounds at 15,000 psi. Sonification was performed in 15 s cycles of sonification and pause with an total time of sonification of 4 min (cycle 5/10, ~50% power output, Bandelin UW 2200 with tip KE 76). For separation of cell fragments from the soluble part, lysate was centrifugate for 1 h at 19,000 rpm (Sorvall<sup>TM</sup> LYNX<sup>TM</sup> 6000 centrifuge, rotor T29). After centrifugation the lysate was filtrated with 0.45 µM PVDF syringe filters. For heme reconstitution of proteins produced in BL21(DE3) 0.1 mM hemin (freshly made 4.6 mM stock in DMSO) was added to the cell free lysate and incubated for 45 min on ice prior affinity chromatography.

##### Buffer W

100	mM	Tris/HCl pH 8.0
150	mM	NaCl
1	mM	EDTA

#### 2.4.6 Purification of recombinant produced *StrepII*-tagged proteins

Recombinant *StrepII*-tagged proteins were purified by affinity chromatography. The *Strep*-Tactin chromatography column (IBA) was equilibrated with buffer W. After the lysate flow through the column material unwanted proteins were washed off with 10 column volumes (CV) of buffer W. Tagged proteins were eluted by buffer E and desired fractions were combined for dialysis. MA0863 full-length proteins were dialyzed against dialysis buffer pH 8.0. MsmS variants were dialysed against dialysis buffer pH 7.0 (for full-length, G2P1 and G2G1 5% (v/v) glycerol and 0.05% (v/v) was added).

##### Dialysis buffer pH 7.0

50	mM	Na <sub>2</sub> HPO <sub>4</sub>
50	mM	NaH <sub>2</sub> PO <sub>4</sub>
100	mM	NaCl

##### Dialysis buffer pH 8.0

20	mM	TES
100	mM	KCl
10	% (v/v)	glycerol
0.05	% (v/v)	Tween-20

##### Buffer E

buffer W
2.5 mM desthiobiotin



### 2.4.7 SDS-polyacrylamide gel electrophoresis

Sodium dodecyl sulfate polyacrylamide gel electrophoresis (SDS-PAGE) was used for separation of protein mixtures or protein preparations as discontinuative SDS-PAGE after Laemmli (1970). The gels were prepared with 5.25% polyacrylamide stacking gel (pH 6.8) and either 10% acrylamide (for proteins with >100 kDa MW) or 12.5% acrylamide (for proteins with <100 kDa MW) separating gel (pH 8.8). SDS is a negatively charged, denaturing detergent which binds proteins in a ratio nearly one molecule SDS per two amino acid side chains, resulting in an almost constant mass:charge ratio. Thereby, it allows separation of proteins in the electric field depending on their molecular weight. Protein samples were denatured by 4x SDS sample buffer and incubation for 5 min at 95 °C prior to loading onto the gel for reducing conditions. For non-reducing conditions the samples were denatured with 4x sample buffer without  $\beta$ -mercaptoethanol and directly loaded onto the gel. The electrophoresis was performed with a constant voltage of 200 V for 12.5% gels and 180 V for 10% gels until tracking dye reached the bottom of the gel. After electrophoresis proteins were visualized by staining with Coomassie Brilliant Blue G250 and subsequent destaining by shaking in destaining solution.

10x SDS running buffer		4x stacking gel buffer		4x separating gel buffer	
250	mM	Tris/HCl	0.5 M	Tris/HCl	1.5 M
		pH 8.8		pH 6.8	
1.92	M	glycine	0.4 % (w/v)	SDS	0.4 % (w/v)
1	% (w/v)	SDS			

#### Stacking gel (5.25%), 4 mini gels

1.4	ml	Rotiphorese Gel 30 (30% acrylamide, 0.8% bisacrylamide)
2	ml	4x stacking buffer
4.6	ml	A.dest
30	$\mu$ l	10% (w/v) ammonium persulfate
20	$\mu$ l	TEMED

#### Separating gel (10%), 4 mini gels

5.3	ml	Rotiphorese Gel 30 (30% acrylamide, 0.8% bisacrylamide)
4	ml	4x separating buffer
6.7	ml	A.dest
80	$\mu$ l	10% (w/v) ammonium persulfate
8	$\mu$ l	TEMED

#### Separating gel (12.5%), 4 mini gels

6.7	ml	Rotiphorese Gel 30 (30% acrylamide, 0.8% bisacrylamide)
4	ml	4x separating buffer
5.3	ml	A.dest
80	$\mu$ l	10% (w/v) ammonium persulfate
8	$\mu$ l	TEMED

#### 4x SDS sample buffer

100	mM	Tris/HCl pH 6.8
8	% (w/v)	SDS
40	% (v/v)	glycerol
10	% (v/v)	$\beta$ -mercaptoethanol
1	% (w/v)	bromphenol blue

#### Staining solution

10	% (v/v)	acetic acid
30	% (v/v)	ethanol
0.25	% (w/v)	Coomassie brilliant blue G250

#### Destaining solution

10	% (v/v)	acetic acid
30	% (v/v)	ethanol

### 2.4.8 Immuno-detection of immobilized proteins (Western blot)

For selective detection of a specific protein in a sample the western blotting method was used. After electrophoretic separation and transfer of the proteins to a membrane the specific protein is detected by using an antibody.

Protein samples were separated via SDS-PAGE (2.4.6) and subsequently transferred to a PVDF membrane using a semidry blotting system for 20 min at 15 V. Prior to blotting the gel was equilibrated in Towbin transfer buffer for 5-15 min. The PVDF membrane was activated in 100% methanol and afterwards equilibrated in Towbin transfer buffer together with the gel. The blotting sandwich was assembled as followed: the equilibrated gel and membrane were placed between two pieces of Towbin transfer buffer soaked blot papers (3 mm, Whatman). After transferring the proteins the membrane was either blocked at RT for 1 h or overnight at 4 °C. Upon blocking the membrane was washed twice with PBS-T buffer for 1-5 min. Afterwards fresh PBS-T was added containing 2 µg/ml avidin, before 10 ml of the anti-Strep-Tactin<sup>®</sup>-AP-conjugate (1:4000, IBA GmbH) was added. After incubating the antibody on the membrane for 1 h at RT the membrane was washed twice with PBS buffer and then equilibrated in 10 ml AP buffer. For detection 33 µl nitro blue tetrazolium chloride (NBT, 100 mg/ml) and 66 µl 5-bromo-4-chloro-3-indolyl phosphate (BCIP, 50 mg/ml) were added. The reaction was stopped by removing the buffer and by addition of A. dest.

#### Towbin transfer buffer

25 mM Tris/HCl pH 8.3  
192 mM glycine

#### PBS buffer, pH 7.4

5 mM Na<sub>2</sub>HPO<sub>4</sub> × 2H<sub>2</sub>O  
1.5 mM NaH<sub>2</sub>PO<sub>4</sub> × H<sub>2</sub>O  
2.7 mM KCl  
137 mM NaCl

#### PBS-T buffer

PBS buffer  
0.1 % (v/v) Tween-20

#### Blocking buffer

PBS buffer  
0.5 % (V/v) Tween-20  
3 % (w/v) Albumin Fraction V

#### AP buffer

100 mM Tris/HCl pH 9.5  
100 mM NaCl  
5 mM MgCl<sub>2</sub>

### 2.4.9 Determination of protein concentration

Protein concentration was determined by measuring the A<sub>280</sub> and using the calculated ε<sub>280</sub> [39] for the respective protein for calculation (Tab. 2.6). The three amino acid residues tryptophane (Trp), tyrosine (Tyr) and cysteine (Cys) absorb light at 280 nm. The molar extinction coefficient can be calculated as followed:

$$\begin{aligned}\epsilon_{280} &= (n_{Trp} * 5690 + n_{Tyr} * 1280 + n_{Cys} * 120)M^{-1}cm^{-1} \\ n_x &= \text{number of the specific amino acid in the protein} \\ \epsilon_{280} &= \text{molar extinction coefficient at 280 nm}\end{aligned}$$

The protein concentration of the sample was calculated by application of the Lambert Beer's law:

$$c\left[\frac{\text{mol}}{\text{l}}\right] = \frac{A_{280}}{\epsilon_{280}} * d$$

$c$  = protein concentration in  $\frac{\text{mol}}{\text{l}}$   
 $A_{280}$  = absorbance at 280 nm  
 $\epsilon_{280}$  = molar extinction coefficient at 280 nm in  $\text{M}^{-1}\text{cm}^{-1}$   
 $d$  = path length of cuvette in cm

To convert the concentration based on the weight the molar concentration was multiplied with the calculated relative molecular weight ( $M_r$ )(Tab. 2.6).

$$c\left[\frac{\text{g}}{\text{l}}\right] = M_r * c\left[\frac{\text{mol}}{\text{l}}\right]$$

$M_r$  = relative molecular weight of a protein in  $\frac{\text{g}}{\text{mol}}$

**Table 2.6** Extinction coefficients

Protein variant	$\epsilon_{280} [\text{M}^{-1} \text{cm}^{-1}]^1$
MsmS- <i>StrepII</i>	123,920
MsmS_sGAF2- <i>StrepII</i>	34,280
MsmS_G2P1- <i>StrepII</i>	107,870
MsmS_G2G1- <i>StrepII</i>	58,820
MsmS_G2P2- <i>StrepII</i>	46,490
MsmS_GAF2- <i>StrepII</i>	50,330
RdmS- <i>StrepII</i>	115,080
RdmS_sGAF2- <i>StrepII</i>	31,720
BphP- <i>StrepII</i>	66,720
KatG- <i>StrepII</i>	150,070
PhuS- <i>His</i> <sub>6</sub>	65,270
H-NOX- <i>StrepII</i>	21,150

<sup>1</sup> calculated from amino acid sequence with *Protein Calculator v3.3*  
 (<http://www.scripps.edu/~cdputnam/protcalc.html>)

## 2.4.10 Size exclusion chromatography

The oligomerization state of affinity purified proteins, was analyzed by size exclusion chromatography (Moore, 1964). The SEC experiments were performed using an Äkta Pure FPLC-system with Superdex<sup>TM</sup> 200 Increase 10/300 GL and Superose<sup>TM</sup> 6 Increase 10/300 GL column (GE Healthcare). The columns were equilibrated with 1.5 column volumes of the appropriate buffer prior to use and the flow rate was set to 1 ml/min. The samples were transferred onto the column using a 500  $\mu\text{l}$  loop. The elution profile was determined by measuring the absorbance at 280 nm for the proteins and at 412 nm for the heme cofactor. For size determination a calibration curve was created by plotting the log of the MW of standard proteins against the quotient of the elution volume ( $V_e$ ) and the void volume ( $V_0$ ). The void volume of the columns was determined by the elution volume of Blue Dextran 2000 (MW 2000 kDa). For calibration 100  $\mu\text{g}$  of following standards were applied to the column: apoferritin (MW = 443 kDa),  $\beta$ -amylase (MW = 200 kDa), alcohol Dehydrogenase (MW= 150 kDa), albumin (MW = 66 kDa), carbonic anhydrase (MW = 29 kDa) and cytochrome C (MW

= 12.4 kDa). The void volume of the column was determined by the elution volume of Blue Dextran 2000 (MW 2000 kDa).

SEC buffer for MsmS			SEC buffer for RdmS		
50	mM		20	mM	TES pH 8
100	mM	NaCl	100	mM	KCl
5	% (v/v)	glycerol	10	% (v/v)	glycerol

#### 2.4.11 Optical absorption spectroscopy (UV/vis)

UV/vis spectra were recorded on a 8453 UV/visible spectrophotometer (Agilent Technologies) at RT. For anaerobic conditions a rubber-sealed cuvette was used. For reduction of Fe(III) complex, the sample was purged with N<sub>2</sub> gas for 10 min and 5 mM sodium dithionate (DTH) was added. For preparation of Fe(II)-CO complex the solution was flushed with CO gas for 5 min. For addition of liquid compounds, anaerobic stocks were prepared to add specific concentrations.

#### 2.4.12 Electron paramagnetic resonance spectroscopy

Electron paramagnetic resonance spectroscopy (EPR) is a technique which detects unpaired electrons in a sample by applying an externally magnetic field. Unpaired electrons can adopt two different states with different energy levels in this field. The electrons can switch between the two levels by emitting or absorbing a photon which are supplied by a microwave source. The frequency of the microwave is kept constant during the experiment but the magnetic field is varied. When the variable magnetic field leads to a difference between the two states equivalent to the supplied energy by the microwave, the electrons can absorb these photons, yielding a detectable signal.

The protein was produced with heme incorporation during protein production. 30  $\mu$ l of 1 mM protein solution was filled up with buffer to 300  $\mu$ l (pH 6: MES, pH 7: HEPES, pH 8: HEPES, pH 9: TAPS, pH 10:CAPS). Immediately afterwards the sample was transferred into a quartz EPR-tube and flash frozen in liquid nitrogen. The samples were analyzed using a Bruker Elexsys E580 spectrometer. The EPR measurements were carried out at a constant temperature of 12 K with a microwave frequency of 9.35 GHz, a modulation frequency of 100 kHz, a modulation amplitude of 1.5 mT and a microwave power of 2 mW. The EPR-experiments were carried out in a cooperation with Antonio Pierik and Dominique Bechtel (Biochemistry group, TU Kaiserslautern).

#### 2.4.13 Circular dichroism spectroscopy

CD spectroscopy was performed in cooperation with Florian Mahler (Molecular biophysics group, TU Kaiserslautern). CD measurements were performed to verify correct folding of variant MA0863\_O216K/C620A in comparison to the wild-type. Measurements were conducted on a Chirascan Plus Spectropolarimeter (Applied Photophysics, Leatherland, UK) at 4 °C with a 1 mm quartz glass cuvette. Spectra were acquired from 195 nm to 290 nm using a bandwidth of 1 nm and in 0.5 nm steps. Triplicates were averaged and subsequently baseline-corrected by subtracting blank measurements.

#### 2.4.14 Mass spectrometry

For mass spectrometry proteins were separated on a SDS-PAGE and stained with colloidal Coomassie. The gel was fixed twice for 10 min in 40% (v/v) ethanol and 10% (v/v) acetic acid. After fixation the gel was washed twice with water for 5 min. The gel was stained overnight in the dye stock solution with freshly added 20% (v/v) methanol. Upon staining the gel was destained with 1% (v/v) acetic acid until all Coomassie particles were removed. The area corresponding to the desired protein was cut out and the protein was in-gel digested with trypsin. Samples were measured via ESI-LC-MS.

##### Dye stock solution

80 g (NH<sub>4</sub>)<sub>2</sub>SO<sub>4</sub> in 765 ml H<sub>2</sub>O  
18.8 ml phosphoric acid (final conc. 3% (v/v))  
1g Coomassie Brilliant G-250 in 20 ml H<sub>2</sub>O

#### 2.4.15 Acidified butanone extraction

To test whether the heme cofactor is bound covalently or not, acidified butanone extraction was performed [147]. The aqueous protein sample was acidified with 1 M HCl to a pH of 1.5-2.0. An equal volume of ice-cold 2-butanone was added, mixed gently and incubated on ice. After cooling the upper organic phase is separated from the lower aqueous phase. If the heme cofactor is bound covalently it stays together with the protein in the aqueous phase, which color then is brown. If the heme cofactor is not covalently bound it can be extracted to the organic phase.

#### 2.4.16 Catalase activity assay

Catalase activity of 10 nM KatG was measured spectroscopically by the decomposition of 20 mM H<sub>2</sub>O<sub>2</sub> in 50 mM sodium phosphate buffer (pH 7.0) and 100 mM NaCl at room temperature [8]. Absorbance was measured every 30 sec for 10 min at 220 nm.

#### 2.4.17 Protein kinase assay

To analyze autophosphorylation activity 20 μM protein was mixed with 50 mM Tris/HCl pH 8.0, 0.2 mM EDTA, 100 mM NaCl and 5 mM MgCl<sub>2</sub>, 0.2 mM ATP and 0.185 MBq [ $\gamma$ -P<sup>32</sup>]ATP at RT. To test the impact of different compounds on the autophosphorylation activity specific concentrations were added prior to phosphorylation. For reducing conditions samples were prepared in short thread bottle ND9 with addition of sodium dithionite and were purged with N<sub>2</sub> gas for 5 min. Assays were stopped after different time points by the additions of SDS-sample buffer without β-mercaptoethanol. For the titration assays with reducing agent 10-200 μM 2-mercaptoethanesulfonate (coenzyme M, CoM-SH), DTT or tris(2-carboxyethyl)phosphine (TCEP) was mixed with protein and incubated for 15 min at RT. Afterwards proteins were phosphorylated for 5 min. Samples were separated in a 10% SDS-PAGE (1 mm thickness) and transferred onto a PVDF membrane. The membrane was exposed to a imagerplate overnight at RT and signals were recorded using the Packard Cyclone PhosphoImager (Perkin Elmer). For control experiments the histidine kinase BphP from *P. aeruginosa* was used. 20 μM of BphP was mixed with 25 mM Tris/HCl pH 7.7, 0.2 mM EDTA, 5 mM MgCl<sub>2</sub> and 2.4 mM β-mercaptoethanol.

5x ATP mix			Reaction mix		
1.85	kBq	$\gamma$ -[P32]-ATP	20	$\mu$ M	Protein
1	mM	ATP	2.5	$\mu$ l	5x Kinase buffer
2.5	$\mu$ l		2.5	$\mu$ l	5x ATP mix
			x	$\mu$ l	A.dest
			12.5	$\mu$ l	

#### 2.4.18 Acid-base treatment of phosphorylated proteins

Proteins were phosphorylated and separated as described before. After blotting, the membrane was exposed to an imager plate. After detecting the signals, the membrane was incubated for 1 h at RT in 1 M HCl, 3 M NaOH or H<sub>2</sub>O. Membrane were again exposed to an imager plate and phosphorylation signals detected.

#### 2.4.19 Thin layer chromatography of phosphorylated proteins

After electrophoresis and transfer of the phosphorylated protein onto a PVDF membrane, the membrane was stained with Ponceau S. The area of the labeled protein was cut out and wash with water until most of the Ponceau S was removed. Afterwards the excised protein was hydrolyzed for 2 h in 5.7 M HCl at 110 °C. After a short centrifugation the supernatant was dried in a vacuum centrifuge, washed twice with water and dried again. After the last drying step the amino acids were resolved in 8  $\mu$ l of a phosphoamino acid standards mix (Sigma, 1 mg/ml of each standard in A.dest). The samples were spotted onto a 0.1 mm cellulose thin layer chromatography (TLC) plate (Merck) and subjected to one-dimensional TLC. The dimension was performed with butanol, formic acid and H<sub>2</sub>O (5:2:1, v/v/v). The TLC plates were treated with 0.25% ninhydrin (in acetone) and incubated at 65 °C until the positions of phosphoamino acid standards were visible. The plate was then exposed to an imager plate (Fuji Film) for 3 days and the signal was recorded using a Typhoon<sup>TM</sup> FLA 7000 biomolecular imager (GE Healthcare).

#### 2.4.20 Pyridine hemochrome assay

The pyridine hemochrome assay is used to determine which type of heme is bound to a protein [9]. To 500  $\mu$ l of a 10  $\mu$ M protein sample 62.5  $\mu$ L 100% (v/v) pyridine and 62.5  $\mu$ l 0.5 M NaOH were added. The sample was then reduced with excess of DTH. The spectrum of reduced pyridine-hemochromogen was measured via UV/vis spectroscopy.

#### 2.4.21 Redox titration

Redox titration experiments were conducted by Christoph Laurich and Wolfgang Lubitz at the Max-Planck-Institute for Energy Conversion (Mühlheim a.d.R., Germany). For determination of redox potentials electrochemical experiments were performed in an electrochemical cell with an optical path length of 0.0125 mm. A gold mesh (82 mesh per inch, wire diameter 0.06 mm, 65% transmission, Advent Materials) was used as a working electrode. Glassy carbon and Ag/AgCl (1 M KCl) electrodes were used as auxiliary and reference electrodes, respectively. The potential was controlled by a potentiostat (EG&G 273 A). A diode array spectrophotometer HP8451 (Hewlett-Packard) with 320 nm cutoff filter was used to follow the UV/vis spectral changes. The following redox mediator dyes were

used (values of midpoint potentials versus normal hydrogen electrode, NHE, of the mediator dyes are given in parenthesis): 1,2-naphthoquinone (+145 mV), 1,4-benzoquinone (+78 mV), phenazine ethosulfate (+55 mV), methylene blue (+13 mV), duroquinone (+5 mV), 5,5,7-indigo trisulfonate (-35 mV), phenazine (-125 mV), 2-hydroxy-1,4-naphthoquinone (-145 mV) and anthra-quinone-1,5-disulfonate (-170 mV). The experiment was performed in an anaerobic glove box. A MsmS\_sGAF2\_C656A-*StrepII* solution at pH 7.0 containing the mediator dyes was injected into the electrochemical cell and a potential of -700 mV was applied for 1 min to completely reduce residual oxygen in the cell. Afterwards, the potential was reset to +200 mV to produce the Fe(III) complex of MsmS\_sGAF2\_C656A. The potential was reduced in 10 mV steps and the reaction was equilibrated for 15 min. A UV/vis spectrum was recorded and the potential was again reduced. The redox reactions were followed by the absorbance changes of the Soret band at 410 nm. For accurate measurements of the reduction and oxidation, mediator mixtures were added (concentration 0.1 mM). For the reduction mixture of 1,2-naphthoquinone, phenazine ethosulfate, 1,4-benzoquinone, duroquinone, 2-hydroxy-1,4-naphthoquinone was employed. The oxidation was measured starting from the reduced state (-350 mV) to +150 mV with the following redox mediators: 1,2-naphthoquinone, phenazine ethosulfate, 1,4-benzoquinone, duroquinone, methylene blue, 5,5,7-indigo trisulfonate, phenazine and anthra-quinone-1,5-disulfonate. The obtained data points were fitted to the Nernst equation.

### 2.4.22 Resonance Raman spectroscopy

Resonance Raman (RR) spectroscopy was conducted in cooperation with Christine J. Querebillo and Peter Hildebrandt (Biophysical chemistry group, TU Berlin). It was performed using a Kr<sup>+</sup> laser at a 413 nm excitation wavelength (Coherent Innova 300c) coupled to a confocal Raman spectrometer (Jobin-Yvon, LabRam 800 HR) with a back-illuminated CCD detector cooled by liquid N<sub>2</sub>. The light was focused on the sample using a Nikon 20× objective (NA = 0.35, WD = 20 mm) at a ~2.0 mW laser power. The spectral resolution was ~1.2 cm<sup>-1</sup>. The typical total accumulation time was in the range of 0.5–1 h. Prior to measurements, samples were chemically oxidized or reduced using sodium peroxodisulfate (Sigma-Aldrich, ≥99%) or NaDT (Fluka, ≥82 RT), respectively. Reduction was performed in a box purged with argon or in an anaerobic glovebox. These samples were then flash frozen using liquid N<sub>2</sub>. All RR measurements presented here were carried out at -120 °C in a cryostat (Linkam Scientific Instruments, Surrey, U.K.) mounted on an XY stage (OWIS GmbH, Germany). The samples were continuously moved through the laser beam to reduce unwanted laser-induced photochemical processes. Spectra were calibrated with respect to mercury lines and the Raman spectrum of toluene. A polynomial function was used for the background subtraction of the spectra. Band fitting and component analysis were carried out according to the procedure described elsewhere [85].

### 2.4.23 Determination of disulfide bonds

The number of disulfide bonds can be determined by comparing the number of free thiols in the unfolded protein before and after reduction. This can be done by the colorimetric Ellmann's assay using 5,5'-dithionitrobenzoic acid (DTNB). DTNB reacts with free thiols and the yellow product nitrothiobenzoate (NTB) can be measured using a UV/vis spectrophotometer. 20 μM of protein was diluted in 6 M guanidinium chloride (GdmCl), 0.1 M phosphate buffer (pH 7.3) and 1 mM EDTA. A reference sample was mixed without the protein. The sample was blanked in UV/vis photometer. For each millilitre of sample 50 μl of 3 mM

DTNB (in 0.1 M phosphate buffer, pH 7.3) was added to the cuvette to start the reaction. The absorbance was measured at 412 nm for 10 min at 20 °C with constant mixing. After the absorbance stopped increasing, the measured absorbance of the reference was substituted from the protein sample absorbance. The reduction reaction was conducted inside an anaerobic chamber. 30 mM freshly made DTT was added to 20  $\mu$ M protein in 6 M GdmCl and 0.1 M Tris-HCl (pH 8.0) and incubated at RT for 20 min. After reduction the reducing agent was removed by using a Sephadex<sup>TM</sup> G-25 column (GE Healthcare). The column was equilibrated with 6 M GdmCl in 3 M sodium-acetate (pH 5) to avoid air oxidation after transferring the sample out of the anaerobic chamber. The reaction was started and measured as described before. The molar concentration of thiols present can be calculated from the molar absorbance of the NTB anion with  $\epsilon_{412}$  13,700/M cm.



# 3 Results Part 1 - Improved method for heme protein production in *Escherichia coli*

## 3.1 Introduction

In order to analyze heme proteins, several different methods are available for their production in *E. coli*. The most common used method is to produce the protein in a common lab strain (e.g. BL21(DE3)) and to add hemin to the cell-free lysate before protein purification [21, 91]. By this method, the heme cofactor is reconstituted (Hrc) into the completely folded protein what often results in non-native heme coordination and therefore, influences the biological function [144, 150]. Due to this reason different methods were established for heme incorporation during protein production. One method is the addition of  $\delta$ -amino levulinic acid ( $\delta$ -ALA) to the growth medium. The synthesis of  $\delta$ -ALA is the rate-limiting step during *E. coli*'s heme biosynthesis [159]. Therefore, addition of  $\delta$ -ALA increases the rate of *E. coli*'s heme biosynthesis itself. However,  $\delta$ -ALA is needed in large amounts, making it to a cost expensive method. In order to avoid using  $\delta$ -ALA one approach would be to add hemin to the growth medium, but common lab strains are not able to take up heme. Thus, another method is the heme protein expression (HPEX) system which coexpresses the heme receptor gene *chuA* [150]. Using the plasmid pHPEX-3, the heme receptor ChuA is coproduced in *E. coli* enabling it to take up heme from the growth medium. An disadvantage of this method is the use of an additional plasmid within *E. coli*, limiting the choice of selection markers for protein production. A second plasmid can also have an impact on the growth behaviour and yield of protein. During this work a new method for heme protein production was established using the non-pathogenic *E. coli* strain Nissle 1917 (O6:K5:H1) (EcN). This strain was isolated in 1917 from Alfred Nissle from faeces of a soldier who did not suffer on diarrhoe like his comrades [104]. Today EcN is used as a probiotic (Mutaflor<sup>®</sup>) against various diseases and dysfunctions of the intestinal tract [83, 137]. Interestingly, the genome of EcN encodes for the heme receptor ChuA [43]. Due to this, the strain was tested whether it can be used for protein production and heme incorporation during protein production.

The result and discussion chapter 3.3 with exception of Ch. 3.3.6 was published in *Biochemistry* by Fiege *et al.* (2018) [30]. The RR spectroscopy measurements were conducted by Christine J. Querebillo and Peter Hildebrandt (TU Berlin). In addition, they have written the result part about RR spectroscopy in chapters 3.3.3 and 3.3.4.

## 3.2 Used plasmids and oligonucleotides

The following tables contain all vectors for the expression of the different genes and construction of an EcN-T7 strain. Furthermore, they contain all oligonucleotides used for the construction of expression vectors and cloning.

**Table 3.1** Used plasmids

No.	Vector	Characteristics	Reference
1	pHPEX-3	contains <i>chuA</i> for heme receptor	[150]
2	pYPRUB311-1	source of Kan <sup>r</sup> resistance cassette	B. Masepohl
3	pHPEX-3-Kan	Kan <sup>r</sup> inserted in EcoRI	this study/ [30]
4	pASK-IBA3	expression vector, Amp <sup>r</sup>	IBA GmbH
5	pASK- <i>msmS</i>	<i>msmS</i> inserted into (4)	[95]
6	pASK- <i>msmS</i> -sGAF2	<i>msmS_sGAF2</i> inserted into (4)	[95]
7	pASK-2815(H-NOX)	<i>D. shibae</i> orf2815 inserted into (4)	master thesis, F. Olbrisch
8	pAHP4	<i>P. aeruginosa</i> <i>phuS</i> inserted in 2nd MCS of pACYCDuet1, N-terminal His <sub>6</sub> tag	lab collection
9	pASK- <i>katG</i>	<i>E. coli</i> <i>katG</i> inserted into (4)	this study/ [30]
10	pYPRUB168	backbone plasmid for blunt-end cloning of T7-FRT-Kan integration cassette	B. Masepohl
11	pUC-T7-FRT-Kan	containing T7-FRT-Kan integration cassette, Amp <sup>r</sup>	this study
12	pKD13	template plasmid for FRT-sites flanking a <i>kan<sup>r</sup></i> cassette	[22]
13	pKD46	<i>P<sub>araB</sub></i> $\gamma$ $\beta$ <i>exo</i> (red recombinase), Amp <sup>r</sup>	[22]

**Table 3.2** Used oligonucleotides

Primer	Sequence (5'-3')
<i>katG</i> -BsaI-fwd	ATGGTAGG <u>TCTCAAATGAGCACGTCAGACGATATCC</u>
<i>katG</i> -BsaI-rev	ATGGTAGG <u>TCTCAGCGCTCAGCAGGTCGAAACGG</u>
Kan-SalI-fwd	GGATCCG <u>TTCGACCTGCAGTTCGAAGTTCCTAT</u>
Kan-SbfI-rev	GATCCCCT <u>GTCAGGGGCATCAAATAAAACGAAAG</u>
T7-SalI-rev	GCTAGT <u>CGACTTACGCGAACGCGAAGTCCG</u>
lacOp-T7-fwd	AATGTGTGGAATTGTGAGCGGATAACAATTTACTAACTGG AAGAGGCACTA
lacUV5-T7-fwd	CCAGGCTTTACTACTTTATGCTTCCGGCTCGTATAATGTGTG GAATTGTGAGCGG
T7-mal-fwd	AAGGTAAACTGGTAATCTGGATTAACGGCGATAAAGGCTATAAC GGTCTCGCTGCCAGGCTTTACTACTTTATGCTTCCGGCTCG
T7-mal-rev	GATCGGTAATGCAGACATCACGGCAGCGGCGGCAAAGTCACCC CACAGGTAGTTTIGCGATTGTGTAGGCTGGAGCTGCTTCGAAG

The restriction sites are underlined.

### 3.3 Results and Discussion

In order to test whether EcN can serve as a production host for recombinant heme proteins, the model protein MsmS\_sGAF2 of *M. acetivorans* was employed in test expression experiments. EcN harboring plasmid pASK-*msmS*-sGAF2 and heme in the growth medium was compared to the two other existing methods employing BL21(DE3) (heme reconstitution before purification) and BL21(DE3) pHPEX3-Kan (termed HPEX system hereafter, heme in growth medium) harboring the same expression plasmid. Interestingly, expression cultures of EcN exhibited a higher growth rate resulting in a higher final OD<sub>578</sub> after the same incubation time compared to the other two systems (data not shown). Consequently, gene expression in EcN cultures was induced at a higher OD<sub>578</sub> of 1.2 to yield a larger cell mass. The total amount of protein produced by the three methods was evaluated by a simple comparison. For each method, an identical aliquot of affinity purified MsmS\_sGAF2 from a 1 L bacterial culture was loaded onto a SDS-PAGE gel. As already expected from the obtained fresh cell weight, the largest amount of protein was produced in EcN and the smallest from the HPEX system (Fig. 3.1 A) [150]. Quantification revealed that EcN yielded 9.41 mg of MsmS\_sGAF2/L bacterial culture compared to 1.92 and 5.16 mg from HPEX and BL21(DE3), respectively.

#### 3.3.1 Protein heme saturation by *E. coli* strain Nissle 1917

Since EcN was shown to produce large amounts of recombinant protein, we next tested the efficiency of heme incorporation into the recombinant protein. Therefore, MsmS\_sGAF2 was produced in EcN with the addition of heme to the culture medium, to the cell-free lysate (heme reconstitution), or to both culture and lysate. The results were compared to protein production without additional heme. Heme saturation was quantified using the  $R_Z$  value representing the ratio between the Soret band and  $A_{280}$ . Previous heme titration experiments resulted in a ~10% heme saturation of MsmS\_sGAF2 when produced in BL21(DE3) without additional heme ( $R_Z = 0.19$ ). The  $R_Z$  value for heme reconstitution (BL21(DE3)) was set to 100% as an excess of heme was used ( $R_Z = 1.74$ ) [95]. Production of MsmS\_sGAF2 in EcN with heme addition only to the growth culture ( $R_Z = 1.30$ ) or in excess to the cell-free lysate ( $R_Z = 1.38$ ) resulted in no significant differences (Tab. 3.3). This demonstrates that the heme addition to the growth medium alone is sufficient for high heme saturation of MsmS\_sGAF2. The values obtained for EcN with heme in the culture medium are comparable to those of the HPEX system (Tab. 3.3). Although additional heme reconstitution resulted in an even higher  $R_Z$  value of 1.61 (Tab. 3.3), we refrained from this additional heme incorporation as this might be the cause for the observed heterogeneity of the sample (see below). For future studies, we therefore decided to add heme only to the growth medium as this might represent the most natural heme reconstitution system. Furthermore, we were able to show that EcN is able to incorporate more than twice the amount of heme in comparison to BL21(DE3)

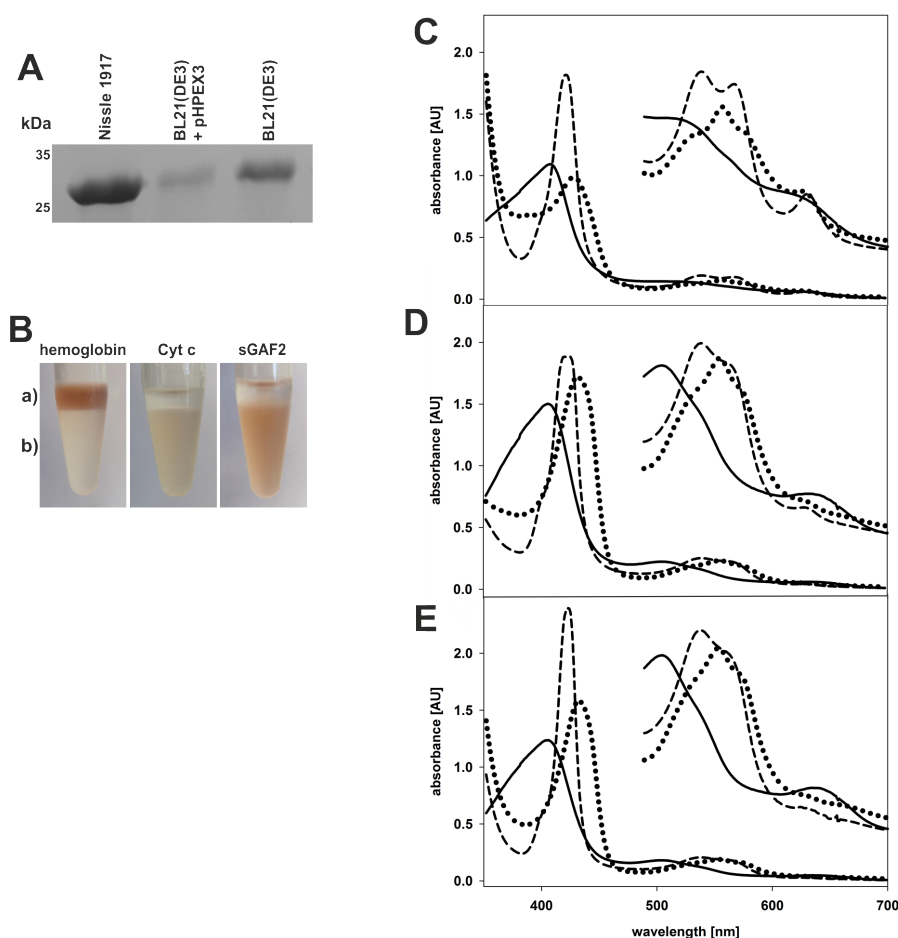


**Figure 3.1 MsmS\_sGAF2 produced by three different heme incorporation methods.** MsmS\_sGAF2 produced by three different heme incorporation methods. **(A)** SDS-PAGE of MsmS\_sGAF2 yield obtained by different methods from the same culture volume. **(B)** Acidified butanone extraction of MsmS\_sGAF2 produced in EcN: (a) organic phase with non-covalently bound heme cofactor and (b) aqueous phase with covalently bound heme cofactor. **(C)** UV/vis spectroscopy of MsmS\_sGAF2 from *E. coli* BL21(DE3) with heme reconstitution. **(D)** *E. coli* BL21(DE3) with coexpression of the *chuA* encoding plasmid pHPEX3-Kan and **(E)** EcN with heme addition to the growth medium. The ferric form of the heme iron (solid line) is shown, as indicated by the ferrous form (dotted line) and the complex of the ferrous form with CO (dashed line) [30].

in the absence of any additional heme ( $R_Z = 0.42$ ). We have previously reported that the heme cofactor is covalently bound to MsmS\_sGAF2 via a single cysteine residue (Cys656) [95]. To test whether the use of EcN has an impact on covalent heme incorporation, the purified protein was treated with acidified butanone to extract the cofactor. The brownish color of the heme cofactor was observed in the aqueous phase, indicating that the heme cofactor is covalently bound to MsmS\_sGAF2 (Fig. 3.1 B).

**Table 3.3** Quantification of heme incorporation into MsmS\_sGAF2

	<b>purity value <math>R_Z</math></b> <b>(<math>A_{\text{Soretband}}/A_{280}</math>)</b>	<b>heme content</b>
BL21(DE3), without heme	0.19	10%
BL21(DE3), heme reconstitution	1.74	100%
HPEX, heme in culture	1.36	48%
EcN, without heme	0.42	23%
EcN, heme in culture	1.30	74%
EcN, heme reconstitution	1.38	79%
EcN, heme in culture and reconstitution	1.61	92%

### 3.3.2 UV/vis spectroscopy of MsmS\_sGAF2 produced with different heme incorporation methods

To determine whether the new method of employing EcN has any effect on the heme coordination, we characterized the purified protein using UV/vis spectroscopy. Purification of MsmS\_sGAF2 employing all three heme incorporation methods yielded protein with typical heme spectra (Fig. 3.1 C–E). The heme iron of the three samples was present in its ferric (Fe(III)) state and could be reduced by DTH. In all three MsmS\_sGAF2 samples, the Soret band for the Fe(III) was observed between 406 and 408 nm (Tab. 3.4). Addition of DTH led to the reduction of the heme iron indicated by a shift of the Soret band to longer wavelengths (428–432 nm). The ferrous form of all three samples displayed an additional peak in the visible region at 555 nm with more or less pronounced shoulders at shorter and longer wavelengths (Fig. 3.1 C–E, Tab. 3.4). The spectrum of the Fe(II) form of MsmS\_sGAF2 isolated from BL21(DE3) further showed a charge transfer band at 625 nm. Incubation of the Fe(II) complex with CO led to a shift of the Soret band to 421 and 423 nm (Tab. 3.4). In addition, in the Q-band region, significant changes were noticeable. While the reconstituted protein displayed two strong  $\beta/\alpha$ -bands in the Q-region, MsmS\_sGAF2 from the other two systems showed only a distinct  $\beta$ -band and a shoulder in the  $\alpha$ -band region. Although only minor differences were seen in the UV/vis spectra, we wished to explore whether incorporation of heme by these methods had an influence on the previously reported heterogeneity of the samples in terms of coordination state. Therefore, resonance Raman (RR) spectroscopy was employed to compare the protein produced by EcN to that reconstituted from BL21(DE3).

**Table 3.4** Heme absorption maxima (in nm) of recombinant MsmS\_sGAF2 produced by three different methods

<b>method</b>	<b>Fe(III)</b>		<b>Fe(II)</b>			<b>Fe(II)-CO</b>			
	Soret		Soret			Soret	$\beta$	$\alpha$	
BL21(DE3), heme reconstitution	408	-	428	555	625	421	538	567	631
HPEX, heme in culture	406	504	432	555	-	423	538	(565)	(631)
EcN, heme in culture	407	504	432	555	-	423	539	(562)	629

### 3.3.3 Resonance Raman spectroscopy of MsmS\_sGAF2 produced by different methods

Unlike a previous study using Q-band excitation [95], the present experiments were carried out in resonance with the Soret band (413 nm excitation) to predominantly enhance the totally symmetric modes that are the most sensitive spectral markers for the spin and ligation state ( $\nu_3$ ) and for the electron density distribution in the heme ( $\nu_4$ ) (Fig. 3.2). The latter mode is therefore redox state dependent and typically observed at  $\sim 1360$  and  $1373\text{ cm}^{-1}$  for ferrous and ferric iron porphyrins, respectively. RR spectra of MsmS\_sGAF2 produced in BL21(DE3) demonstrate a mixture between a high-spin (HS) and 6-coordinated lowspin (6cLS) species in both oxidation states, consistent with previous RR and MCD (magnetic circular dichroism) spectroscopic results [95]. In the ferrous form (Fig. 3.2, left panel, red traces), the spectra display distinct doublets of these modes with the low-frequency and high-frequency components corresponding to a HS and 6cLS configuration, respectively. For the  $\nu_4$  mode, the frequency difference between both components of  $11\text{ cm}^{-1}$  cannot be exclusively attributed to the different spin and ligation states. Instead, the unusual low frequency of the HS species of  $1352\text{ cm}^{-1}$  points to an increased electron density in the antibonding orbitals of the heme. This effect is expected when the axial His ligand serves as a hydrogen bond donor such that excess electron density is transferred to the heme [136]. In the ferric state, the coexistence of HS and 6cLS species is clearly reflected by the  $\nu_3$  modes (Fig. 3.2, right panel, red trace), which comprise the prevailing 6cLS ( $\nu_3$  at  $1508\text{ cm}^{-1}$ ) and 5-coordinated HS species (5cHS,  $\nu_3$  at  $1493\text{ cm}^{-1}$ ), as well as a smaller contribution of a 6-coordinated HS form ( $\nu_3$  at  $1479\text{ cm}^{-1}$ ). In the ferric state, the  $\nu_4$  mode frequency is not very sensitive to changes in the spin and ligation states, and thus, the respective frequencies of both configurations overlap to afford a peak position at  $1373\text{ cm}^{-1}$ . MsmS\_sGAF2 reconstituted after production in BL21(DE3) displays a higher RR intensity but does not affect the distribution among the various spin and ligation states in the ferric state. This is in contrast to the ferrous state, for which we note an increased 6cLS contribution at the expense of the HS form upon addition of heme (Fig. 3.2, solid red line, left) compared to that of the preparation restricted to the natural heme incorporation (dotted red line). Addition of heme to the growth medium in the EcN MsmS\_sGAF2 preparations has a distinctly smaller effect on the distribution among the various heme configurations (Fig. 3.2, blue traces), which highlights that EcN can produce enough heme so that additional heme has no significant influence on the ligation and spin state distribution and is not necessary for these purposes. Naturally though, similar to the BL21(DE3) preparation, addition of heme increased the amount of heme incorporation as reflected by the higher RR intensities, further confirming the results in Table 3.3. To summarize these findings, the ferric form of the BL21(DE3) preparation favors the 6cLS configuration over the HS species compared to EcN, regardless of further heme addition to the cell lysate. In the ferrous form, however, heme addition increases the amount of HS but only for BL21(DE3), whereas in the absence of additional heme both pre-

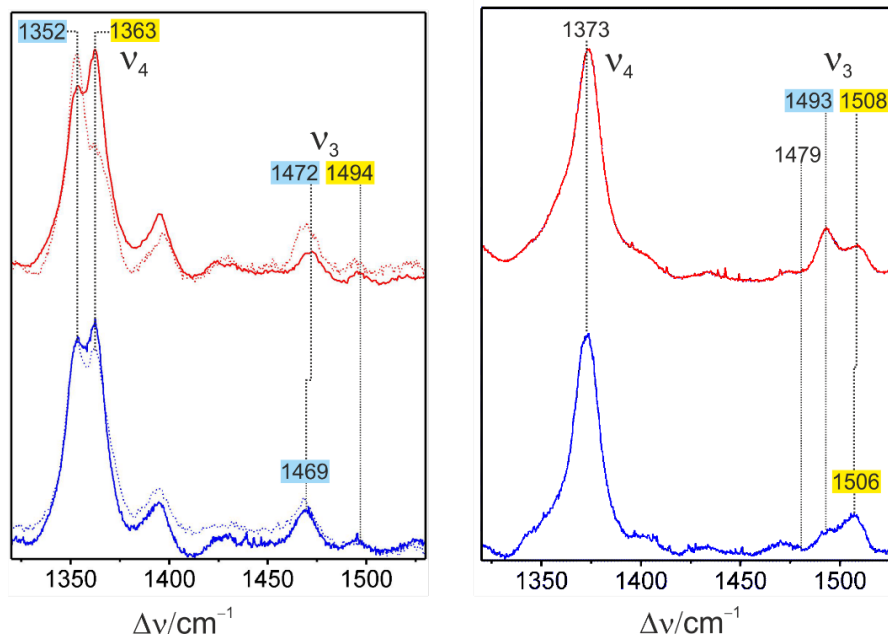


**Figure 3.2** RR spectra of ferrous (left panel) and ferric MsmS\_sGAF2 (right panel) obtained from *E. coli* BL21(DE3) (top, red traces) and EcN (bottom, blue traces) grown and purified under aerobic conditions. The solid and dotted traces refer to the samples with and without heme added to the lysate (i.e. reconstitution, only BL21(DE3) or growth culture (EcN only)), respectively. Unlike to the ferrous form, heme addition had no effect on the spin- and ligations state distribution of the ferric state such that here only the spectra from preparations with additional heme are shown. The bands of the HS and LS configurations are highlighted in blue and yellow, respectively [30]. (RR spectra performed by Christine J. Querebillo and Peter Hildebrandt (Biophysical chemistry group, TU Berlin))

parations give rise to similar spin state distributions. Next we studied the effect of oxygen during growth and purification of MsmS\_sGAF2 from EcN (in each case heme was added to the culture medium) (Fig. 3.3). Aerobic growth and purification affords a spin and ligation state distribution similar to that of anaerobic growth and aerobic purification with the 6cLS and 5cHS species being particularly strong in the ferrous and ferric states, respectively (Fig. 3.2 and 3.3). The situation is reversed if, regardless of the growth conditions, purification is carried out anaerobically (Fig. 3.3). Then, the HS species is the prevailing form in the ferrous state, whereas in the ferric state the 6cLS configuration represents the major fraction.

### 3.3.4 Production of MsmS from Nissle 1917, Resonance Raman, and autophosphorylation activity

Finally, we tested whether full-length MsmS can also be produced as a functional protein in EcN. Interestingly, during these experiments we observed that EcN produced enough heme itself and that there was no need to supply heme to the growth medium for spin and ligation state distribution studies (see also RR spectra shown in Figure 3.3, dotted blue trace). Subsequent spectroscopic analysis of the purified protein revealed a Soret band at 412 nm for the ferric form and a shift to 430 nm for the ferrous form. The Fe(II) complex showed

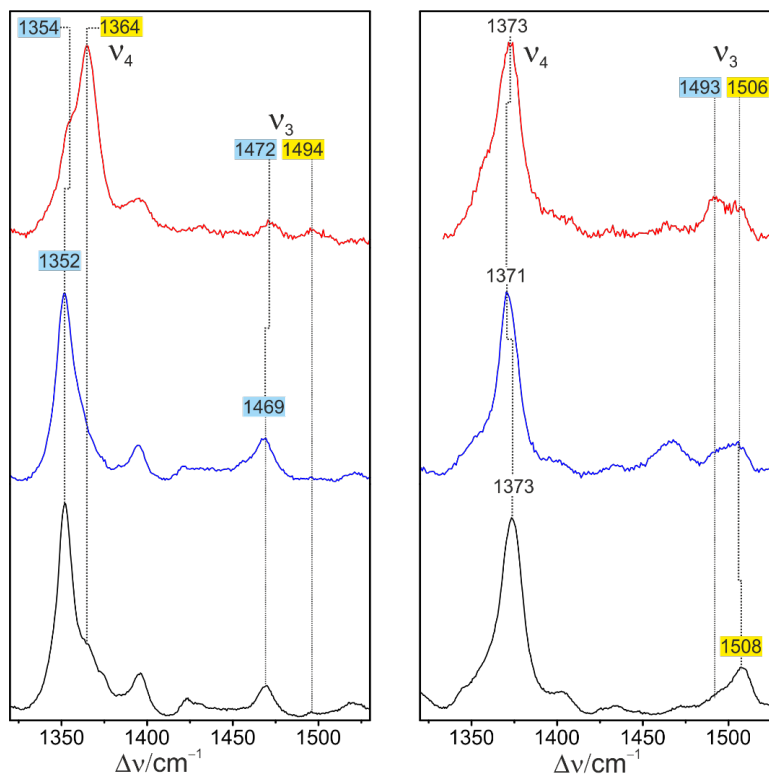


**Figure 3.3 RR spectra of ferrous (left panel) and ferric MsmS\_sGAF2 (right panel) obtained from EcN under different conditions.** Top (red traces), grown anaerobically but purified aerobically; middle (blue traces), grown aerobically but purified anaerobically; bottom (black traces), grown and purified anaerobically. The bands of the HS and LS configurations are highlighted in blue and yellow, respectively [30]. (RR spectra performed by Christine J. Querebillo and Peter Hildebrandt (Biophysical chemistry group, TU Berlin))

two  $\beta/\alpha$ -bands in the Q-region (536 and 562 nm), indicating a 6-fold heme iron coordination. Incubation of the Fe(II) complex with CO gas led to the formation of a Fe(II)–CO complex with a Soret band at 424 nm and two slight peaks in the Q-band region (536 and 556 nm) (Fig. 3.4 A). Hence, the distal ligand was likely changed to CO. It is now interesting to compare the RR spectra of the full-length protein (Fig. 3.5) to those of the MsmS\_sGAF2 produced from EcN (Fig. 3.2, blue traces). In the ferric state, the spin and ligation state distributions of the full-length preparation (Fig. 3.5, blue trace) and the MsmS\_sGAF2 preparations (Fig. 3.2, left panel, blue trace) are essentially the same, with the 6cLS configuration as the prevailing species. In the ferrous state (Fig. 3.5, red trace), the HS species represents the prevailing species. We also note that the distributions for the full-length protein are very similar to those observed for the anaerobically purified MsmS\_sGAF2 samples (Fig. 3.3, black traces), which are dominated by the HS species in the ferrous state. This may indicate that the native state is HS in the ferrous state as observed for the anaerobically purified truncated and the full-length preparations, which are close to the conditions of protein synthesis in the organism, if we consider *M. acetivorans* as an anaerobic Archaeon [76].



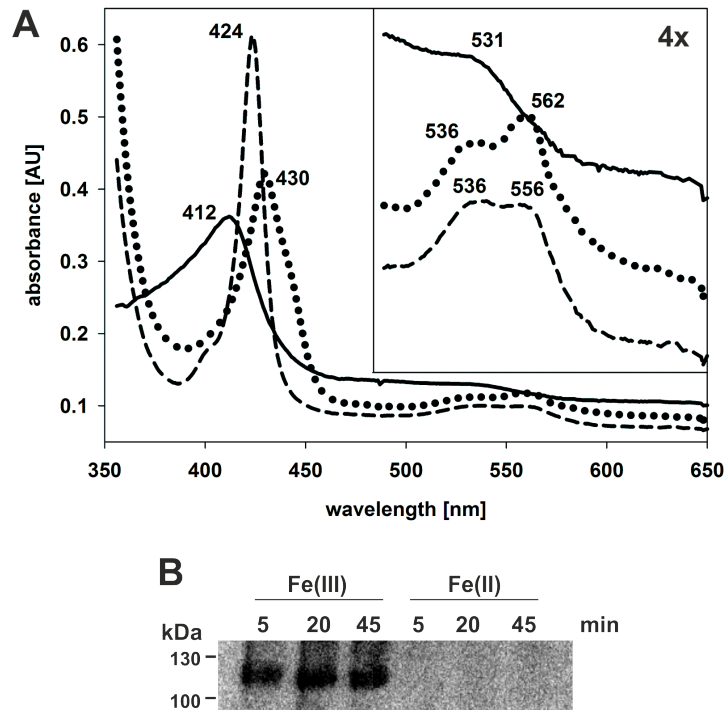


**Figure 3.4 UV/vis spectrum and kinase assay of MsmS. (A)** UV/vis spectrum of MsmS full-length protein produced in EcN without additional heme: ferric heme iron (solid line), ferrous heme iron (dotted line), and complex of the ferrous heme iron with CO (dashed line). The box in the right corner shows a 4× enlargement of the wavelength region from 490 to 650 nm. **(B)** Radio-labeled kinase assay of oxidized Fe(III) and reduced Fe(II) state of MsmS. Samples were taken after different time points [30].

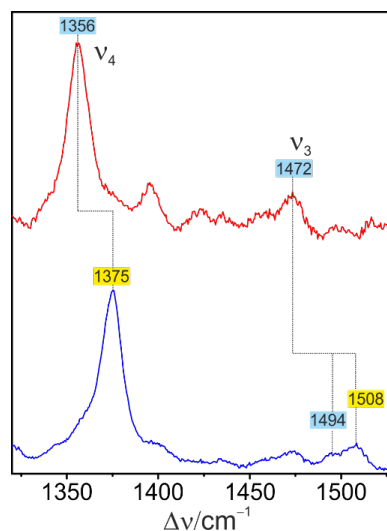


**Figure 3.5 RR spectra of ferrous (top, red trace) and ferric (bottom, blue trace) full-length MsmS obtained from EcN under aerobic conditions (without any additional heme supplement).** The bands of the HS and LS configurations are highlighted in blue and yellow, respectively [30]. (RR spectra performed by Christine J. Querebillo and Peter Hildebrandt (Biophysical chemistry group, TU Berlin))

The considerable extent of LS in the ferrous state obtained from BL21(DE3) and EcN purified aerobically (Fig. 3.2) may possibly mean that such preparations include a fraction of misfolded protein that gives rise to a LS state in the ferrous form. *M. acetivorans* is a strictly anaerobic Archaeon [32, 76, 139]; therefore, we are inclined to consider that the full-length and anaerobic purifications from EcN are the most closely related to its natural conditions. From the RR in both cases, the HS state prevails for the ferrous state and the LS for the ferric state. These states are therefore considered to be the native configurations of MsmS. Autophosphorylation assays with MsmS full-length protein from EcN confirmed earlier results employing *E. coli* BL21(DE3) as a host strain. Phosphorylation was observed only for the ferric form but not for the ferrous complex (Fig. 3.4 B). Hence, MsmS produced in EcN displays full activity as described previously [95].

### 3.3.5 *E. coli* Nissle 1917 is a general suitable host for the expression of heme proteins

The results of employing MsmS\_sGAF2 and full-length MsmS suggest that EcN is a suitable host for the production of heme proteins. To test whether EcN is generally applicable to other heme proteins, three other heme proteins were tested: a heme/nitric oxide/oxygen-binding (H-NOX) protein from *Dinoroseobacter shibae*, the cytoplasmic heme-binding protein PhuS from *Pseudomonas aeruginosa*, and the catalase-peroxidase KatG from *E. coli*. H-NOX domains function as sensors for gaseous signaling molecules such as nitric oxide (NO) or oxygen in eukaryotes and bacteria [116]. The UV/vis spectrum of the H-NOX protein produced in EcN with heme in the growth medium displayed a typical heme UV/vis spectrum. The Soret band for the ferric state was observed at 416 nm, with a second peak at 538 nm (Fig. 3.6 A). The Fe(III) complex of the H-NOX protein can be reduced to Fe(II) by DTH, and the Soret band can thus be shifted to 426 nm. In the visible region two maxima at 531 and 559 nm were obtained, indicating a 6-coordinated heme complex. After addition of NO to the Fe(II) complex, the Soret band shifted to 398 nm, which signifies the binding of NO to the heme iron typical for H-NOX proteins. No clear maxima were observed in the visible region for the Fe(II)–NO complex (Fig. 3.6 A). The spectroscopic behavior of the H-NOX protein from *D. shibae* is comparable with the UV/vis spectrum observed for the H-NOX protein from *Shewanella oneidensis* [122]. PhuS is encoded in the *phu* (*Pseudomonas* heme uptake) operon in *P. aeruginosa* and is responsible for the transfer of heme to the heme oxygenase *pa*-HO [105]. PhuS was produced in EcN with addition of heme to the growth medium. The UV/vis spectrum revealed a Soret band at 413 nm for the ferric state. In the visible region a maximum at 539 nm was observed. Reduction with DTH led to a shift of the Soret band to 424 nm for the ferrous state and a maximum at 555 nm in the Q-band region (Fig. 3.6 B). This spectrum is similar to former UV/vis measurements of PhuS produced in BL21(DE3)*plysS* cells with heme reconstitution but depicts shifts of the peaks (410, 545, and 570 nm for the

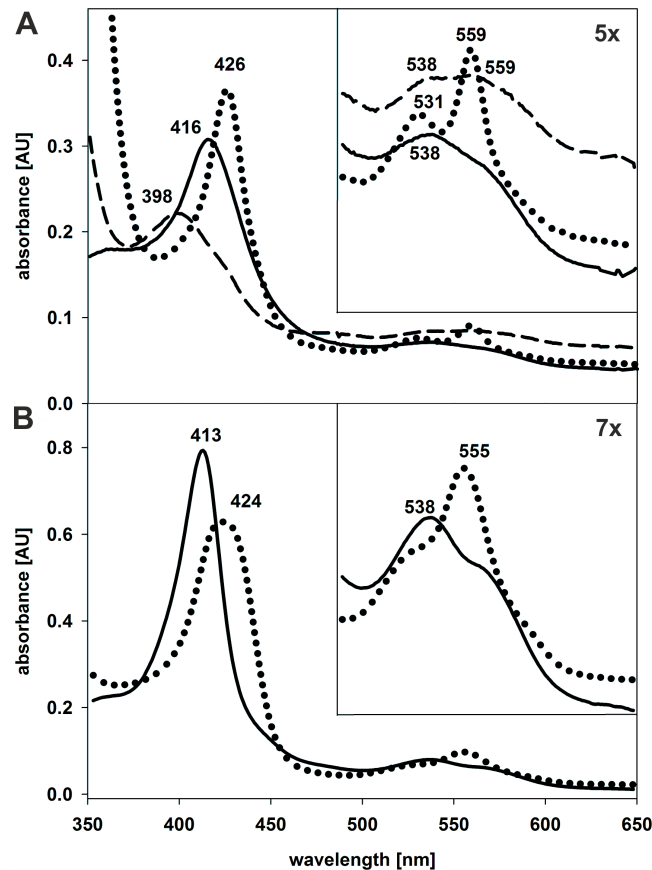


**Figure 3.6** UV/vis spectra of an H-NOX protein from *D. shibae* and PhuS from *P. aeruginosa*. Produced in EcN with 10  $\mu\text{M}$  heme in growth medium: (A) H-NOX protein and (B) PhuS. The ferric form of the heme iron (solid line), the ferrous form (dotted line), and the complex of the ferrous form with NO (dashed line) for the H-NOX protein are included. The boxes in the right corners show enlargements of the wavelength region from 490 to 650 nm [30].

ferric state and 428 and 559 nm for the ferrous form) [73]. Finally, the catalase-peroxidase KatG from *E. coli* was used to confirm that the strain EcN is a useful host. A UV/vis spectrum of purified KatG produced in EcN with addition of heme to the growth medium exhibited a Soret band for the Fe(III) state at 408 nm. In the visible region a second peak at 632 nm was obtained. Reduction with DTH resulted in a shift of the Soret band to a longer wavelength (441 nm) and a second maximum at 560 nm with a shoulder at 590 nm (Fig. 3.7 A). The successful heme incorporation in KatG from EcN is shown in Figure 7B with overlaid UV/vis spectra of KatG obtained from heme reconstitution and EcN (Fig. 3.7 B). In addition to this spectroscopic characterization, we also tested the activity of the produced KatG. To analyze the catalase activity of the purified KatG, the decomposition of  $\text{H}_2\text{O}_2$  was followed via UV/vis spectroscopy. KatG from EcN resulted in a decrease of  $\text{H}_2\text{O}_2$  absorbance measured at 220 nm within 5 min of reaction time. The same result was observed for KatG from BL21(DE3) after heme reconstitution (Fig. 3.7 C). Forms of KatG purified with both methods do not have a significant difference in their activity.

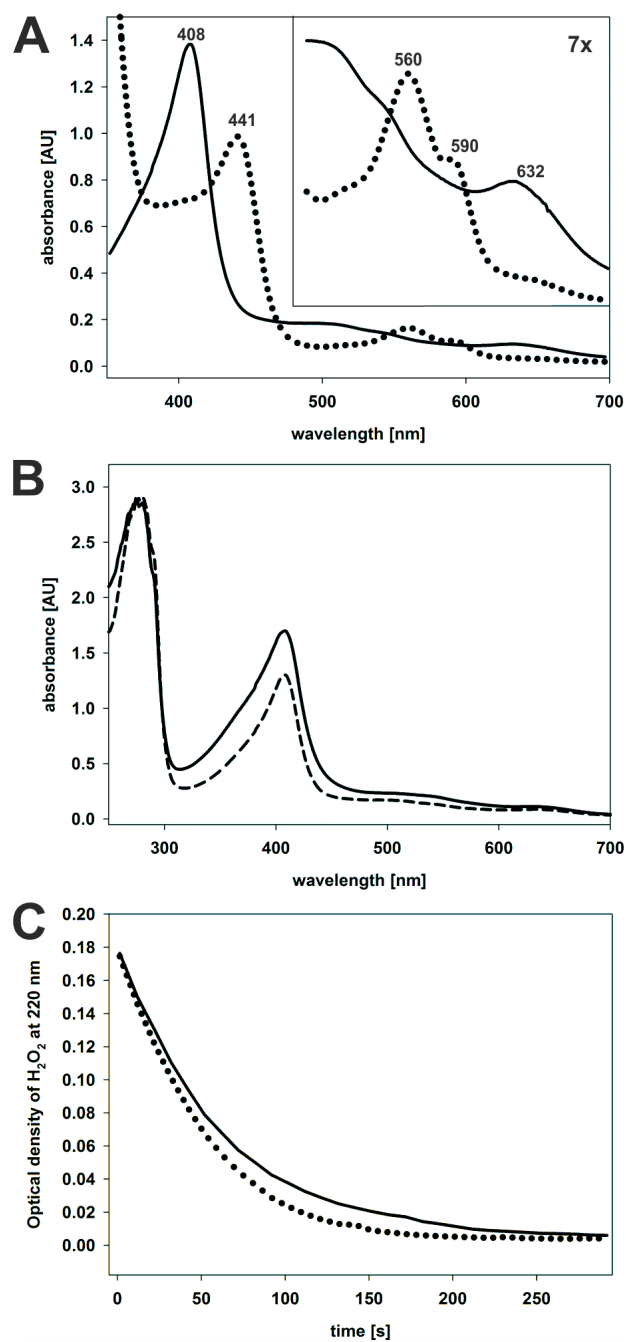


**Figure 3.7 UV/vis spectra and activity of KatG.** (A) UV/vis spectrum of KatG produced in EcN with a 10  $\mu\text{M}$  heme addition to the growth medium: ferric heme iron (solid line) and ferrous heme iron (dotted line). The box in the right corner shows a 7x enlargement of the wavelength region from 490 to 700 nm. (B) Comparison of heme incorporation into KatG produced in BL21(DE3) (solid line) and EcN (dashed line). (C) Catalase activity comparison by  $\text{H}_2\text{O}_2$  consumption of KatG produced in *E. coli* BL21(DE3) with heme reconstitution (solid line) and EcN (dashed line) [30].

### 3.3.6 Construction of an EcN strain for T7-RNA polymerase dependent gene expression

Protein production using the EcN strain is limited to expression systems lacking the T7 promoter. In order to use expression systems like the pET system, it was started to construct an EcN strain containing the gene for the T7-RNA polymerase. Initially, the  $\lambda$ DE3 lysogenization Kit (Novagen) was used to obtain a EcN( $\lambda$ DE3) strain but integration of  $\lambda$ DE3 prophage into EcN chromosome failed. Therefore, homologous recombination was further used for chromosomal integration. Cloning a plasmid containing the T7-RNA polymerase gene under a lacUV5 promoter (together with a kanamycin resistance cassette) with homologous sequences at the 5' and 3' end for the *malEFG* operon of EcN was finished (Plasmid map in Appendix). First recombination experiments of the fragment into the EcN chromosome resulted in kanamycin resistant clones. Unfortunately, the T7-RNA polymerase was not active in these clones due to an incorrect incorporation of the gene.

# 4 Results part 2 - The sensor kinase MsmS

## 4.1 Introduction

The sensor kinase MsmS (MA4561) from *M. acetivorans* is a multi domain protein. It consists of two alternating PAS and GAF domains and a histidine-like ATPase domain at the C-terminus (Fig. 4.1). MsmS lacks the conserved H-box, containing a histidine residue that functions as a phosphorylation site during autophosphorylation of a typical bacterial sensor histidine kinase [64, 142]. In the second GAF domain of MsmS at the cysteine residue 656 a heme cofactor is covalently bound via one of its vinyl groups [95].

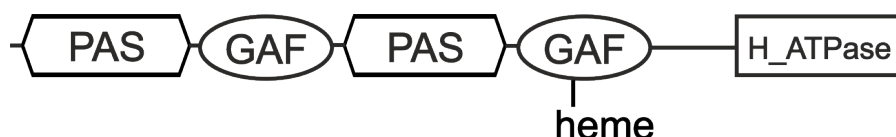


**Figure 4.1 Predicted domain structure of MsmS.** The full-length MsmS consists of two alternating PAS and GAF domains and a histidine-like ATPase (H\_ATPase) domain at the C-terminus. Predicted domains are PAS1: aa 118-293; GAF1: aa 298-470; PAS2: aa 471-585; GAF2: aa 609-761; H\_ATPase: aa 783-998. In the second GAF domain a heme cofactor is covalently bound via cysteine residue 656 [95].

A first characterization of MsmS was performed in a former study. For this, a truncated variant containing only the second GAF domain (MsmS\_sGAF2) produced with a C-terminal *His*<sub>6</sub>-tag in *E. coli* BL21(DE3) by heme reconstitution was used. Resonance Raman (RR) and magnetic circular dichroism (MCD) data of MsmS\_sGAF2 revealed a mix of 6- and 5-coordinated heme species. MCD data further suggested a histidine residue as a putative heme ligand [95]. In order to predict putative heme ligand binding sites a model structure of the second GAF domain of MsmS was generated [95]. In this model several putative ligands like histidine residues (H<sub>646</sub>, H<sub>702</sub>, H<sub>704</sub>, H<sub>708</sub>) (Fig. 4.2 A), methionine (M<sub>645</sub>), tyrosine (Y<sub>665</sub>) or lysine (K<sub>661</sub>) (Fig. 4.2 B) are located near the heme molecule. Several variants of these amino acid residues were already tested as *His*<sub>6</sub>-tag fusions in the former study [94] and histidine residue 702 was suggested to be the most likely proximal ligand. However, on the one hand it was found that imidazole, what is typically used for *His*<sub>6</sub>-tag protein purification influences the heme coordination and on the other hand heme incorporation during production complies more with the native heme coordination than heme reconstitution [30]. To further analyze the heme coordination in MsmS these variants should be revalidated by using *Strep*II-tag fusions and by using the improved method for heme protein production in *E. coli* Nissle 1917 (EcN) [30]. Furthermore, it was shown that MsmS has an autophosphory-

lation activity which is redox dependent. Due to the bound heme cofactor it was assumed that the redox-sensing is dependent on the redox state of the bound heme cofactor. 2D thin-layer chromatography and stability tests of phosphorylation suggested serine and tyrosine residues as the phosphorylation sites [95].

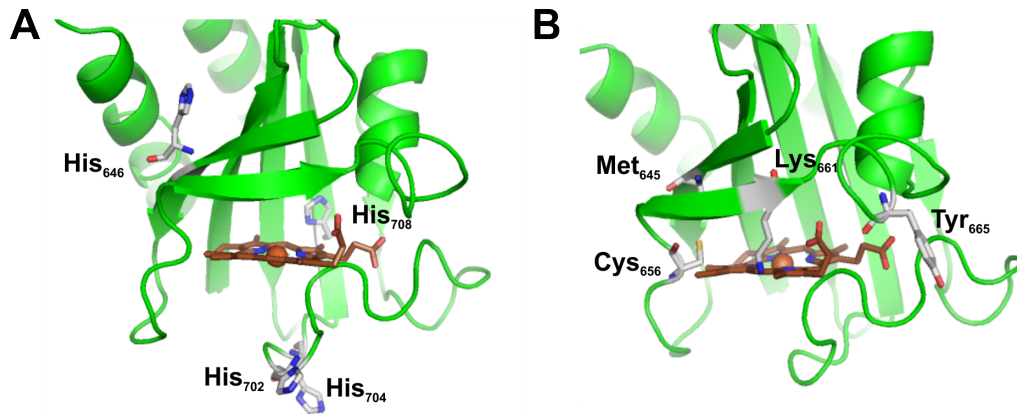


**Figure 4.2 Model of heme-binding pocket of MsmS.** A model structure of the second GAF domain was modeled to predict putative heme binding ligands [95]. **(A)** Histidine residues located close to the heme molecule, **(B)** methionine residue at the proximal, tyrosine and lysine residues at the distal site and cysteine residue for covalent binding (structure models were constructed with *PyMOL*).

## 4.2 Used plasmids and oligonucleotides

The following tables contain all vectors for the expression of the different MsmS variants and BACTH analysis. Furthermore, they contain all oligonucleotides used for the construction of expression vectors and site-directed mutagenesis.

**Table 4.1** Used expression plasmids for MsmS analysis

No.	Vector	Characteristics	Reference
1	pHPEX-3-Kan	gene for heme receptor ChuA, <i>lacUV5</i> promoter, Kan <sup>r</sup> , Tet <sup>r</sup>	[30]
2	pASK-IBA3	expression vector, C-terminal StrepII-tag, Amp <sup>r</sup>	IBA GmbH
3	pASK- <i>msmS</i>	(2) with complete coding region of <i>msmS</i>	[95]
4	pASK- <i>msmS</i> _C656A	(3) with C656→A	master thesis, C. Twittenhoff
5	pASK- <i>msmS</i> _H702G	(3) with H702→G	this study
6	pASK- <i>msmS</i> _H702G/H708G	(5) with H708→G	this study
7	pASK- <i>msmS</i> _G2P1	(2) with coding region from aa 2 to aa 804 of <i>msmS</i>	this study
8	pASK- <i>msmS</i> _G2G1	(2) with coding region from aa 298 to aa 804 of <i>msmS</i>	this study
9	pASK- <i>msmS</i> _G2P2	(2) with coding region from aa 471 to aa 804 of <i>msmS</i>	this study
10	pASK- <i>msmS</i> _GAF2	(2) with coding region from aa 580 until the end of <i>msmS</i>	lab collection
11	pASK- <i>msmS</i> _sGAF2	(2) with coding region from aa 580 to 804 of <i>msmS</i>	[95]
12	pASK- <i>msmS</i> _sGAF2_M645A	(11) with M645→A	master thesis, C. Twittenhoff
13	pASK- <i>msmS</i> _sGAF2_H646A	(11) with H646→A	master thesis, C. Twittenhoff
14	pASK- <i>msmS</i> _sGAF2_C656A	(11) with C656→A	master thesis, C. Twittenhoff
15	pASK- <i>msmS</i> _sGAF2_C656A/H702G	(14) with H702→G	this study
16	pASK- <i>msmS</i> -sGAF2_C656A/H708G	(14) with H708→G	this study
17	pASK- <i>msmS</i> _sGAF2_K661G	(11) with K661→G	this study
18	pASK- <i>msmS</i> _sGAF2_K661G/H702G	(17) with H702→A	this study
19	pASK- <i>msmS</i> _sGAF2_Y665F	(11) with Y665→A	master thesis, C. Twittenhoff
20	pASK- <i>msmS</i> _sGAF2_H702G	(11) with H702→G	master thesis,

- Continuation on next page -



21	pASK- <i>msmS</i> _sGAF2_H704A	(11) with H704→A	C. Twittenhoff master thesis, C. Twittenhoff
22	pASK- <i>msmS</i> _sGAF2_H708G	(11) with H708→G	master thesis, C. Twittenhoff
23	pASK- <i>msmS</i> _sGAF2_H702G/H708G	(20) with H708→G	master thesis, C. Twittenhoff
24	pASK- <i>msmS</i> _sGAF2_H702A/H704A	(21) with H702→A	this study

**Table 4.2** Used plasmids for MsmS BACTH analysis

No.	Vector	Characteristics	Reference
1	pUT18	C-terminal T18 fragment, Amp <sup>r</sup> , <i>lac</i> -promoter	[60]
2	pUT18C	N-terminal T18 fragment, Amp <sup>r</sup> , <i>lac</i> -promoter	[61]
3	pKT25	N-terminal T25 fragment, Kan <sup>r</sup> , <i>lac</i> -promoter	[61]
4	p25N	C-terminal T25 fragment, Kan <sup>r</sup> , <i>lac</i> -promoter	[62]
5	pUT18C- <i>zip</i>	coding region for leucine zipper region of GCN4 yeast protein, positive control	[60]
6	pKT25- <i>zip</i>	coding region for leucine zipper region of GCN4 yeast protein, positive control	[60]
7	pUT18- <i>msmS</i>	(1) with complete coding region of <i>msmS</i>	this study
8	pUT18C- <i>msmS</i>	(2) with complete coding region of <i>msmS</i>	this study
9	p25N- <i>msmS</i>	(4) with complete coding region of <i>msmS</i>	this study
10	pKT25- <i>msmS</i>	(3) with complete coding region of <i>msmS</i>	this study
11	pUT18C- <i>msrG</i>	(2) with complete coding region of <i>msrG</i>	this study
12	p25N- <i>msrG</i>	(4) with complete coding region of <i>msrG</i>	this study
13	pKT25- <i>msrG</i>	(3) with complete coding region of <i>msrG</i>	this study
14	p25N- <i>msrC</i>	(4) with complete coding region of <i>msrC</i>	bachelor thesis, A. Scherhag
15	p25N- <i>msrF</i>	(4) with complete coding region of <i>msrF</i>	bachelor thesis, S. Gluzins
16	pUT18- <i>msmS</i> _GAF1	(1) with coding region from aa 298 until the end of <i>msmS</i>	this study
17	pUT18- <i>msmS</i> _PAS2	(1) with coding region from aa 471 until the end of <i>msmS</i>	this study
18	pUT18- <i>msmS</i> _GAF2	(1) with coding region from aa 580 until the end of <i>msmS</i>	this study

**Table 4.3** Used oligonucleotides for MsmS analysis

No.	Primer	Sequence (5'-3')
1	<i>msmS</i> -BsaI-fwd	ATGGTAGGTCTCAAATGATAGGTGTTGACATG AAACTC
2	<i>msmSG1</i> -gb-fw	GGTCGACCTGCAGGGGGACGAGCTTATCCTGAG CCAGAATCG
3	<i>msmSP2</i> -gb-fw	GGTCGACCTGCAGGGGGACAACAGGTTTCAGGA CAATCTTTGAC
4	<i>msmSP1</i> -gb-fw	GGTCGACCTGCAGGGGGACGCATAGGTGTTGAC ATGAAACTGG
5	<i>msmSG2</i> -gb-rv	CCAAGCGCTGAGACCATGCGTCTCATAATCCAT AATTTCCCC
6	UT18- <i>msmSG1</i> -fw	GCGTATTCTAGAGATGGAGCTTATCCTGAGCC
7	UT18- <i>msmSG1</i> -rv	CGCATAGAGCTCGGCTTTGGGAGTTTCACATAA
8	UT18- <i>msmSP2</i> -fw	GCGTATTCTAGAGATGAACAGGTTTCAGGACAATC
9	UT18- <i>msmSP2</i> -rv	CGCATAGAGCTCGGCTTTGGGAGTTTCACAT
10	UT18- <i>msmSG2</i> -fw	GCGTATTCTAGAGATGATCACCGAACGTAAAA AAGC
11	UT18- <i>msmSG2</i> -rv	CGCATAGAGCTCGGCTTTGGGAGTTTCACAT
12	<i>msrG</i> -BTH-XbaI-fw	GCTCGGTCTAGAGATGAAACTGGAATTGTTGGG
13	<i>msrG</i> -BTH-KpnI-rv	GGCATAGGTACCGCGAGTCCGACGTGGTAAT
14	25- <i>msmS</i> -gb-fw	GGCGGGCTGCAGGGTCGACTATGATAGGTGTTGAC ATG
15	25- <i>msmS</i> -gb-rv	ATTCTTAGTACTTAGGTACCTTTGGGAGTTTCACATG
16	25N- <i>msmS</i> -gb-fwd	TACGGCTGCAGGGTCGACTATGATAGGTGTTGAC ATGA
17	25N- <i>msmS</i> -gb-rev	TTGAATTCGAGCTCGGTACCTTTGGGAGTTTCA CATGC

**Table 4.4** Used oligonucleotides for site-directed mutagenesis of MsmS

Primer	Sequence (5'-3')
4561-K661G-fwd	CGATTGAAGAT <u>GGGC</u> AGTTTG
4561-C656A-fwd	GGTCTGACAGTGC <u>GATGGAAGAGG</u> CTTCGATT GAAGATAAGC
4561-H708G-fwd	GTGCACCTGATCAGGGG <u>ACTGA</u> ATATCCCGGTC
4561-H702G-fwd	GGGTATCCGAAAAACGG <u>AGTGC</u> ACCTGATCAGGC
4561-H708/702G-fwd	GTATCCGAAAAACGG <u>AGTGC</u> ACCTGATCAGGGGA CTGAATATCC
4561-H702A-H704A-fwd	GGTATCCGAAAAACG <u>CTGTGG</u> CCCTGATCAG

Only the forward primers are listed, as the reverse primers are complementary to them.  
The positions where the mutations were introduced are underlined.

### 4.3 Characterization of the sensor kinase MsmS

To further analyze the heme coordination of MsmS the protein was produced in *E. coli*. The recombinant production of MsmS full-length protein resulted in a protein with good purity but a large culture volume was needed to get sufficient protein for spectroscopic analysis (Fig. 4.3 A). For a better analysis of the heme iron coordination the truncated variant MsmS\_sGAF2 was used, which can be produced with a higher yield (Fig. 4.3 B).

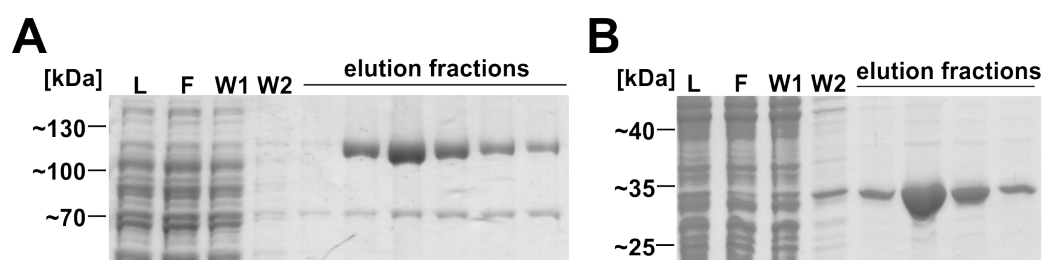


**Figure 4.3 SDS-PAGE of MsmS-*StrepII* and MsmS\_sGAF2-*StrepII* purification by affinity chromatography from EcN.** L = Lysate; F = Flow-through fraction; W1 = Washing fraction 1; W2 = Washing Fraction 2. The elution fractions contain mostly (A) MsmS-*StrepII* (MW = ~115 kDa) from 6 l and (B) MsmS\_sGAF2-*StrepII* (MW = ~27 kDa) from 2 l culture volume.

#### 4.3.1 Mutational analysis of heme binding ligands in MsmS\_sGAF2

In a former study several MsmS\_sGAF2-*His*<sub>6</sub>-tag variants were tested for their heme coordination structure. But as it was found that imidazole influences the heme iron coordination, the variants were cloned into another expression vector carrying a C-terminal *StrepII*-tag [95]. Therefore, interesting variants of MsmS\_sGAF2 of the former tested ones were also constructed carrying a C-terminal *StrepII*-tag fusion. Furthermore, new variants were constructed to further characterize the heme coordination. As it was found that the coordination is influenced by the heme incorporation method (during protein production (EcN) or by heme reconstitution (Hrc) after protein production), the variants were also produced in EcN what is more similar to how heme proteins are produced in their native organism [30]. Comparison of the two methods resulted in slight shifts of the peak maxima for the wild-type MsmS\_sGAF2 (Tab. 4.5). MsmS\_sGAF2 produced in EcN resulted in a Soret band at 407 nm. After reduction the Soret band shifted to 432 nm with a Q-band peak at 555 nm with slight shoulders, indicating a mixture of 5- and 6-coordinated heme species. Addition of CO gas led to the formation of a Fe(II)-CO complex and a sharper Soret band with a maximum at 423 nm. The  $\alpha$ - and  $\beta$ -bands are visible at 539 nm and 562 nm. The absorbance maxima of all MsmS\_sGAF2 variants are pooled in Tab. 4.5.

#### Histidine residues 702 and 708 influence heme coordination

In the vicinity of the heme cofactor four histidine residues (H<sub>646</sub>, H<sub>702</sub>, H<sub>704</sub>, H<sub>708</sub>) are located in the model structure (Fig. 4.2). Exchange of histidine residue 646 and 704 did not result in

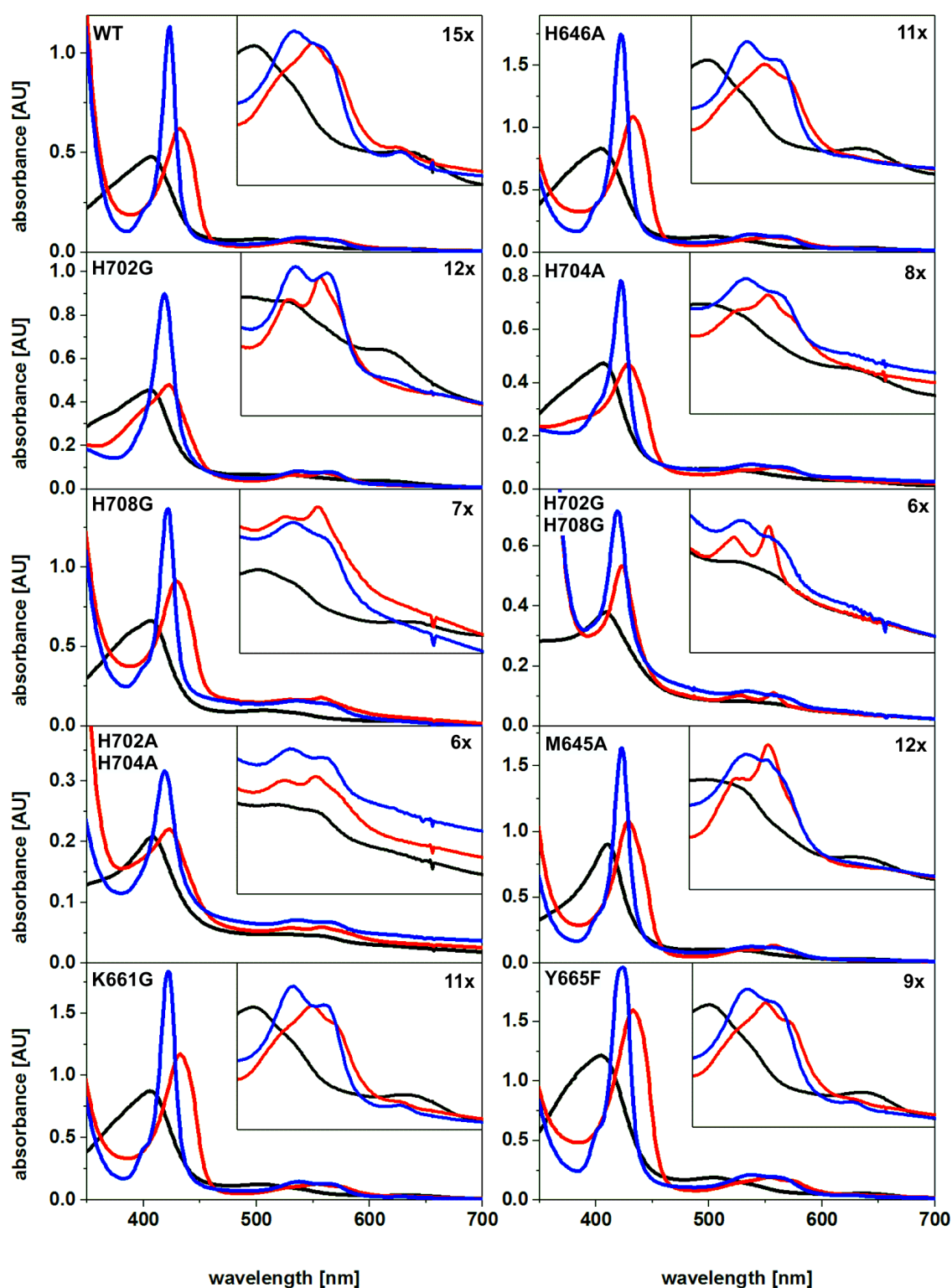


**Figure 4.4 Absorbance spectra of MsmS\_sGAF2 variants.** UV/vis spectra of MsmS\_sGAF2 variants produced in EcN as Fe(III) (black line), Fe(II) (red line) and Fe(II)-CO (blue line). The boxes in the right corners are enlargements of the wavelengths region from 490 to 700 nm by the factors indicated in the spectra.

significant differences using UV/vis spectroscopy in comparison to the wild-type MsmS\_sGAF2 (Fig. 4.4). However, changing histidine 702 to glycine resulted in an obvious different

spectral behaviour. Whereas the Fe(II) complex of the wild-type MsmS\_sGAF2 consists of a mixture of 5- and 6-coordinated heme with an absorbance maximum at 555 nm, the H702G variant showed two distinct Q-bands at 531 nm and 559 nm, implying the presence of a 6-coordinated heme species. The mutation of histidine residue 708 (located at the distal site) showed slight differences to the wild-type. The Soret band of the Fe(II) complex was shifted to 429 nm and the  $\alpha$ - and  $\beta$ -bands resolved at 527 nm and 557 nm indicative for a single 6-coordinated heme species, but here the Q-bands were not as distinct as observed for variant H702G (Fig. 4.4). An additional exchange of histidine residue 702, which is located at the proximal site, in the H708G variant resulted in a shift of the Fe(III) Soret band from 407 nm to 409 nm. Upon reduction, the  $\alpha$ - and  $\beta$ -bands of H702G/H708G variant were observed at the same wavelengths as for the single H708G variant Fe(II) complex, but more distinct. Also the additional exchange of histidine 702 in the H704A variant led to more clearly resolved Q-bands than for the single H704A variant. All variants with exchanges of histidine residue 702 were only able to be purified in small yields in comparison to the wild-type (data not shown).

### **Methionine residue 645 influences heme coordination at the distal site**

To verify the former found result that methionine residue 645 has an influence on the heme coordination [95], the variant MsmS\_sGAF2\_M645A was also produced in EcN and purified via *StrepII*-tag. A deviation of the spectral behavior compared to MsmS\_sGAF2 wild-type was observed (Tab. 4.5). The Soret band of the Fe(III) complex was found at 410 nm. Upon reduction the Soret band shifted to 429 nm and weak  $\alpha$ - and  $\beta$ -bands were observed at 529 nm and 555 nm indicating that more 6-coordinated heme species are present than in the wild-type protein. The other exchanges of distal located residues (K<sub>661</sub>G, Y<sub>665</sub>F) do not show significant changes in their absorbance.

### **Absorbance spectra of MsmS\_sGAF2 cysteine 656 variants**

For the MsmS\_sGAF2\_C656A variant it was shown that the heme cofactor is not covalently bound [95]. UV/vis spectroscopy of MsmS\_sGAF2\_C656A revealed slight shifts of the Soret bands for the Fe(III) complex from 409 nm to 411 nm, for the Fe(II) complex from 429 nm to 433 nm and for the Fe(II)-CO complex from 422 nm to 425 nm compared to the wild-type protein. In the visible region no significant differences were observed for the heme coordination (Fig. 4.5). Addition of a second amino acid exchange of histidine residue 702 or 708 which were shown to have an influence on the heme coordination resulted in obviously different absorbance spectra. The Soret bands of the Fe(III) complexes for both double variants are much broader than for the single cysteine variant with maxima at 391 nm and 390 nm, respectively. Also the Soret band of Fe(II) complex shifted from 429 nm to 392 nm for C656A/H702G and 426 nm for C656A/H708G (Fig. 4.5).

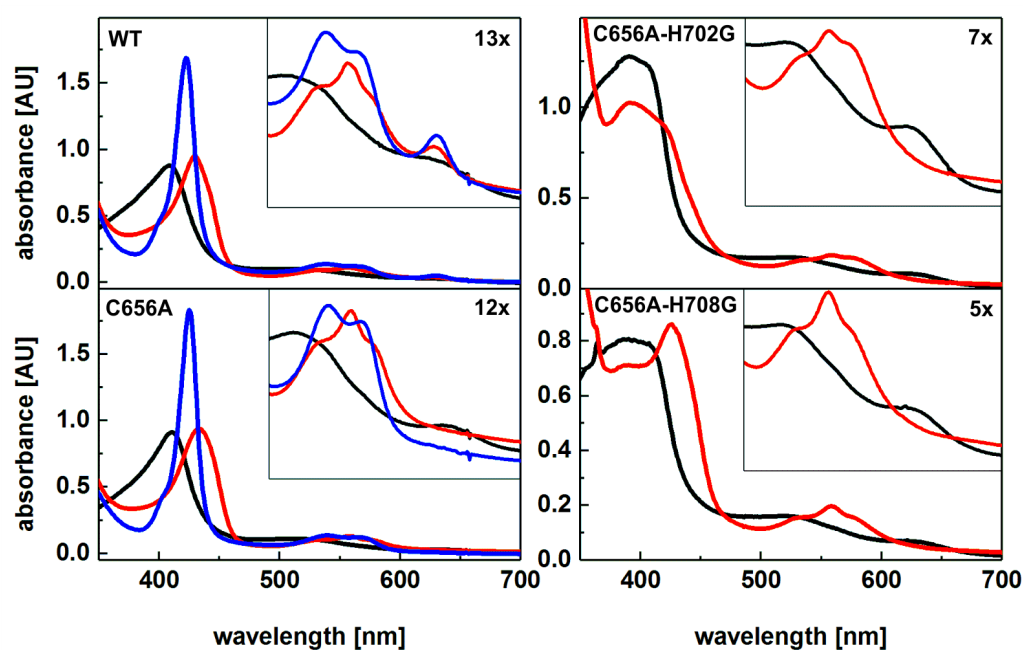


**Figure 4.5 Absorbance spectra of MsmS\_sGAF2\_C656A variants.** UV/vis spectra of MsmS\_sGAF2\_C656A variants produced in BL21(DE3) with heme reconstitution as Fe(III) (black line), Fe(II) (red line) and Fe(II)-CO (blue line). The boxes in the right corners are enlargements of the wavelengths region from 490 to 700 nm by the factors indicated in the spectra.

**Table 4.5 UV/vis peak maxima wavelengths of MsmS\_sGAF2 variants [nm].**

variant	Fe(III)	Fe(II)	Fe(II)-CO
WT (EcN)	407 - 504 - (635)	432 - 555	423 - 539 - 562 - 629
H646A (EcN)	404 - 504 - 633	433 - 553	422 - 538 - 562
H704A (EcN)	407 - (504) - (629)	429 - (529) - 556	422 - 535 - 562
H702G (EcN)	405 - (612)	422 - 531 - 559	419 - 537 - 564
H708G (EcN)	406 - 504	429 - 527 - 557	421 - 536
H702G/H708G (EcN)	409	423 - 527 - 557	420 - 533
H702A/H704A (EcN)	408 - (521) - (555)	423 - 530 - 557	419 - 535 - 562
Y665F (EcN)	405 - 504 - 635	433 - 553 - (573)	423 - 534 - 561 - 627
M645A (EcN)	410 - 504 - 631	429 - 529 - 557	423 - 538 - 555
K661G (EcN)	405 - 504 - 635	432 - 554	422 - 538 - 564 - 628
WT (Hrc)	409 - 502 - 619	429 - 556 - 627	422 - 538 - 565 - 629
C656A (Hrc)	411 - 510	433 - 558	425 - 539 - 566
C656A/H702G (Hrc)	391 - 522 - 622	392 - 559	
C656A/H708G (Hrc)	390 - 518 - (622)	426 - 559	

#### 4.3.2 No impact of pH value on heme coordination in MsmS\_sGAF2

Recombinant MsmS\_sGAF2 produced with heme incorporation during protein production was used to test whether the pH value has an impact on the heme iron coordination. UV/vis spectra of MsmS\_sGAF2 from pH 6 to pH 10 resulted in no significant differences for the absorbance maxima wavelengths (Fig. 4.6). Peak maxima of all spectra are pooled in Tab.

4.6. The Soret bands show slight shifts with an absorbance maxima at 405 nm for the Fe(III) and 504 nm for the Fe(II) complex of the wild-type MsmS\_sGAF2. Under all pH conditions the reduced samples are present as a mixture of 5- and 6-coordinated heme species with one Q-band at approximately 554 nm and slight shoulders. For a more precisely analysis of the heme iron coordination, EPR measurements at different pH values were conducted with MsmS\_sGAF2, produced by coexpression (CoEx) of the heme receptor ChuA. The protein was diluted in the appropriate buffers and directly frozen with liquid nitrogen. EPR spectra did not show any differences for the heme coordination dependent on the pH value.

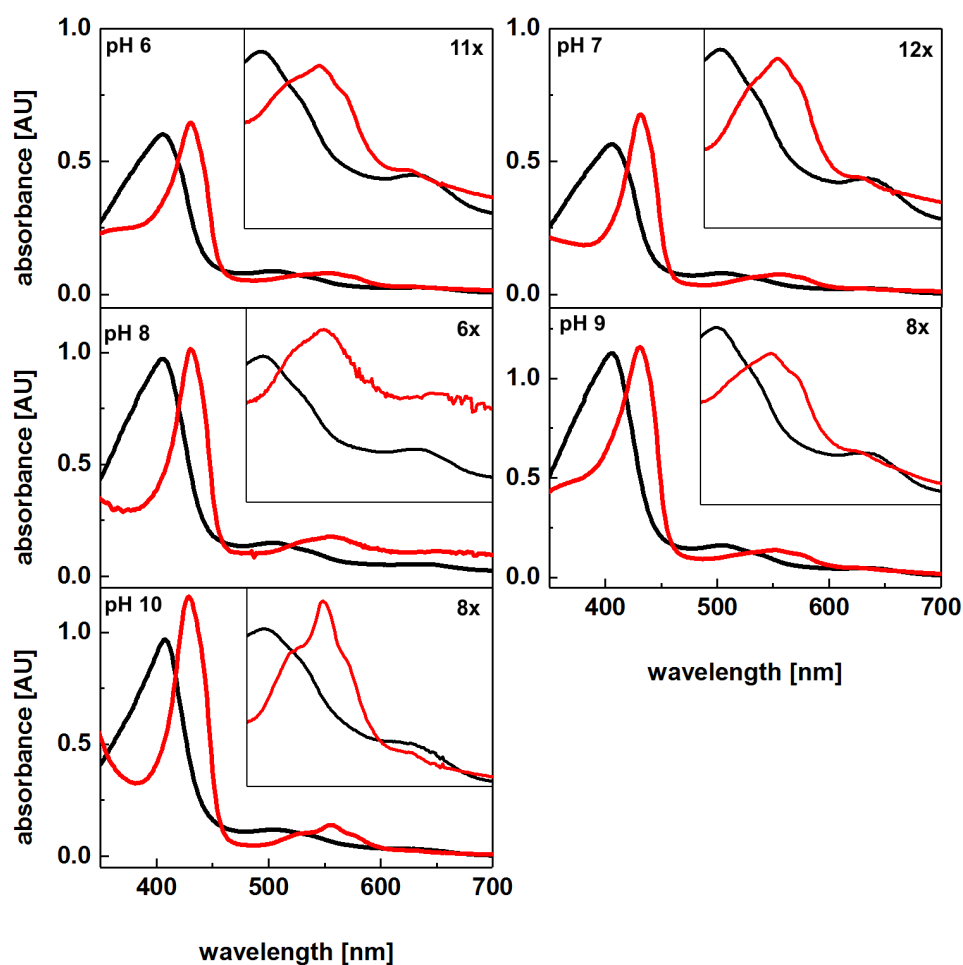


**Figure 4.6** Effects of pH on heme iron coordination of MsmS\_sGAF2. UV/vis spectra of MsmS\_sGAF2 produced in EcN as Fe(III) (black line) and Fe(II) (red line) complexes at pH values from 6 to 10 are shown. The boxes in the right corners show enlargements by the indicated factor.

**Table 4.6** UV/vis peak maxima wavelengths of MsmS\_sGAF2 at different pH values [nm].

pH	Fe(III)	Fe(II)	pH	Fe(III)	Fe(II)
6	405 - 504 - 633	430 - 554	9	406 - 504 - 631	431 - 552
7	406 - 504 - 635	431 - 555	10	408 - 504	429 - 555
8	405 - 504 - 632	432 - 554			

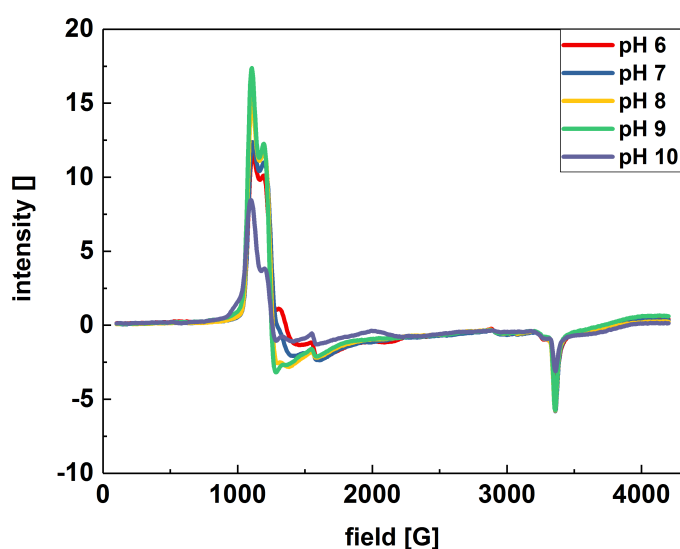


**Figure 4.7** EPR measurements of MsmS\_sGAF2 (CoEx) at different pH values. EPR spectra were measured at 12 K, 9.35 GHz and 2 mW. The experiments were conducted in cooperation with A. Pierik and D. Bechtel (Biochemistry group, TU Kaiserslautern).

### 4.3.3 Redox potential of MsmS\_sGAF2\_C656A

In a former study it was shown that the heme cofactor in MsmS\_sGAF2 is covalently bound via cysteine residue 656 [95]. This result could be confirmed using acidified butanone extraction and pyridine hemochromogen assay with the full-length MsmS and MsmS\_C656A proteins (data not shown). Moreover, the redox potential of MsmS\_sGAF2 was determined [95]. To understand the role of covalent heme binding for the protein function, the redox potential of the recombinant variant MsmS\_sGAF2\_C656A was measured at pH 7.0 by redox titration. These measurements obtained midpoint potentials of  $-111 \pm 10$  mV and  $-123 \pm 10$  mV for the oxidation and reduction reaction of MsmS\_sGAF2\_C656A, respectively (Fig. 4.8). With a midpoint potential of  $-85$  mV for MsmS\_sGAF2 [95] the covalent binding led to a difference of about 30 mV between the two variants.



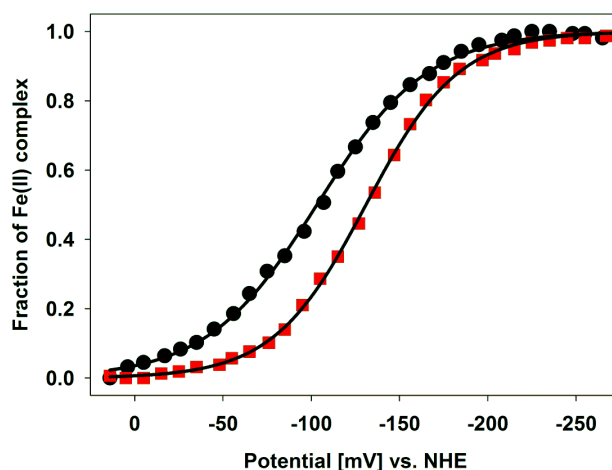


**Figure 4.8 Redox potential determination of MsmS\_sGAF2\_C656A (Hrc).** Reductive (black circles) and oxidative (red squares) titration of MsmS\_sGAF2\_C656A at pH 7.0. Redox titration experiments were performed by C. Laurich and Prof. Dr. W. Lubitz (Max-Planck-Institute for Energy Conversion, Mühlheim a.d.R., Germany).

#### 4.3.4 Full-length domain structure influences heme iron coordination

UV/vis spectroscopy revealed that the heme in MsmS\_sGAF2 is present as a mixture of 5- and 6-coordinated heme iron. To test whether one of the other domains of MsmS have an impact on the heme iron coordination several extended variants of MsmS\_sGAF2 were constructed (Fig. 4.9 A) and UV-vis spectra measured. All peak maxima of the extended variants are pooled in Tab. 4.7. The Soret bands of the Fe(III) complex of MsmS\_sGAF2 (I) and GAF2 (II) have their peak maxima at 409 nm.

The Fe(II) complexes of both proteins have a Soret band at 429 nm and a Q-band at 557 nm with slight shoulders indicating a mix of 5- and 6- coordinated heme species (Fig. 4.9 B). This mixture can be observed also for the variants G2P2 (III) and G2G1 (IV). For these two variants also the Soret band of the Fe(III) complex shifts from 409 nm to 405 nm implying a slightly different heme coordination in these variants. The UV/vis spectrum of variant G2P1 (V) has two  $\alpha$ - and  $\beta$ -bands at 532 nm and 556 nm in the visible region indicating that the ratio is more on the side of the 6-coordinated heme species than for the shorter variants. These  $\alpha$ - and  $\beta$ -bands were more resolved for the full-length MsmS (VI) with peaks at 528 nm and 566 nm (Fig. 4.9 B). The full-length protein structure led to a 6-coordinated heme instead of a mix of 5- and 6-coordinated heme species.

**Table 4.7** UV/vis peak maxima wavelengths of MsmS\_sGAF2 extension variants [nm].

variant	Fe(III)	Fe(II)	variant	Fe(III)	Fe(II)
I	409 - 502	429 - 557	IV	404	430 - 553
II	409	429 - 557	V	410	429 - 532 - 556
III	405 - 495 - 642	430 - 554	VI	411	429 - 528 - 566

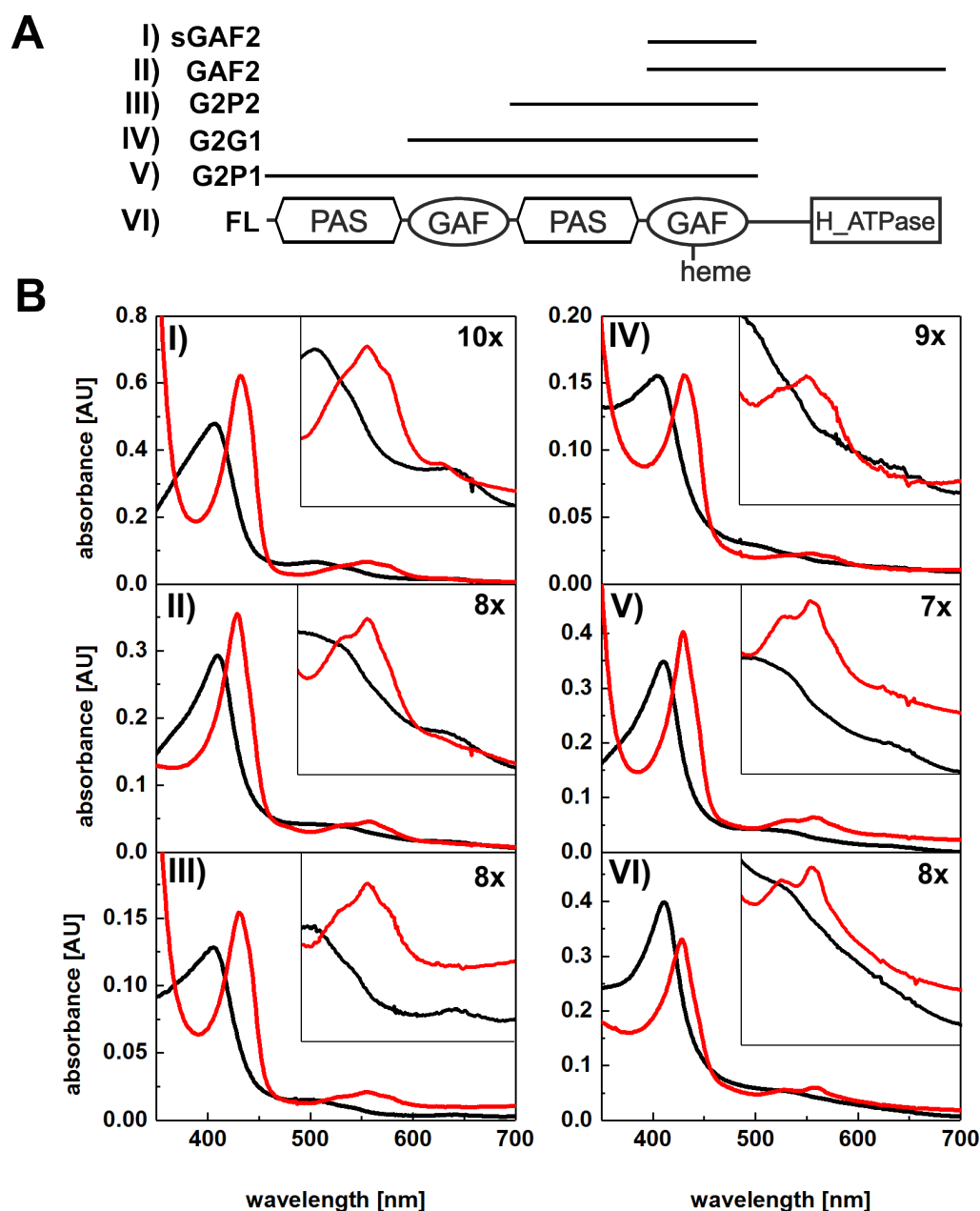


**Figure 4.9 Effect of other domains on heme iron coordination.** (A) Scheme of extended MsmS-sGAF2 variants and (B) UV/vis spectra of these variants produced in EcN as the Fe(III) (black line) and Fe(II) (red line) complex. Roman numbers indicate the variant. The boxes in the right corners show enlargements of the wavelengths region 490 nm to 700 nm indicated by the factors shown in the spectra.

#### 4.3.5 UV/vis spectroscopy of MsmS full-length variants

The extended variants of MsmS\_sGAF2 have shown that the heme coordination is not only influenced by the second GAF domain to which the heme cofactor is bound. Therefore, full-length variants were constructed for a non-covalent bound heme (C656A) and for histidine residue 702 and 708 which were shown to have an impact on heme iron coordination in MsmS\_sGAF2. The peak maxima of all full-length spectra are pooled in Tab. 4.8. UV/vis spectrum of the wild-type MsmS showed a Soret band at 412 nm for the Fe(III) complex. The

Soret band shifted to 430 nm for the Fe(II) complex with  $\alpha$ - and  $\beta$ -bands at 536 nm and 562 nm. Upon addition of CO gas the Soret band shifted to 424 nm and slight  $\alpha$ - and  $\beta$ -bands were observed at 536 nm and 556 nm (Fig. 4.10). For variant C656A with non-covalently bound heme UV/vis spectroscopy revealed no significant differences (Tab. 4.8). The exchange of histidine residue 702 led to a shift of the Fe(III) Soret band to 409 nm, a more obvious shift from 430 to 426 nm for the Fe(II) complex and, from 424 nm to 416 nm for the Fe(II)-CO complex with  $\alpha$ - and  $\beta$ -bands at 532 nm and 557 nm, and 533 nm and 560 nm, respectively (Fig. 4.10). The double exchange of histidine residue 702 and 708 showed only slight shifts indicating a major role for histidine residue 702. For MsmS\_sGAF2 it was shown that the heme cofactor is covalently bound to cysteine residue 656 [95]. This result was varied also for the full-length MsmS by acidified butanon extraction and pyridine hemochrome assay, revealing a pyridine-hemochromogen peak at 553 nm (data not shown).

**Table 4.8** UV/vis peak maxima wavelengths of MsmS full-length variants [nm].

variant	Fe(III)	Fe(II)	Fe(II)-CO
WT	412	430 - 536 - 562	424 - 536 - 556
C656A	414	430 - 533 - 558	425 - 537 - 560
H702G	409	426 - 532 - 557	416 - 533 - 560
H702G/H708G	411	425 - 532 - 558	415 - 536 - 566

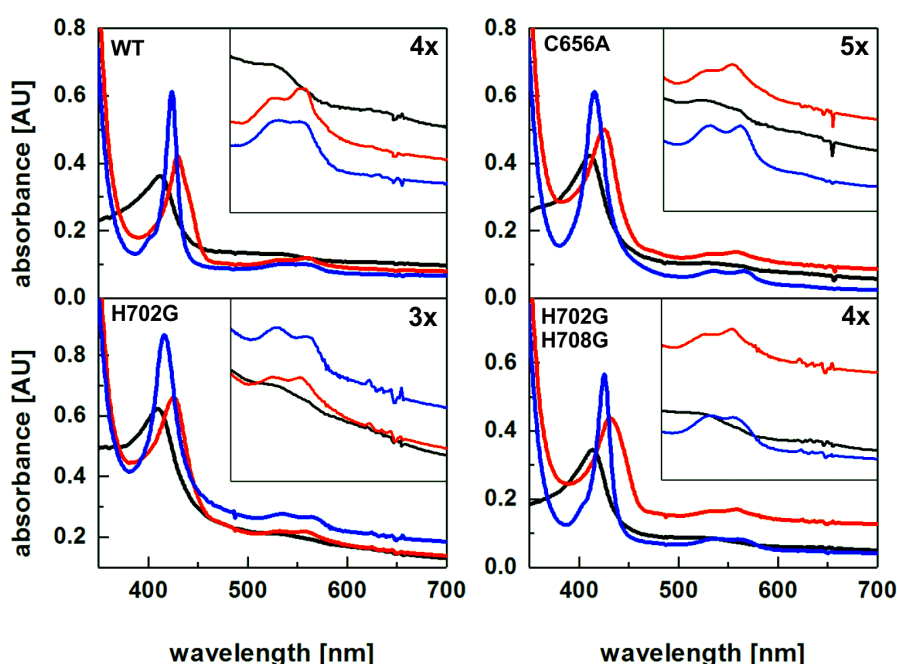


**Figure 4.10** UV/vis spectroscopy of different MsmS full-length variants. UV/Vis spectra of MsmS WT, C656A, H702G and H702G/H708G produced in EcN as Fe(III) (black line), Fe(II) (red line) and Fe(II)-CO complex (blue line). The boxes in the right corner show enlargements of the wavelengths region 490 nm to 700 nm by the factor indicated in the spectra.

### 4.3.6 Analyzing the autophosphorylation activity of MsmS

For MsmS it was shown that it has a redox-dependent autophosphorylation activity. Moreover, 2D thin layer chromatography with standard phospho-amino acids revealed that MsmS is phosphorylated most likely at serine and tyrosine residues [95]. To further analyze the phosphorylation site of MsmS mass spectrometry was used and revealed several serine, tyrosine and threonine residues as putative phosphorylation sites (data not shown). However, these results are only first hints and have to be repeated for a more precise statement. To establish whether the activity is dependent on specific metal-ions, kinase assays of MsmS with different divalent metal-ions in the kinase buffer were tested. For the five tested ions,  $\text{Mg}^{2+}$  and  $\text{Mn}^{2+}$  resulted in the strongest autophosphorylation activity in comparison to the protein amount (Fig. 4.11). Autophosphorylation was also observed with  $\text{Zn}^{2+}$  ions, whereas  $\text{Ca}^{2+}$  and  $\text{Cu}^{2+}$  ions led to no significant autophosphorylation of MsmS.

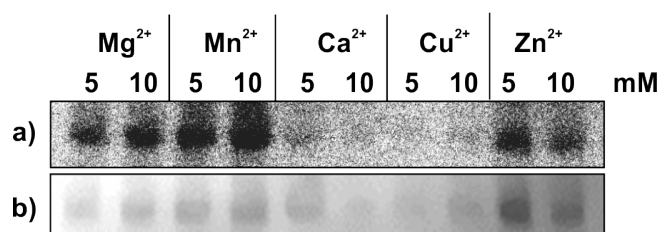


**Figure 4.11 Ion-dependent kinase assay of MsmS.** Kinase assay of MsmS with different divalent metal-ions under oxidizing conditions: (a) auto radiogram of  $[\gamma\text{-P}^{32}]$ -ATP phosphorylated MsmS stopped after 30 min and (b) Ponceau S stain of blotted proteins.

#### MsmS variants have no impact on autophosphorylation

UV/vis spectroscopy of full-length MsmS showed that histidine residue 702 has an impact on the heme iron coordination. Therefore, the single H702G and also the double variant H702G/H708G were tested, whether the heme coordination has an impact on the autophosphorylation activity. Moreover, the full-length variant C656A, in which the heme cofactor is not covalently bound, was used to test the impact of the covalent binding on the autophosphorylation activity. For all three variants phosphorylation signals were already observed after one minute under oxidizing conditions. No signals were observed under reducing conditions like for wild-type MsmS (Fig. 4.12).

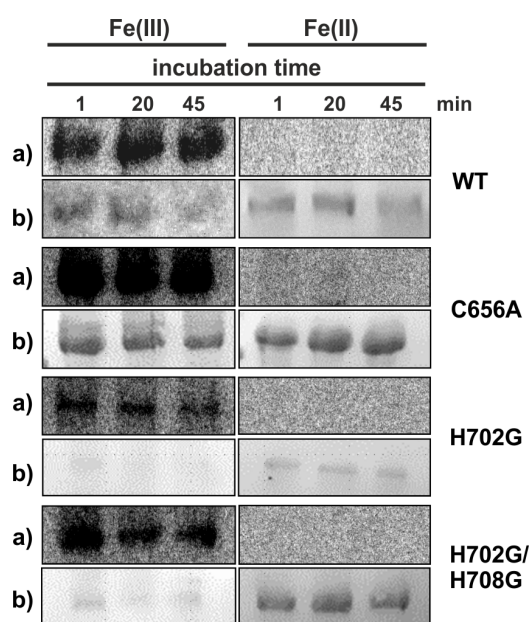


**Figure 4.12 Kinase assays of MsmS heme ligand variants.** Kinase assays of MsmS C656A, H702G and H702G/H708G full-length variants as Fe(III) and Fe(II) complexes: (a) auto radiogram of  $[\gamma\text{-P}^{32}]$ -ATP phosphorylated proteins and (b) Ponceau S stain of blotted proteins. The reactions were stopped after different time points.

#### 4.3.7 Coenzyme M influences autophosphorylation activity but not heme coordination

First kinase assays revealed that the autophosphorylation activity of MsmS is redox dependent. Putative signals inside *M. acetivorans* are oxidized cofactors during methanogenesis which can result in oxidation and "activation" of MsmS. Coenzyme M is part of the last steps of methanogenesis and is commercial available as CoM-SH (Sigma-Aldrich). Therefore, it was used to test whether it has an impact on the autophosphorylation activity of MsmS. Incubation of MsmS with increased concentrations of CoM-SH prior phosphorylation resulted in a decrease of autophosphorylation activity (Fig. 4.13 A).

Interestingly, UV/vis spectroscopy of MsmS revealed no changes for the heme coordination dependent on CoM-SH (Fig. 4.13 C). The reducing agent TCEP is usually used to break disulfide bonds. Incubation of MsmS with increased amounts of TCEP resulted also in a decreased autophosphorylation activity of MsmS (Fig. 4.13 B), indicating the presence of disulfide bonds in MsmS.

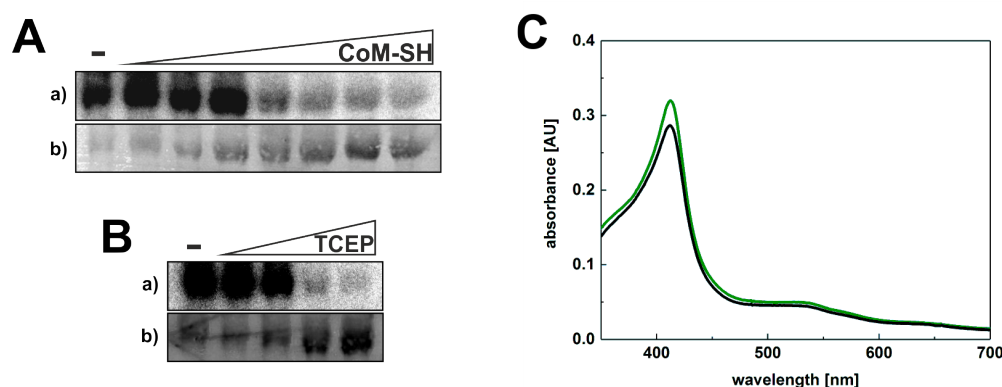


**Figure 4.13 Impact of CoM-SH and TCEP on autophosphorylation activity and heme coordination of MsmS.** Kinase assay of 20  $\mu\text{M}$  MsmS with (A) increased concentrations of CoM-SH (10-200  $\mu\text{M}$ ) and (B) increased concentrations of TCEP (10-200  $\mu\text{M}$ ). Shown are (a) autoradiogram of  $[\gamma\text{-P}^{32}]\text{-ATP}$  phosphorylated protein and (b) Ponceau S stain of blotted proteins. (C) UV/vis spectrum of 20  $\mu\text{M}$  MsmS as Fe(III) complex (black line) and after addition of 200  $\mu\text{M}$  CoM-SH (green line).

#### 4.3.8 Oligomerization state of MsmS is independent of redox state

Sensor kinases often form dimers in which one molecule phosphorylate the other. To investigate how MsmS is present in solution, analytical size exclusion chromatography was used to determine the oligomerization state. Under oxidizing conditions an  $A_{280}$  peak was observed with an elution volume of  $\sim 10.35$  ml. This corresponds to a relative molecular weight of  $\sim 504.55$  kDa. At the same position also a peak at 412 nm was measured for the heme cofactor indicating holo-MsmS. The peak at 8.53 ml elutes before the void volume and represents aggregates. The peak at 12.33 ml corresponds to a molecular weight of 178.66 kDa but only a slight absorbance at 412 nm for the heme cofactor was measured (Fig. 4.14 A, left). Therefore, the peak at 10.35 ml likely represents a long stretched dimer of holo MsmS, whereas the peak at 12.33 ml possibly represents a long stretched monomer. Under reducing conditions the elution profile shows no significant differences to the oxidizing condition. All precipitated fractions contain full-length MsmS (Fig. 4.14 C). Hence, the redox condition has no impact on the oligomerization state.

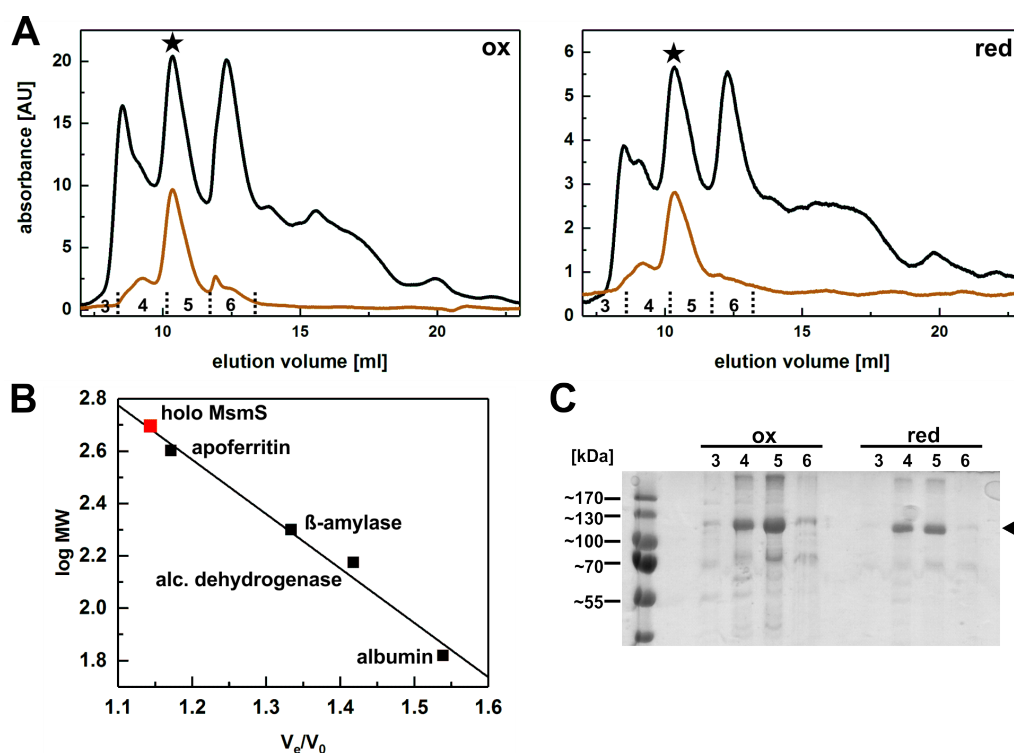


**Figure 4.14 Determination of oligomerization state of MsmS under oxidizing and reducing conditions.** (A) Size exclusion chromatography of purified MsmS under oxidizing (left) and reducing conditions (right). The experiment was performed with a Superdex<sup>TM</sup> 200 Increase 10/300 GL column equilibrated with 50 mM phosphate buffer, pH 7.0 containing 5% glycerol. For reducing conditions the buffer was degassed prior usage and 2 mM DTT was added. Eluted proteins were detected using their absorbance at 280 nm (black line) and the absorbance of the heme cofactor at 412 nm (brown line). Elution peak of holo-MsmS is marked with an asterisk. (B) Calibration curve of Superdex<sup>TM</sup> 200 Increase 10/300 GL column with phosphate buffer pH 7.0 and 5% glycerol. The standards used were: apoferritin (MW = 400 kDa),  $\beta$ -amylase (MW = 200 kDa), alc. dehydrogenase (MW = 150 kDa) and albumin (MW = 66 kDa). The void volume was determined using Blue Dextran 2000. The log of the MW (log MW) was plotted against the quotient of the elution volume and the void volume ( $V_e/V_0$ ) (black squares). The calibration curve was calculated using a linear regression in *Origin*. The red square presents the position of holo-MsmS. (C) SDS-PAGE of TCA precipitated fractions indicated in elution graphs (A). The arrow indicates the position of full-length MsmS.

#### 4.3.9 Protein-protein interaction studies of MsmS with Msr regulator proteins

Current literature suggests that MsmS forms a two-component system with the directly downstream encoded regulator protein MsrG [14, 95]. Therefore, the bacterial two-hybrid adenylate cyclase system (BACTH) was used for protein-protein interaction studies of MsmS and MsrG. For sufficient incorporation of the heme cofactor  $\delta$ -amino levulinic acid was added to the agar plates. The genes for both proteins were cloned into several vectors to receive different terminal fusions with the T18 and T25 fragment of the adenylate cyclase domain.



### The sensor kinase MsmS interacts with the regulator protein MsrG

For BACTH interaction studies the proteins of interest were fused to the T25 and T18 fragments of the adenylate cyclase domain. This fusion can hinder the interaction of the two putative interaction partners. Therefore, the proteins were fused at both C-terminus and N-terminus to test which fusion works best. Interaction studies of MsmS with MsrG revealed that only the N-terminal fusion of MsmS (18-*msmS*) resulted in a positive interaction with MsrG, indicating that the C-terminal fusion disturbed the interaction. Moreover, only the combination of MsmS cloned into pUT18 resulted in a positive interaction but not when cloned into p25N. Both plasmids led to a C-terminal fusion of the adenylate cyclase fragments to MsmS. For MsrG both fusions with T25 fragment interact with MsmS (Fig. 4.15 A). It was further tested whether MsmS and MsrG are able to form homo-multimers. Combinations of MsmS with itself did not result in a positive reaction under the used condition. However, MsrG was found to form homo-multimers (Fig. 4.15 B).

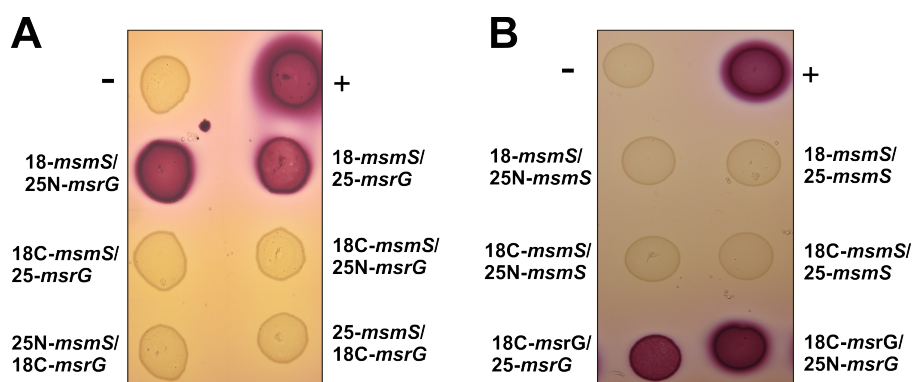


**Figure 4.15 Bacterial two-hybrid analysis of MsmS and MsrG protein interaction.** Different combinations of (A) *msmS* and *msrG* and (B) *msmS* and *msrG* for homo multimerization in pUT18 (18), pUT18C (18C), pKT25 (25) and p25N (25N) were cotransformed into BTH101 and incubated at 30 °C for 24 h under aerobic conditions. Negative control: pUT18C + pKT25 (empty vectors), positive control: pUT18C-zip + pKT25-zip(leucine zipper).

### Interaction studies of MsmS and MsrG with truncated MsmS variants

First interaction studies have shown that MsmS is able to interact with MsrG. To further analyze the interaction region of MsmS with MsrG, truncated variants of MsmS were constructed (Fig. 4.16 A). Combinations of MsrG with the truncated MsmS variants resulted only in an interaction with full-length MsmS. Varying redox conditions during incubation did not influence the interaction (Fig. 4.16 B/C). For combinations of full-length MsmS with the truncated MsmS variants no interaction was observed under aerobic conditions. However, full-length MsmS was able to interact with all truncated MsmS variants under anaerobic conditions (Fig. 4.16 C).



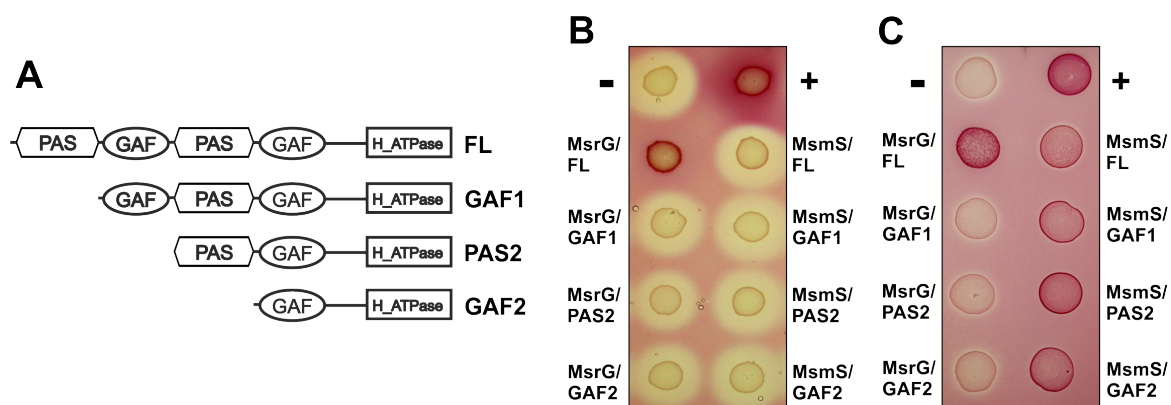


**Figure 4.16 Bacterial two-hybrid analysis of MsrG and MsmS with truncated MsmS variants.** Full-length MsmS (p25N) or MsrG (pKT25) were cotransformed into BTH101 with (A) truncated variants of MsmS (pUT18); FL: full-length. Interaction plates were incubated at 30 °C for 48 h under (B) aerobic and (C) anaerobic conditions. Negative control: pUT18 + p25N (empty vectors), positive control: pUT18-zip + pKT25-zip (leucine zipper).

### MsmS interacts also with regulators MsrF and MsrC

BACTH analysis revealed that the sensor kinase MsmS interacts with the regulator MsrG. The analysis of the  $\Delta msmS$  strain revealed that MsmS has an impact on the biosynthesis of the corrinoid/methyltransferase fusion protein MtsF [95] which expression is activated by the regulator protein MsrC [95]. Hence, the assumption is that MsmS has to interact also with the regulator protein MsrC. In order to test this assumption, BACTH analysis was also performed by combining MsmS with the other two homologous regulators MsrF and MsrC. Combinations of MsmS with all three regulators MsrG/F/C resulted in a positive interaction under the used conditions (Fig. 4.17).

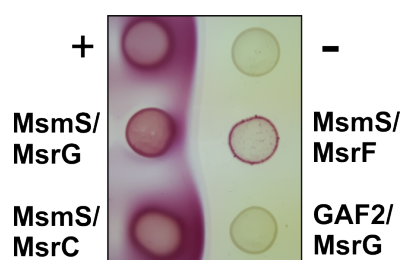


**Figure 4.17 Bacterial two-hybrid analysis of MsmS with Msr regulator proteins.** Full-length *msmS* (pUT18) was cotransformed with *msrG*, *msrF*, *msrC* (p25N) into BTH101 and incubated at 30 °C for 40 h under aerobic conditions. Positive control: pUT18-zip + pKT25-zip (leucine zipper), negative control: pUT18 + p25N (empty vectors), second negative control: GAF2 + MsrG.

### 4.3.10 RNAseq analysis of wild-type *M. acetivorans* vs. *msmS* deletion strain

To test the impact of the kinase MsmS on the transcriptome of *M. acetivorans* RNAseq analysis with the wild-type and  $\Delta ms m S$  strain was performed with methanol as growth substrate. RNAseq analysis was performed by Konrad Förstner and Claus Scholz of the Core Unit Systems Medicine of the University of Würzburg. Comparison of the gene expression profile of the wild-type and  $\Delta ms m S$  strain revealed  $\sim 160$  genes (adjusted p-value  $< 0.05$ ) which were differentially expressed (data not shown). Under these genes the highest log<sub>2</sub>FoldChange (log<sub>2</sub>FC) value was 2.0018 for MA4171 (hypothetical protein). Only the log<sub>2</sub>FC of *msmS* reached a value which represent a significant difference (log<sub>2</sub>FC  $\geq 3$ ) with 4.1597 (Fig. 4.18 A). Part of the strongest differentially expressed genes are several genes belonging to nitrogen, methane and carbon metabolism in *M. acetivorans* (Fig. 4.18 B).

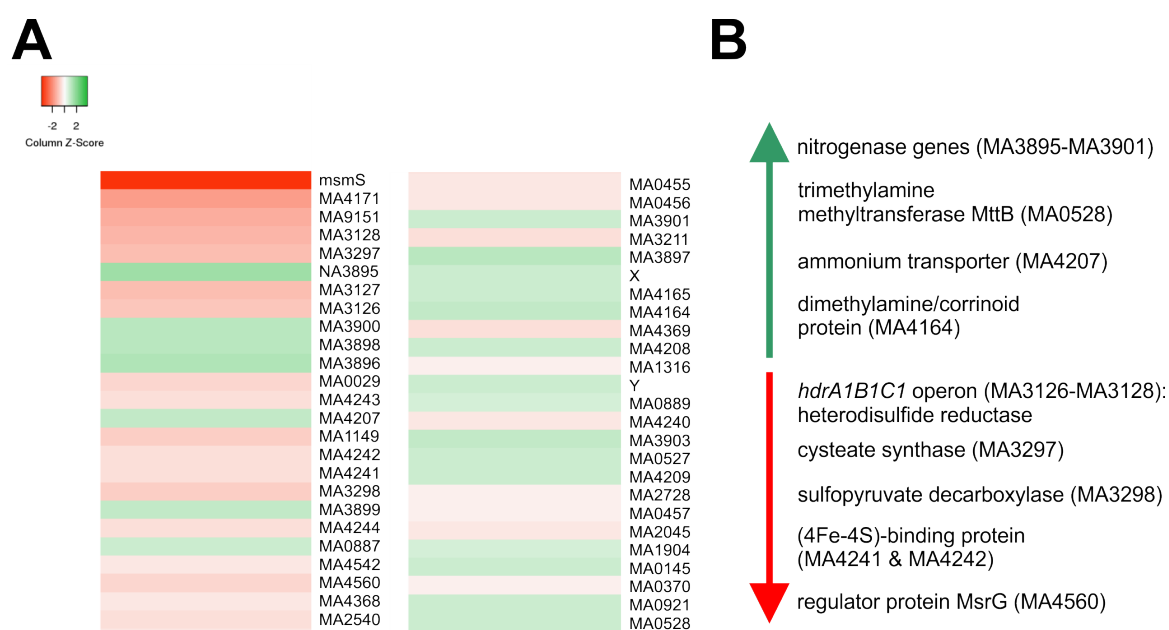


**Figure 4.18** RNAseq analysis of wild-type vs.  $\Delta ms m S$  strain grown on methanol. **(A)** Heat map of first 50 differentially expressed genes between wild-type and  $\Delta ms m S$  strain (adjusted p-value  $< 0.05$ ). The heat map was created using the log<sub>2</sub>FC and the online tool *Heatmapper* (<http://heatmapper.ca/expression/>). **(B)** Some specific genes differentially expressed in the mutant in comparison to the wild-type strain (down regulated = red; up regulated = green).

# 5 Results part 3 - The putative sensor kinase MA0863

## 5.1 Introduction

The putative sensor kinase MA0863 is a multi domain protein with significant homology to MsmS (60% identity and 76% similarity). In comparison to MsmS, it contains an additional PAS domain at the N-terminus and lacks the conserved H-box found in typical histidine kinases (Master thesis, K. Kwiatkowski). Moreover, MA0863 possesses an amber codon in the second PAS domain encoding for pyrrolysine (Pyl216/O216) (Fig. 5.1). First analysis of MA0863 were conducted in the master theses of Kathrin Kwiatkowski and Christian Twittenhoff at the Ruhr-University of Bochum. They revealed that MA0863 also binds a heme cofactor in the second GAF domain, like MsmS. This heme cofactor is covalently bound to cysteine residue 620. UV/vis spectroscopy of MA0863\_sGAF2 (truncated variant containing only the second GAF domain) showed that the heme cofactor is able to bind small molecules like CO and DMS. Furthermore, MA0863 possesses an autophosphorylation activity which was found to be dependent on the heme redox state (Master thesis, K. Kwiatkowski, Bochum). MA0863 is genomically located upstream of a gene encoding for the transcriptional regulator MsrF which activates the expression of the corrinoid/methyltransferase fusion protein MtsD (Fig. 1.6). Parts of the MA0863 results were published in *Environmental Microbiology* by Fiege and Frankenberg-Dinkel (2019) [29].

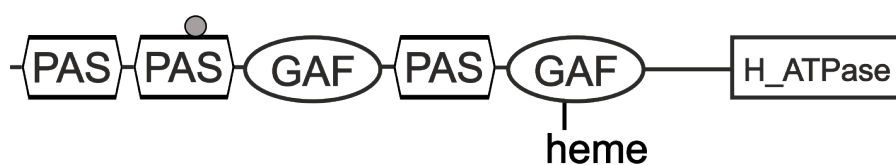


**Figure 5.1 Predicted domain structure of MA0863.** The full-length MA0863 consists of three PAS, two GAF and a histidine-like ATPase (H\_ATPase) domain at the C-terminus. In the second PAS domain an amber codon encodes for the amino acid pyrrolysine (grey circle). In the second GAF domain a heme cofactor covalently binds to cysteine residue 620. Predicted domains are PAS1: aa 33-118; PAS2: aa 163-251; GAF1: aa 277-422; PAS3: aa 458-541; GAF2: aa 572-716; H\_ATPase: aa 852-964. (modified from [29])

## 5.2 Used plasmids and oligonucleotides

The following tables contain all vectors for the expression of the different MA0863 variants and BACTH analysis. Furthermore, they contain all oligonucleotides used for the construction of expression vectors and site-directed mutagenesis.

**Table 5.1** Used Plasmids for MA0863 analysis

No.	Vector	Characteristics	Reference
1	pASK-MA0863	MA0863 inserted into pASK-IBA3	master thesis, K. Kwiatkowski
2	pASK-MA0863_O216K	(1) with O216→K	master thesis, K. Kwiatkowski
3	pASK-MA0863_O216K/C620A	(2) with C620→A	lab collection
4	pASK-MA0863_O216K/H666G	(2) with H666→G	lab collection
5	pASK-MA0863_O216K/H672G	(2) with H672→G	lab collection
6	pASK-MA0863_O216K/C22S	(2) with C22→S	this study
7	pASK-MA0863_O216K/C73S	(2) with C73→S	this study
8	pASK-MA0863_O216K/C78S	(2) with C78→S	this study
9	pASK-MA0863_O216K/C119S	(2) with C119→S	this study
10	pASK-MA0863_O216K/C155S	(2) with C155→S	this study
11	pASK-MA0863_O216K/C214S	(2) with C214→S	this study
12	pASK-MA0863_O216K/C300S	(2) with C300→S	this study
13	pASK-MA0863_O216K/C315S	(2) with C315→S	this study
14	pASK-MA0863_O216K/C376S	(2) with C376→S	this study
15	pASK-MA0863_O216K/C514S	(2) with C514→S	this study
16	pASK-MA0863_O216K/C933S	(2) with C933→S	this study
17	pASK-MA0863_sGAF2	MA0863 coding sequence from aa 566 to aa 740	master thesis, K. Kwiatkowski
18	pASK-MA0863_sGAF2_C620A	(17) with C620→A	master thesis, K. Kwiatkowski
19	pASK-MA0863_sGAF2_H666G	(17) with H666→G	master thesis, K. Kwiatkowski
20	pASK-MA0863_sGAF2_H672G	(17) with H672→G	this study
21	pASK-MA0863_sGAF2_H666G/H672G	(19) with H672→G	bachelor thesis, M. Merz
22	pASK-MA0863_sGAF2_H666G/H672Q	(19) with H672→Q	this study
23	pASK-MA0863_sGAF2_H666G/H668G/H672G	(21) with H668→G	this study
24	pASK-MA0863_sGAF2_	(23) with H672→Q	this study

- Continuation on next page -

H666G/H668G/H672Q			
25	pASK-MA0863_sGAF2_K625G	(17) with K625→G	this study
26	pASK-MA0863_sGAF2_K625G/ H666G	(19) with K625→G	this study
27	pRSFDuet-pylDBC	expression vector for <i>pylDBC</i>	D. Söll & I. Heinemann
28	pCDFDuet-pylST	expression vector for <i>pylST</i>	D. Söll & I. Heinemann
29	pASK- <i>bphP</i>	<i>Pa-bphP</i> inserted into pASK-IBA3	lab collection

Table 5.2 Used plasmids for BACTH analysis of MA0863

No.	Primer	Sequence (5'-3')	
1	pUT18	C-terminal T18 fragment, Amp <sup>r</sup> , <i>lac</i> -promoter	[61]
2	pUT18C	N-terminal T18 fragment, Amp <sup>r</sup> , <i>lac</i> -promoter	[61]
3	p25N	C-terminal T25 fragment, Kan <sup>r</sup> , <i>lac</i> -promoter	[62]
4	pUT18- <i>zip</i>	coding region for leucine zipper region of GCN4 yeast protein, positive control	[60]
5	p25N- <i>zip</i>	coding region for leucine zipper region of GCN4 yeast protein, positive control	[60]
6	p25N-MA0863_O216K	MA0863_O216K inserted into (1)	this study
7	pUT18C- <i>msrG</i>	<i>msrG</i> inserted into (2)	this study
8	p25N- <i>msrG</i>	<i>msrG</i> inserted into (3)	this study
9	pUT18- <i>msrF</i>	<i>msrF</i> inserted into (1)	bachelor thesis, S. Gluzins
10	pUT18- <i>msrC</i>	<i>msrC</i> inserted into (1)	bachelor thesis, A. Scherhag
11	pUT18- <i>msmS_GAF2</i>	<i>msmS</i> coding sequence from aa 580 to the end into (2)	this study

Table 5.3 Used oligonucleotides for MA0863 BACTH analysis

Primer	Sequence (5'-3')
<i>msrG</i> -BTH-XbaI-fw	GCTCGGTCTAGAGATGAAACTGGAATTGTTGGG
<i>msrG</i> -BTH-KpnI-rv	GGCATAGGTACCGCGAGTTCCGACGTGGTAAT
25N-0863-gb-f	TTACGGCTGCAGGGTCTGACTATGAAAAAGTTCGATAT AAATCTTG
KT25-0863-gb-r	TCTTAGTTACTTAGGTACCCGAGACTCTATTTGATTCATGC

**Table 5.4** Used oligonucleotides for site-directed mutagenesis of MA0863

Primer	Sequence (5'-3')
MA0863-K625G-fwd	GTGCTATCGAAGAC <u>CGGGCGCTTC</u> ATTATCC
MA0863-H672Q-fwd	CACCTTACCCGCCAG <u>ATGAATGTTCC</u> AG
MA0863-H666/668/ 672G-fwd	CCTAAAGACGGAGTAG <u>GCCTTACCCGCGGA</u> ATG
MA0863-H672G-fwd	CGTACACCTTACCCGCGGA <u>ATGAATGTTCC</u> AGTG
MA0863-H668G/ H672Q-fwd	GTAGGCCTTACCCGCC <u>AAATGAATGTTCC</u> AG
MA0863-C22S-fwd	CCCTATAGTCATTTTTTTA <u>AGCAAGGCG</u> ACTGAAA <u>ACTGG</u>
MA0863-C73S-fwd	GAGGAAGTTGCCAGA <u>AGTTCGG</u> AAAAAGGC
MA0863-C78S-fwd	GTTCCGAAAAAGGC <u>AGTGC</u> GGAGCTGAC
MA0863-C119S-fwd	CCAGGGTACTCTC <u>AGTGATGCT</u> ACCC
MA0863-C155S-fwd	GTGTTTGTGTTTCTG <u>AGCAAGCCGGA</u> AAGAAAG
MA0863-C214S-fwd	GAAGGGTATGAAGAA <u>AGCACCAAGG</u> AGTAC
MA0863-C300S-fwd	GCCCGGTTTCGAGA <u>AGCTCGATA</u> ATGC
MA0863-C315S-fwd	CACCTCTTTTAC <u>AGCGTTGCC</u> CCCG
MA0863-C376S-fwd	CGGGATTAAAGCC <u>AGCTGGTCC</u> GAAC
MA0863-C514S-fwd	TATGAAGCCGGGGCGGTC <u>AGCAAGGACGGC</u> ACTGTT
MA0863-C933S-fwd	GAATCGGGGTTCTATATC <u>AGCAAAA</u> CATTGTCAACG

<sup>1</sup> Only the forward primers are listed, as the reverse primers are complementary to them. The positions where the mutations were introduced are underlined.

## 5.3 Characterization of the putative sensor kinase MA0863

In order to analyze MA0863, two main variants were constructed and produced in *E. coli*. The first one was the full-length protein MA0863\_O216K in which the pyrrolysine codon was changed to a lysine codon, because *E. coli* is not able to synthesize and incorporate pyrrolysine but recognizes the UAG amber codon as a stop codon. This variant was used as an alternative "wild-type" protein. The second variant was a truncated one, consisting only of the second GAF domain (sGAF2). Both proteins were produced in EcN with good yields (Fig. 5.2 A). To further analyze the heme iron coordination in MA0863 a model structure of the second GAF domain was constructed using the PHYRE2 server. The alignment of both predicted second GAF domains of MsmS and MA0863 illustrates a high sequence and structural similarity between both domains (Fig. 5.2 B & 5.3). The full-length proteins MsmS and MA0863 share 60% identity and 76% similarity (NCBI blastp alignment). In MA0863\_sGAF2 the cysteine residue 620 corresponds with Cys<sub>656</sub> in MsmS and also the putative heme ligands analyzed in MsmS can be found in MA0863 (Fig. 5.2 C & 5.3). As putative heme ligands the amino acid residues Lys<sub>625</sub>, His<sub>666</sub>, His<sub>668</sub> and His<sub>672</sub> were mutated to study the heme iron coordination in MA0863.

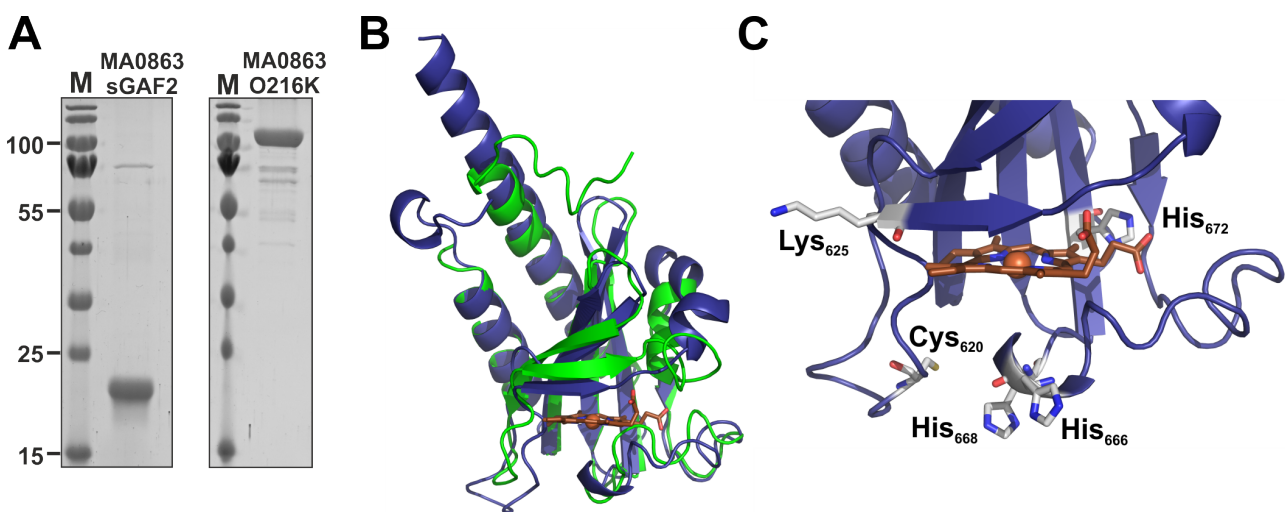


**Figure 5.2 Purification of MA0863\_O216K and MA0863\_sGAF2 and predicted structure model of MA0863-sGAF2.** (A) Affinity purified MA0863\_sGAF2-*Strep*II (MW =~21 kDa) and MA0863\_O216K-*Strep*II (MW =~113 kDa) from 2 l EcN culture volume. (B) Alignment of predicted model structures of second GAF domains of MsmS (green) and MA0863 (blue). The models were constructed using the PHYRE2 server and the alignment was performed with PyMOL. (C) Histidine and lysine residues located next to the heme molecule and cysteine residue to which the heme cofactor is covalently bound. (A modified from [29])







### 5.3.1 Covalent binding of heme cofactor is mediated by Cys620

In the master thesis of K. Kwiatkowski it was shown that the heme cofactor in MA0863\_sGAF2 is covalently bound via cysteine residue 620. To verify this finding acidified butanone extractions and pyridine hemochrome assays of the full-length MA0863\_O216K and MA0863\_O216K\_C620A variants were conducted (Fig. 5.4). Both methods revealed a loss of covalent binding by the exchange of Cys620 to alanine. The heme cofactor in MA0863\_O216K cannot be extracted from the protein, whereas it can be extracted in MA0863\_O216K\_C620A indicating that it is not longer covalently bound in the C620A variant (Fig. 5.4 A). The pyridine hemochrome assay of MA0863\_O216K revealed a peak at 553 nm and MA0863\_O216K\_C620A at 556 nm (Fig. 5.4 B). From literature it is known that a pyridine-hemochromogen of a non-covalently bound heme b shows a peak at 556 nm and a covalent binding via two cysteine residues at 550 nm [9]. To rule out an impact of uncorrect folding in the C620A variant leading to the loss of covalent binding circular dichroism (CD) spectroscopy of both variants were performed but showed no considerable differences (Fig. 5.4 C). Covalent binding via one cysteine residue is a rare phenomenon. In order to exclude the involvement of an additional cysteine residue in covalent heme binding, additional cysteine residues within MA0863 were changed to serine residues. Due to lack of time, only five out of eleven cysteine variants (C22S, C78S, C155S, C300S and C933S) were tested. None of these five variants possessed a non-covalently bound heme cofactor, only C620A (Fig. 5.4 D).

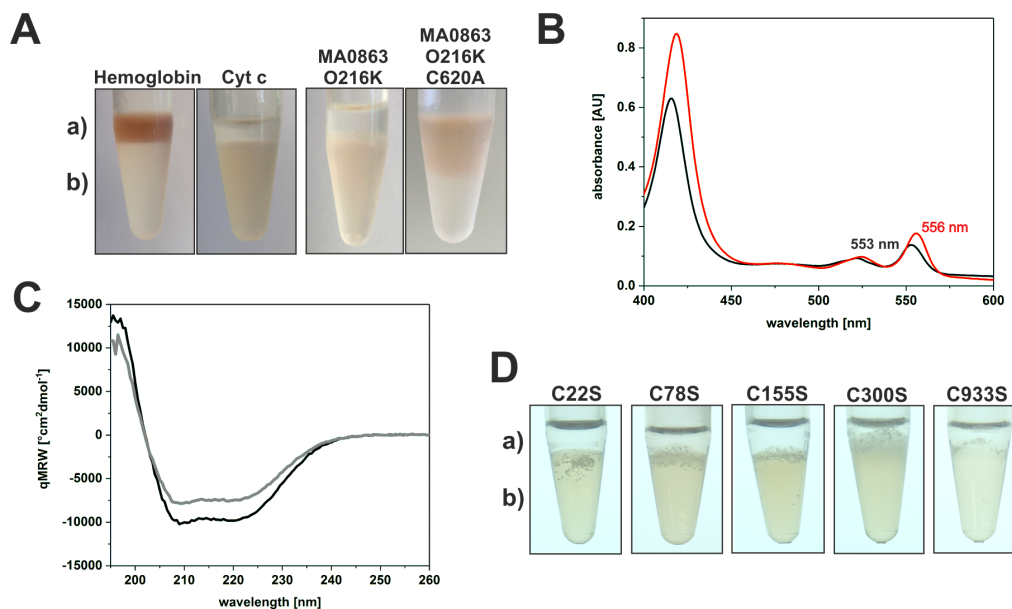


**Figure 5.4 Heme cofactor of MA0863\_O216K is covalently bound via Cys620.** Acidified butanone extractions of (A) MA0863\_O216K and MA0863\_O216K/C620A and (D) five Cys variants. (a) Organic phase with non-covalently bound heme cofactor, like in hemoglobin, and (b) aqueous phase with covalently bound heme cofactor, like in cytochrome c. (B) Pyridine hemochrome assay of MA0863\_O216K (black) and MA0863\_O216K/C620A (red). (C) CD spectroscopy of MA0863\_O216K (black) and MA0863\_O216K/C620A (grey). CD measurements were performed in cooperation with F. Mahler (Molecular biophysics group, TU Kaiserslautern). (modified from [29])

### 5.3.2 Mutational analysis of heme binding ligands in MA0863\_sGAF2 produced by heme reconstitution

Corresponding to the analyzed MsmS\_sGAF2 variants, also MA0863\_sGAF2 variants were constructed and UV/vis spectra measured. MA0863\_sGAF2 produced with heme reconstitution (Hrc) resulted in a Soret band at 410 nm for the Fe(III)-complex. Upon reduction the band shifted to 427 nm and two distinct Q-bands at 528 nm and 559 nm appeared, indicating the presence of a 6-coordinated heme species. Addition of CO gas to the sample resulted in the formation of a Fe(II)-CO complex with a shift of the Soret band to 423 nm. The  $\beta$ - and  $\alpha$ -bands were observed at 534 nm and 556 nm, respectively (Fig. 5.5, Tab. 5.5). Changing the histidine residue 666 to glycine resulted in a different spectral behavior than for the wild-type MA0863\_sGAF2. The Soret band of the Fe(III)-complex shifted to 412 nm and for the Fe(II)-complex to 423 nm (Tab. 5.5). After reduction a Q-band at 559 nm appeared with a shoulder at 535 nm, in comparison to the two distinct Q-bands of the wild-type protein. Also the Fe(II)-CO complex of the H666G variant revealed two more distinct Q-bands at 539 nm and 569 nm than the wild-type (Fig. 5.5). The H672G variant showed also shifts of the Soret bands of 2 or 3 nm in comparison to the wild-type sGAF2 but not as clear as for the H666G variant (Tab. 5.5). Moreover, the exchange of lysine residue 625 to glycine did not show a significant impact on the heme iron coordination. Only the double mutant K625G/H666G resulted in clear change of the heme coordination similar to that of the single H666G variant from a 6-coordinated Fe(II)-complex (two Q-bands) to a mixture of 5- and 6-coordinated heme species (one Q-band with shoulders) (Fig. 5.5). Furthermore, the C620A variant with a non-covalently bound heme revealed only small shifts, indicating no significant coordination differences to the wild-type protein. However, the C620A variant depicts an additional peak 619 nm.

**Table 5.5** UV/vis peak maxima wavelengths of MA0863\_sGAF2 variants [nm].

variant	Fe(III)	Fe(II)	Fe(II)-CO
WT (EcN)	413 - 531 - (559)	425 - 526 - 555	423 - 528 - (559)
H666G (EcN)	410 - 528	423 - 529 - 556	418 - 535 - 562
H666G/H672Q (EcN)	412 - 533	424 - 529 - 557	421 - 538
H666G/H668G/H672Q (EcN)	412 - 534	424 - 528 - 557	421 - 536 - (565)
WT (Hrc)	410 - 528	427 - 528 - 559	423 - 534 - 556
H666G (Hrc)	412 - 527	423 - (535) - 559	421 - 539 - 569
H672G (Hrc)	407 - 526	424 - 531 - 558	421 - 539 - 566
K625G (Hrc)	414 - 528	425 - 529 - 558 - (629)	423 - 538 - 565 - 629
K625G/H666G (Hrc)	411 - 528	419 - 558	425 - 540 - 569
C620A (Hrc)	411 - 529	426 - 531 - 559	426 - 540 - 566

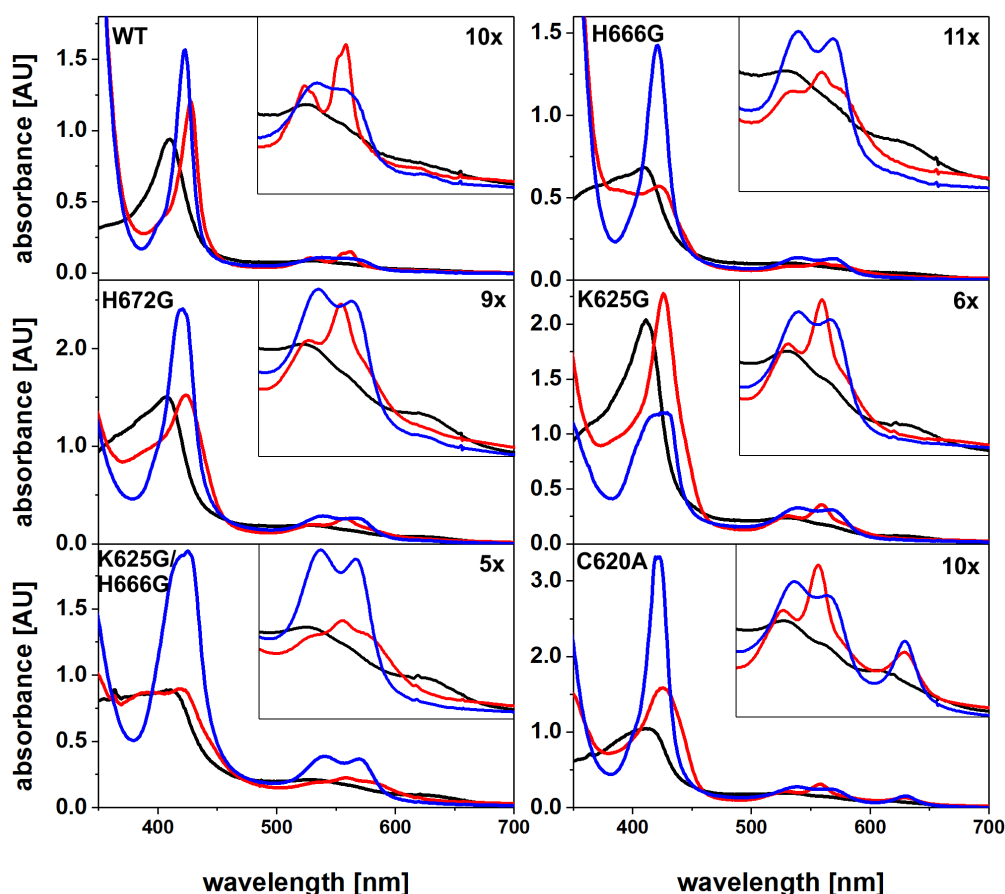


**Figure 5.5 Absorbance spectra of MA0863\_sGAF2 variants.** UV/vis spectra of MA0863\_sGAF2 variants produced in BL21(DE3) with heme reconstitution as Fe(III) (black line), Fe(II) (red line) and Fe(II)-CO (blue line). The boxes in the right corners are enlargements of the wavelengths region from 490 to 700 nm by the factors indicated in the spectra.

### 5.3.3 Mutational analysis of heme binding ligands in MA0863\_sGAF2 produced in *E. coli* Nissle 1917

After establishing the improved heme protein production method, MA0863\_sGAF2 variants of the three histidine residues (His<sub>666</sub>, His<sub>668</sub> and His<sub>672</sub>) next to the heme molecule were produced in *E. coli* Nissle 1917 (EcN). The wild-type MA0863\_sGAF2 showed slight shifts of the maxima in comparison to the production with heme reconstitution (Tab. 5.5). The Fe(II) complex was present as two distinct bands indicating a 6-coordinated heme species. After addition of CO to the sample the Fe(II)-CO complex did not show two separate maxima (Fig. 5.6). For the MA0863\_sGAF2\_H666G variant the maxima shifted in comparison to the wild-type. The Soret bands of the Fe(III), Fe(II) and Fe(II)-CO complex shifted to a shorter wavelengths with 410 nm, 423 nm and 418 nm, respectively (Tab. 5.5). When produced in BL21(DE3) with heme reconstitution, the variant H666G showed a more significant different spectral behavior than the wild-type sGAF2. Addition of further histidine exchanges, revealed the variants H666G/H672Q and H666G/H668G/H672Q, led to small maxima shifts in comparison to variant sGAF2\_H666G but no significant differences for the Q-bands (Fig.

5.6, Tab. 5.5). In the double and triple variant the histidine 672 was changed to glutamine instead of glycine because the glycine variant could not be produced in EcN. For all three histidine variants it was observed that their production yield in EcN was much weaker than for wild-type sGAF2 (indicated by the low absorbance values of the spectra, Fig. 5.6).

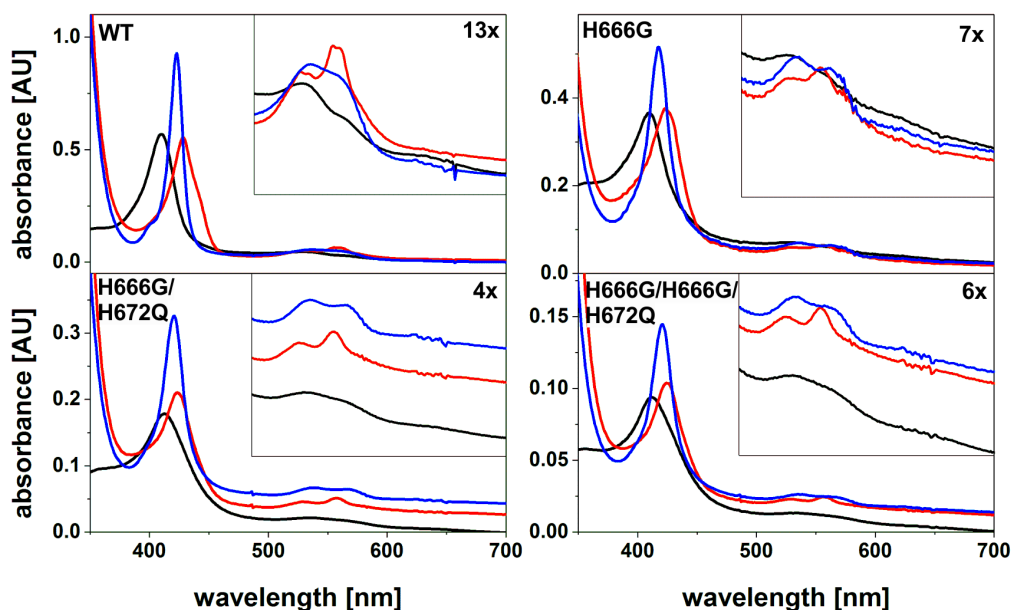


**Figure 5.6 Absorbance spectra of MA0863\_sGAF2 variants.** UV/vis spectra of MA0863\_sGAF2 variants produced in EcN as Fe(III) (black line), Fe(II) (red line) and Fe(II)-CO (blue line). The boxes in the right corners are enlargements of the wavelengths region from 490 to 700 nm by the factors indicated in the spectra.

### 5.3.4 Mutational analysis of heme iron ligands in MA0863\_O216K full-length protein

After analysing the impact of different amino acid residues on the heme coordination in MA0863\_sGAF2, some of the single exchanges were also introduced into the full-length MA0863\_O216K (C620A, H666G, H672G, H672Q) and produced in EcN. The Fe(III) complex of MA0863\_O216K has a Soret band at 413 nm, a maximum at 531 nm and a shoulder at 559 nm. The Soret band shifted to a longer wavelength of 425 nm after reduction with DTH and two very distinct Q-bands were observed at 526 nm and 555 nm, indicating a 6-coordinated heme. Upon addition of CO gas a Fe(II)-CO complex was formed and the Soret band shifted to 423 nm. In the Q-band region the formation of the Fe(II)-CO complex led to a shift of the maxima to 528 nm and 559 nm (Fig. 5.7, Tab. 5.6). For the C620A variant no differences for the present heme species was observed. Both the Fe(II) and Fe(II)-CO complex revealed two Q-bands for a 6-coordinated heme. However, the Q-bands of C620A were less distinct than for the "wild-type" full-length MA0863 and shifted to other wavelengths (Fig. 5.7, Tab. 5.6). Single exchange of histidine residue 666 to glycine led to significant shifts of the Soret bands for the Fe(III) complex to 407 nm, the Fe(II) complex to

423 nm and the Fe(II)-CO complex to 418 nm (Tab. 5.6). The Q-bands were less distinct than for the "wild-type" but shifted significantly to other wavelengths (Fig. 5.7, Tab. 5.6). For the histidine residue 672 two different variants were constructed. First, the H672G variant was produced and measured. Interestingly, exchange of His<sub>672</sub> to glycine led to a very low yield of protein (2.7  $\mu\text{g/g}$  cell pellet). Thus, the second variant H672Q was constructed which resulted in a much higher yield (750  $\mu\text{g/g}$  cell pellet). Both H<sub>672</sub> variants differed slightly in the absorbance spectra. The low yield of H672G might be due to an instable folding of the protein. The spectral data can be influenced by this, hence, the H672Q variant

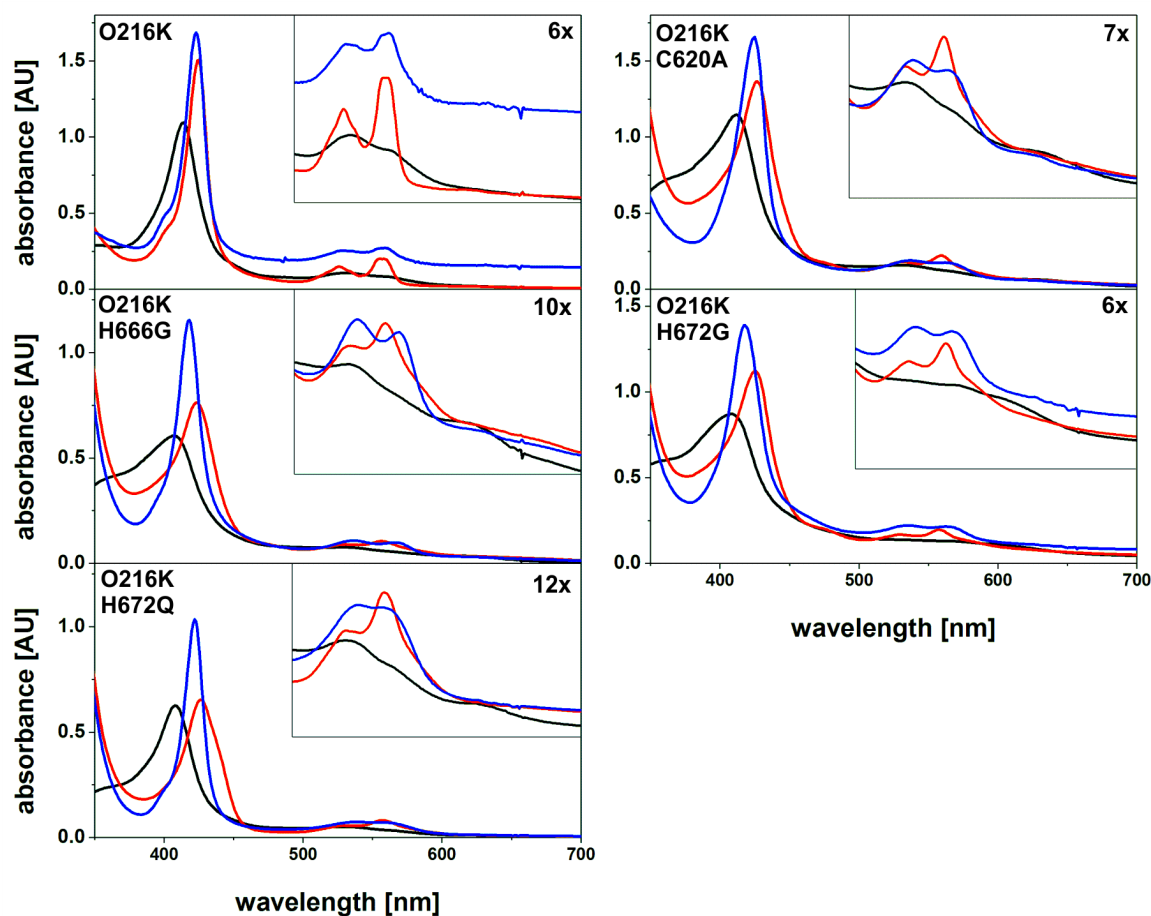


**Figure 5.7 UV/vis spectroscopy of different MA0863 full-length variants.** UV/vis spectra of MA0863\_O216K, O216K/C620A, O216K/H666G, O216K/H672G and O216K/H672Q produced in EcN as Fe(III) (black line), Fe(II) (red line) and Fe(II)-CO complexes (blue line). The boxes in the right corner show enlargements of the wavelengths region 490 nm to 700 nm by the factor indicated in the spectra.

**Table 5.6 UV/vis peak maxima wavelengths of MA0863\_O216K variants [nm].**

variant	Fe(III)	Fe(II)	Fe(II)-CO
O216K (EcN)	413 - 531 - (559)	425 - 526 - 555	423 - 528 - 559
O216K/C620A (EcN)	412 - 530	427 - 531 - 559	425 - 537 - 562
O216K/H666G (EcN)	407 - 531	423 - 531 - 557	418 - 536 - 566
O216K/H672G (EcN)	408	425 - 530 - 558	418 - 535 - 562
O216K/H672Q (EcN)	408 - 529 - 625	426 - 530 - 557	422 - 538 - 554

was used for the comparison with the "wild-type" protein. The Soret band of the Fe(III) complex shifted from 413 nm to 408 nm, whereas for the Fe(II) and Fe(II)-CO complexes no significant shifts of the Soret bands were observed. The Q-bands for both Fe(II) and Fe(II)-CO complexes shifted considerable and were less distinct (Tab. 5.6). Especially for the Fe(II)-CO complex the maxima were very less separable (Fig. 5.7).

### 5.3.5 Resonance Raman spectroscopy for determination of heme coordination

UV/vis spectroscopy revealed first insights into the heme coordination in MA0863. However, Raman Resonance spectroscopy is more sensitive for measuring the heme iron coordination. Here the pyrrole rings of the heme are excited by a laser at a specific wavelength. The so called Raman scattering is detected and can be used to draw inferences about the coordination of the heme iron. The RR spectra of MA0863\_O216K full-length protein indicated a 6-coordinated heme species for both, the oxidized ( $1376\text{ cm}^{-1}$ ) and reduced state ( $1363.2\text{ cm}^{-1}$ ) (Fig. 5.8, pink and light blue, respectively). In contrast, MsmS\_sGAF2 revealed a mix of 5- and 6-coordinated heme ( $1353.4\text{ cm}^{-1}$  and  $1362.2\text{ cm}^{-1}$ ) in its reduced and a 6-coordinated heme ( $1373.2\text{ cm}^{-1}$ ) in its oxidized state (Fig. 5.8, blue and red, respectively).

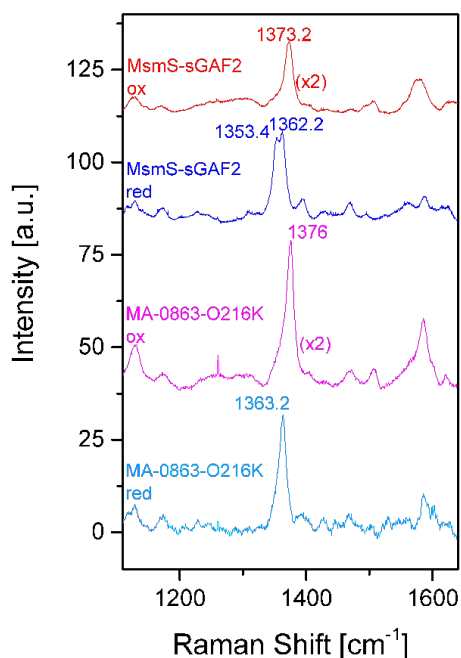


**Figure 5.8 Resonance Raman spectroscopy of MA0863\_O216K in comparison to MsmS\_sGAF2.** MsmS\_sGAF2 and MA0863\_O216K were measured each in their oxidized (MsmS\_sGAF2: red, MA0863\_O216K: pink) and reduced state (MsmS\_sGAF2: blue, MA0863\_O216K: light blue). RR spectroscopy experiments were conducted in cooperation with C. J. Querebillo and P. Hildebrandt (Biophysical chemistry group, TU Berlin).



### 5.3.6 Autophosphorylation activity of MA0863\_O216K is redox dependent

UV/vis spectroscopy revealed that MA0863\_O216K contains a redox-active heme cofactor within one of its sensory GAF domains. In addition, the protein was predicted to have a H\_ATPase domain at the C-terminus. In order to analyze whether MA0863\_O216K has a kinase activity dependent on the heme cofactor, kinase assays were performed under different redox conditions. Under oxidizing conditions, the Fe(III) complex (as it was present after purification) showed an increasing phosphorylation signal. Under reducing conditions with the presence of the Fe(II) complex (addition of DTH, anaerobic) no signal was observed (Fig. 5.9 A). In the master thesis of K. Kwiatkowski (Bochum) it was shown that the heme cofactor of MA0863\_O216K is able to bind CO and DMS which are both present during methanogenesis. Therefore, the impact of these heme ligands on the autophosphorylation activity was also investigated. Kinase assays were performed under different redox conditions in presence and absence of DMS- and CO-heme complexes. Interestingly, autophosphorylation was also only observed under oxidizing conditions, independent of a bound ligand (Fig. 5.9 B). In addition, variants of MA0863\_O216K were tested for their autophosphorylation activity. The C620A variant in which the heme cofactor is non-covalently bound, as well as the two histidine variants (H666G and H672Q) revealed the same redox dependent autophosphorylation activity as MA0863\_O216K itself (Fig. 5.9 C).

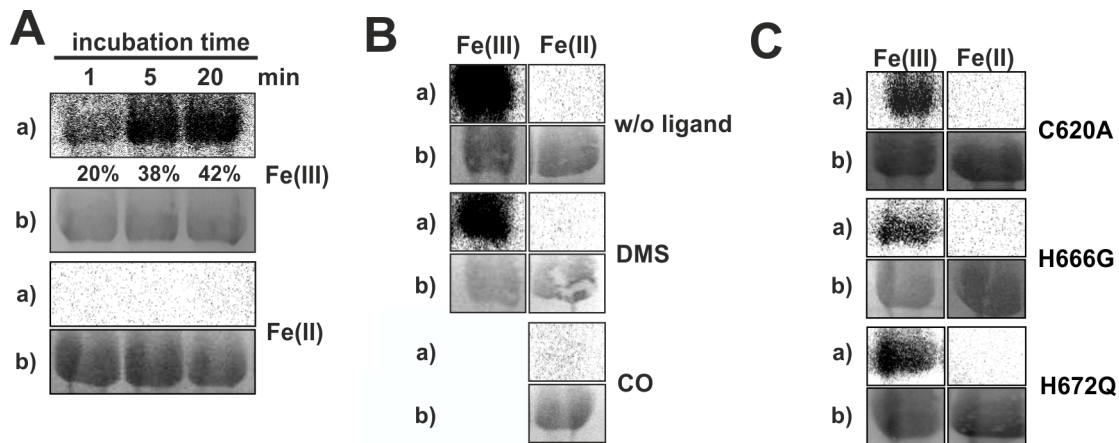


**Figure 5.9 Autophosphorylation activity of MA0863\_O216K.** (A) Kinase assays under oxidizing (w/o DTH) and reducing (w/ DTH) conditions. The reactions were stopped after different time points. Quantification of phosphorylation signals of the oxidized protein via *ImageJ* is shown. (B) Kinase assays without a ligand, and with bound DMS and CO as Fe(III) and Fe(II) complexes. (C) Kinase assay of MA0863\_O216K C620A, H666G and H672Q full-length variants as Fe(III) and Fe(II) complexes. (a) Autoradiogram of  $\gamma$ -[P<sup>32</sup>]-ATP phosphorylated proteins and (b) Ponceau S stain of blotted proteins. The Fe(II) complex was revealed by addition of DTH. The assays were stopped after 15 min (B,C). (modified from [29])

## 5.3.7 MA0863\_O216K is no typical histidine sensor kinase

In order to analyze the nature of the phosphorylation site an *in silico* analysis was performed. Sequence analysis and classification of different prediction databases (InterPro, Pfam, SMART) revealed no conserved H-box for MA0863. An alignment of kinase domains of several bacterial histidine kinases supported this finding (Fig. 5.10 A). Therefore, the stability of the phosphorylation after treatment with acid and base was investigated. The phosphoamidates of histidine phosphorylations are stable under basic conditions but labile under acidic condition as it was shown for the SHK *PaBphP* (Fig. 5.10). In comparison, the phosphorylation of MA0863\_O216K was found to be stable under acidic conditions (Fig. 5.10), supporting the *in silico* analysis result that MA0863 is not phosphorylated on a histidine residue.

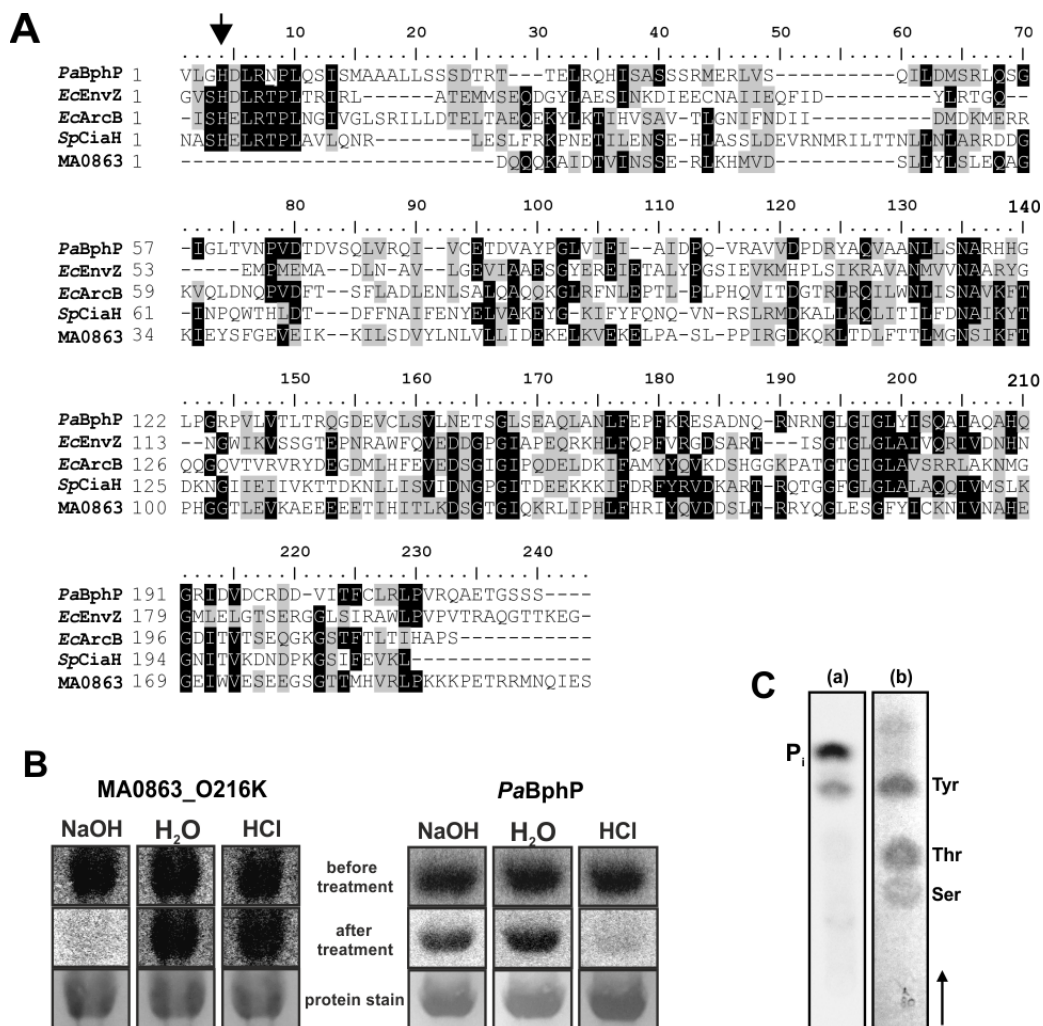


**Figure 5.10 Determination of phosphorylation site.** (A) Protein sequence alignment of kinase domains of four classical bacterial histidine kinases and MA0863 (aa 773-964). The arrow marks the position of the conserved H-box. The alignment was conducted using the programme *BioEdit* and *ClustalW*. (B) Acid-base treatment of  $\gamma$ -[P<sup>32</sup>]-ATP phosphorylated MA0863\_O216K and histidine kinase BphP from *P. aeruginosa*. (C) Thin layer chromatography of (a)  $\gamma$ -[P<sup>32</sup>]-ATP phosphorylated, hydrolyzed MA0863\_O216K and (b) standard phosphoamino acids. (modified from [29])



### 5.3.8 Production of wild-type MA0863 with pyrrolysine in *E. coli*

All previous experiments have been conducted with the variant MA0863\_O216K. At the position 216 the wild-type MA0863 possesses an amber codon for pyrrolysine. In order to rule out any impact of the pyrrolysine residue on the autophosphorylation activity or heme coordination, MA0863 was produced in coexpression of the genes *pylST* and *pylDBC* for Pyl synthesis, pyrrolysyl-tRNA and the cognate aminoacyl-tRNA-synthetase [102]. The protein was fused to a C-terminal *StrepII*-tag. Production of MA0863 in *E. coli* mainly resulted in the production of a truncated protein, due to the recognition of the Pyl encoding amber codon UAG as a stop codon (~25 kDa, Fig. 5.11 asterisk). However, at a size of around 113 kDa also a small amount of produced full-length MA0863 with incorporated pyrrolysine was purified via the C-terminal *StrepII*-tag. With this protein further experiments were conducted.

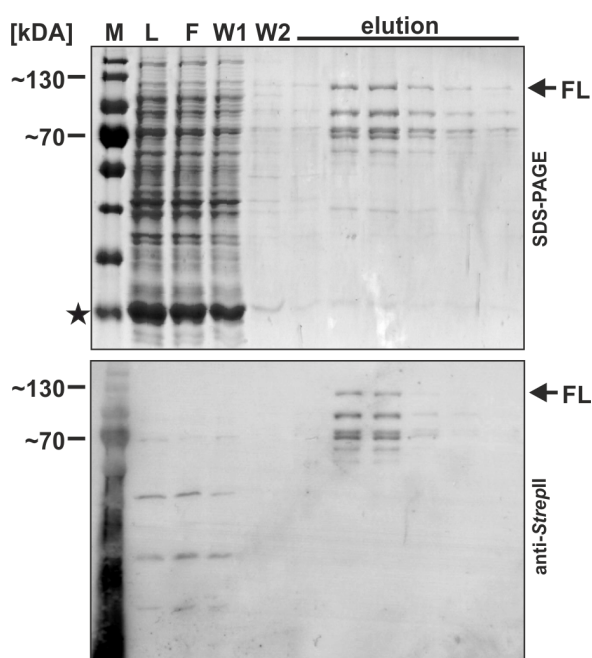


**Figure 5.11 Affinity purification and immuno detection of MA0863 after pyrrolysine coproduction.** MA0863 was produced in BL21(DE3) with coexpression of genes for Pyl synthesis and tRNA. The heme cofactor was reconstituted by adding heme to the cell-free lysate. SDS-PAGE of purified MA0863-*StrepII* and immuno detection against the C-terminal *StrepII*-tag. Marker (M), lysate (L), flow-through (F), washing fraction 1 (W1), washing fraction 2 (W2) and elution fractions 1-6. The migration positions of standards with known molecular weight are shown ( $M_r \times 1000$ ). The arrows mark the position of full-length MA0863 in which pyrrolysine was incorporated. The asterisk marks the position of truncated protein in which the amber codon was recognized as a stop codon. (modified from [29])

UV/vis spectroscopy of MA0863 wild-type revealed a Soret band of the Fe(III) complex at 412 nm. Upon reduction the Soret band shifted to 425 nm and two distinct Q-bands at 526 nm and 560 nm were observed for the Fe(II) complex, indicating a 6-coordinated heme species like for MA0863\_O216K. Formation of the Fe(II)-CO complex led to a shift of the Soret band to 418 nm. In the Q-band region a maximum at 535 nm and a shoulder at 559 nm was present (Fig. 5.12 A, Tab. 5.7). These results indicated a 6-coordinated heme species for

the wild-type MA0863 as it was also observed for the variant Ma0863\_O216K (Fig. 5.12 B, Tab. 5.7). Spectra of both proteins showed shifts of the maxima wavelengths but the heme coordination was the same. To further test whether the covalent binding of the heme cofactor is influenced by Pyl, an acidified butanon extraction was performed, indicating that the Pyl residue did not have an impact on the covalent binding (Fig. 5.12 C). In addition, kinase assays was conducted. Like MA0863\_O216K, MA0863 wild-type protein showed an increasing autophosphorylation activity over time only under oxidizing conditions but not in the presence of the reducing agent DTH (Fig. 5.12 D). A later performed control of pyrrolysine incorporation with mass spectrometry did not successfully show that pyrrolysine was incorporated but an amino acid with the mass of lysine plus an additional mass without unknown identity (data not shown). Therefore, the results have to be considered with caution.

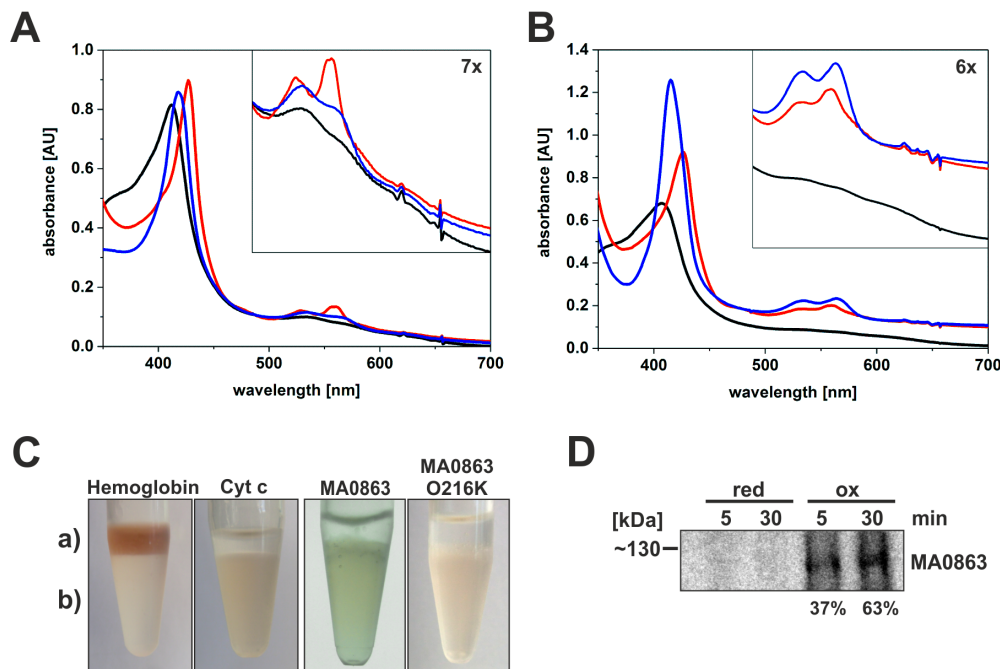


**Figure 5.12 Analysis of MA0863 wild-type protein.** UV/vis spectra of (A) MA0863 and (B) MA0863\_O216K produced with heme reconstitution as Fe(III) (black line), Fe(II) (red line) and Fe(II)-CO complexes (blue line). The boxes in the right corner show enlargements of the wavelength regions from 490 nm to 700 nm indicated by the factor in the spectra. (C) Acidified butanon extraction of MA0863 and MA0863\_O216K. (a) Organic phase with extractable non-covalently bound heme cofactor, like in hemoglobin, and (b) aqueous phase with non-extractable covalently bound heme cofactor, like in cytochrome c. (D) Kinase assay of  $\gamma$ -[P<sup>32</sup>]-ATP phosphorylated MA0863 under oxidizing and reducing (w/ DTH) conditions. The reaction was stopped after different time points. Phosphorylation signals were quantified via *ImageJ*. (modified from [29])

**Table 5.7** UV/vis peak maxima wavelengths of MA0863 and MA0863\_O216K after heme reconstitution [nm].

protein	Fe(III)	Fe(II)	Fe(II)-CO
MA0863	412 - 533	427 - 528 - 560	418 - 535 - (559)
MA0863_O216K	407	426 - 534 - 560	415 - 535 - 564

### 5.3.9 CoM-SH influences the autophosphorylation activity of MA0863\_O216K

Kinase assays of MA0863 have shown that the protein has a redox-dependent autophosphorylation activity. In the genome, MA0863 is located directly upstream of the regulator gene *msrF*. This regulator protein activates the expression of the corrinoid/methyltransferase fusion protein MtsD associated to the methylotrophic pathway of methanogenesis [14]. In order to identify a putative signal sensed by MA083 (i.e. "oxidizing conditions"), it was hypothesized that the signal is part of the methylotrophic pathway. One important role during methanogenesis plays the heterodisulfide CoM-S-S-CoB. It is part of the energy conserving step at the end of the methanogenesis pathway. Due to changing conditions or absence of preferred substrates CoM-S-S-CoB can be accumulated inside the cell. Accumulation of such an oxidized species might result in an oxidation of the kinase MA0863. Due to the oxidation signal the expression of the methyltransferase would be activated to utilize alternative substrates like DMS for methanogenesis. However, synthesis of the heterodisulfide CoM-CoB is not easy to perform, therefore, the commercial available reduced CoM-SH (Sigma-Aldrich) was tested to have an impact on MA0863. Interestingly, incubating oxidized MA0863\_O216K with increasing amounts of CoM-SH and subsequently phosphorylation resulted in a decreased phosphorylation signal (Fig. 5.13 A). To verify the result the SHK BphP was incubated with CoM-SH under the same conditions and did not show an impact of CoM-SH (Fig. 5.13 A). In comparison to the clear influence of CoM-SH on the autophosphorylation activity, it had no impact on the redox state of the heme cofactor as the UV/vis spectra with and without CoM-SH revealed the same spectral behavior (highest concentration of CoM-SH used as for kinase assay) (Fig. 5.13 B).

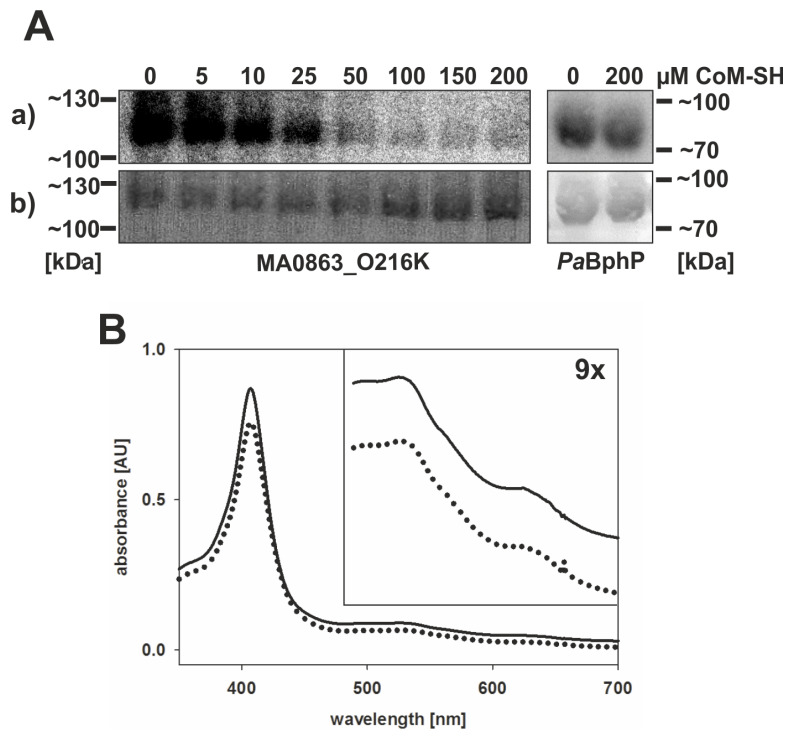


**Figure 5.13 Influence of CoM-SH on autophosphorylation activity.** MA0863\_O216K produced in *E. coli* Nissle 1917 with heme. **(A)** Incubation of 20  $\mu\text{M}$  MA0863\_O216K and PaBphP with increasing amounts of CoM-SH under oxidizing conditions. After incubation the kinase was phosphorylated for 30 min; a) autoradiogram, b) Ponceau S stain of blotted proteins. **(B)** UV/vis spectrum of oxidized heme iron (solid line) and with addition of 10 $\times$  excess of CoM-SH (dotted line). The box in the right corner shows a 9 $\times$  enlargement of the wavelengths region from 490 to 700 nm. (modified from [29])

### 5.3.10 Heme cofactor is not essential for redox dependent autophosphorylation activity

If the autophosphorylation activity is influenced by CoM-SH but not the heme cofactor, the heme cofactor might not be the primary receiver of the sensed signal. In order to verify the assumption that not the heme cofactor is sensing the redox change, MA0863\_O216K was produced without a heme cofactor. For this the *E. coli* strain RP523 was used which contains a *hemB* gene disruption and is not able to produce heme by itself. To produce a heme-free protein the strain was cultivated under anaerobic fermentative conditions when it is able to grow without heme [160]. Purification of the protein from RP523 resulted in a heme-free protein (Fig. 5.14 A). Interestingly, kinase assays of heme-free MA0863\_O216K with (red) and without DTH (ox) resulted in the same redox dependence of autophosphorylation as it was observed for the holo-protein (Fig. 5.14 B). Furthermore, incubation of the apo-protein with CoM-SH and DTT also led to a decreased phosphorylation signal like it was found for the holo-protein (Fig. 5.14 C/D). All in all, these results strongly suggest that it is not the heme cofactor sensing the redox changes which led to the differences in autophosphorylation activity.

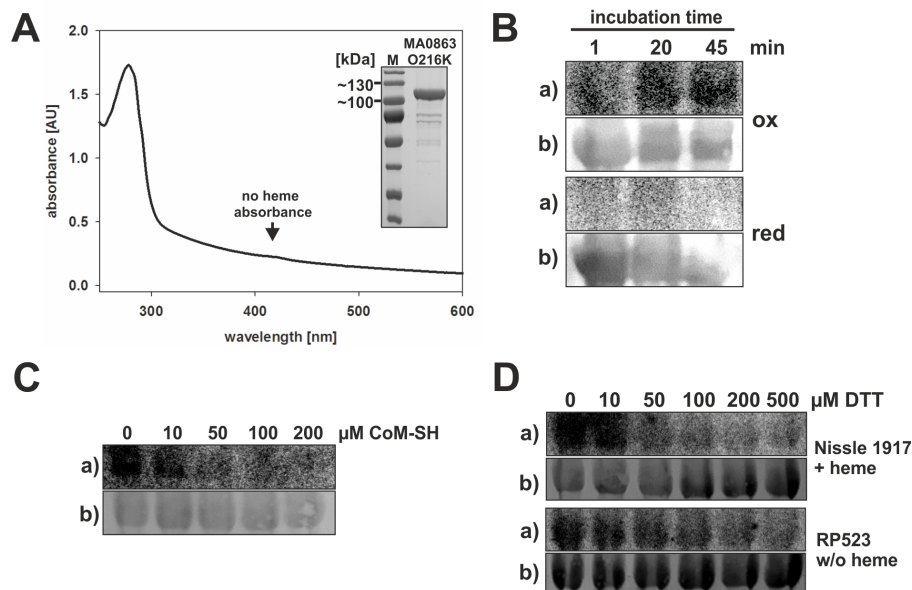


**Figure 5.14 UV/vis spectrum and autophosphorylation assays of MA0863\_O216K produced without heme cofactor.** (A) UV/vis spectrum of MA0863\_O216K produced in RP523 without heme cofactor. The figure in the right part of the spectrum shows a SDS-PAGE of the purified protein. (B) Kinase assays of  $\gamma$ -[ $P^{32}$ ]-ATP phosphorylated MA0863\_O216K with (red) and without (ox) DTH. (C) Kinase assay of 20  $\mu$ M MA0863\_O216K w/o heme with increasing amounts of CoM-SH. (D) Kinase assays of 20  $\mu$ M MA0863\_O216K with and w/o heme cofactor, incubated with increasing amounts of DTT. (modified from [29])

### 5.3.11 MA0863\_O216K contains putative redox active disulfide bonds

Redox changes can be sensed by different mechanisms. After it was shown that not the heme cofactor is sensing the redox changes, it was thought that disulfide bonds might be present in the oxidized form of the protein interacting with the CoM-SH. Overall, MA0863 contains 12 cysteine residues, one of which is the covalent linkage to the heme cofactor. Any of the other 11 remaining cysteine residues can be involved in the formation of disulfide bonds. Therefore, the free thiol groups in the protein in its oxidized (putative disulfide bonds present) and completely reduced state (all cysteine residues present as thiol groups) were determined using the Ellmann's assay. In this method, the Ellmann's reagent 5,5-dithio-bis-(2-nitrobenzoic acid) (DTNB) reacts with the thiol groups and the yellow product 2-nitro-5-chlorobenzoate can be measured by spectroscopy. The increased absorbance of the reduced sample indicates a higher amount of free thiols than in the oxidized form (Fig. 5.15), implying the presence of disulfide bonds in MA0863\_O216K.

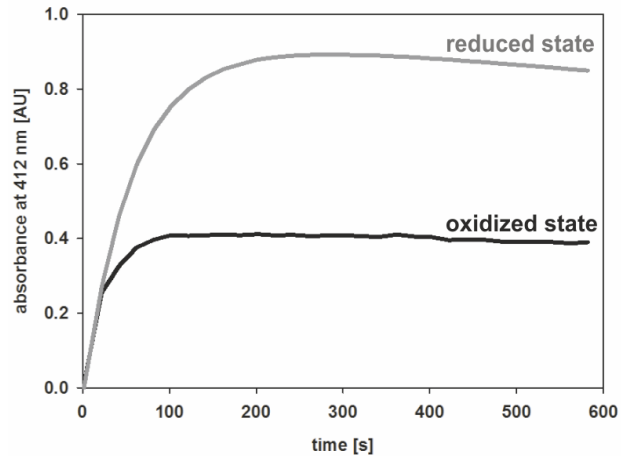


**Figure 5.15 Determination of free thiols in MA0863\_O216K.** Ellmann's assay for determination of thiol-groups in the oxidized (black) and reduced (DTT) (grey) state of the protein. Reaction was measured at 412 nm every 15 sec for 10 min. (modified from [29])

### 5.3.12 Oligomerization state of MA0863\_O216K is independent on redox condition and disulfide bonds

To investigate the oligomerization state of MA0863\_O216K and its dependence on the redox condition, analytical size exclusion chromatography was performed. Under oxidizing conditions the protein ( $A_{280}$ ) was eluted with a volume of  $\sim 14.4$  ml (Fig. 5.16 A, left) corresponding to a calculated molecular weight of 605.05 kDa (calibration curve, Fig. 5.16 B). This finding indicated that MA0863\_O216K was not present as a monomer. At the same position also the absorbance of the bound heme cofactor was measured. Under reducing conditions (degassing of buffer, 2 mM DTT), the protein eluted with the same volume as under oxidizing conditions, indicating that the redox condition has no impact on the oligomerization. Therefore, no intermolecular disulfide bonds led to the formation of the oligomer. To verify this finding, a non-reducing SDS-PAGE was performed. If intermolecular disulfide bonds are present between two molecules of MA0863\_O216K, the protein would run slower at the height of a bigger protein complex in the gel. The result of the non-reducing SDS-PAGE supported the gelfiltration because the protein was observed with a size calculated for the monomer (Fig. 5.16 C). Overall, these results led to the assumption that MA0863 contains intramolecular disulfide bonds instead of intermolecular ones.

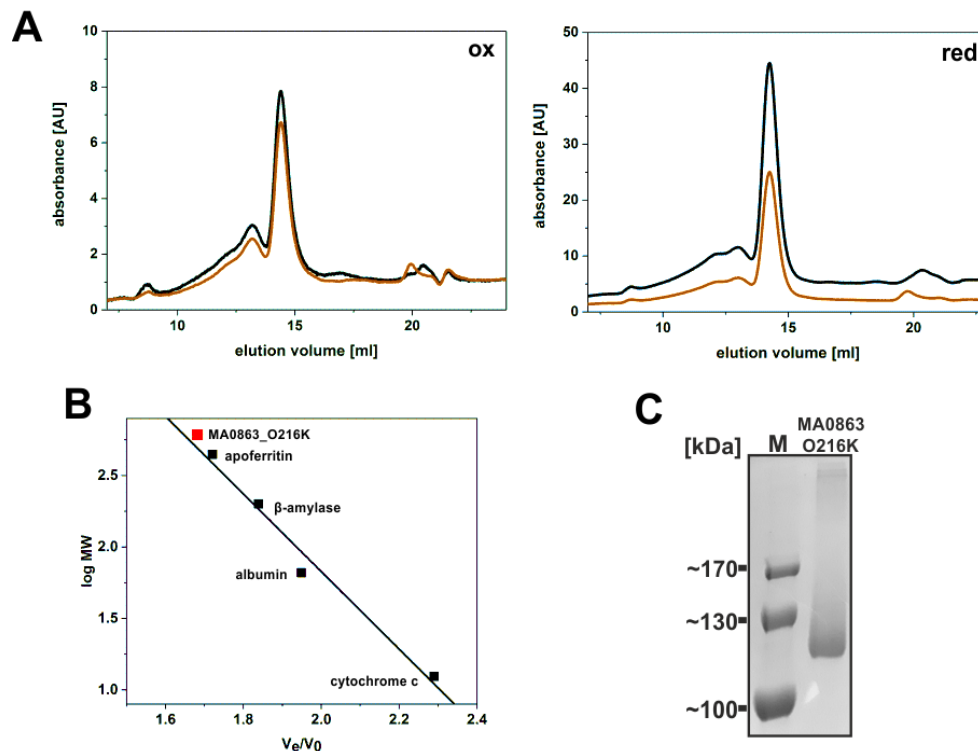


**Figure 5.16 Determination of oligomerization state of MA0863\_O216K under oxidizing and reducing conditions. (A)** Size exclusion chromatography of purified MA0863\_O216K under oxidizing (left) and reducing conditions (right). The experiment was performed with a Superose<sup>TM</sup> 6 Increase 10/300 GL column equilibrated with 20 mM TES/KOH, 100 mM KCl, pH 8.0 containing 10% glycerol. For reducing conditions the buffer was degassed prior usage and 2 mM DTT was added. Eluted proteins were detected using their absorbance at 280 nm (black line) and the absorbance of the heme cofactor at 412 nm (brown line). **(B)** Calibration curve of Superose<sup>TM</sup> 6 Increase 10/300 GL column with 20 mM TES/KOH, 100 mM KCl, pH 8.0 containing 10% glycerol. The standards used were: apoferritin (MW = 400 kDa),  $\beta$ -amylase (MW = 200 kDa), albumin (MW = 66 kDa) and cytochrome c (MW = 12.5 kDa). The void volume was determined using Blue Dextran 2000. The log of the MW (log MW) was plotted against the quotient of the elution volume and the void volume ( $V_e/V_0$ ) (black squares). The calibration curve was calculated using a linear regression in *Origin*. The red square presents the position of holo-MA0863\_O216K. **(C)** Non-reducing SDS-PAGE of MA0863\_O216K. Oxidized protein was run with SDS sample buffer without  $\beta$ -mercaptoethanol to reveal putative disulfide bonds. (C modified from [29])

### 5.3.13 First analysis of cysteine variants reveal no differences

In order to identify the cysteine residues involved in disulfide bond formation, single variants in which each cysteine was changed to serine were constructed. Due to time restriction only nine of eleven variants could be tested during this study (Fig. 5.17 A). Gelfiltration of the nine oxidized Cys variants did not reveal differences for the oligomerization state (Fig. 5.17 B). All proteins, including MA0863\_O216K, eluted after 14.3 ml. In addition, kinase assays of the Cys variants were conducted and all variants revealed an autophosphorylation activity similar to MA0863\_O216K. Interestingly, the variants ran slightly different in the SDS-PAGE than MA0863\_O216K (Fig. 5.17 C).



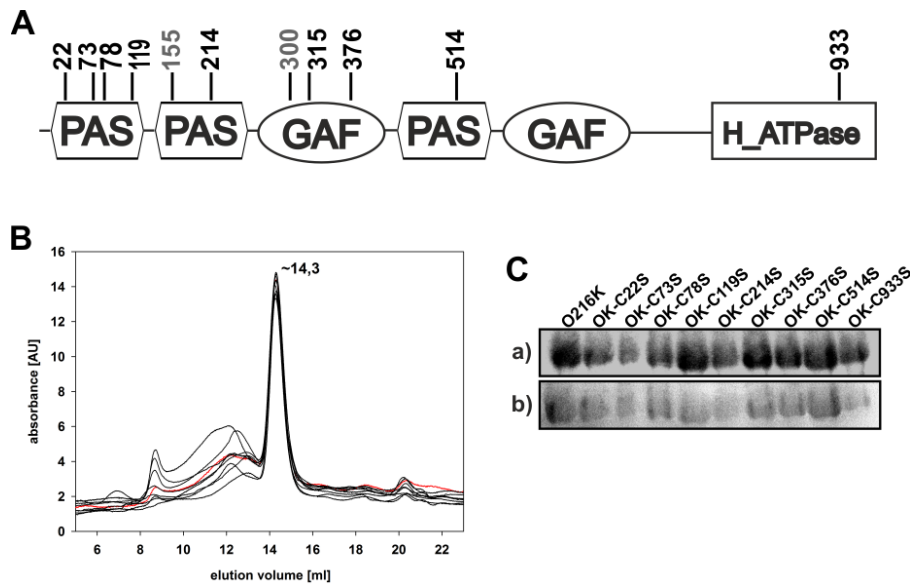


**Figure 5.17 Gelfiltration and kinase assays of MA0863\_O216K cysteine variants.** (A) Schematic overview of cysteine location in the different domains of MA0863. Cysteine residues in grey weren't tested. (B) Comparison of size exclusion chromatography of nine Cys variants (black) to the "wild-type" MA0863\_O216K (red) under oxidizing conditions. The experiment was performed with a Superose<sup>TM</sup> 6 Increase 10/300 GL column equilibrated with 20 mM TES/KOH, 100 mM KCl, pH 8.0 containing 10% glycerol. Eluted proteins were detected using their absorbance at 280 nm. (C) Kinase assays of  $\gamma$ -[P<sup>32</sup>]-ATP phosphorylated nine Cys variants. The proteins were phosphorylated for 10 min.

### 5.3.14 Protein-protein interaction analysis of MA0863\_O216K and Msr-regulators

All former experiments analyzed the protein MA0863 itself. For a better understanding of the function of MA0863 it was also important to investigate its role in *M. acetivorans*. As mentioned before, MA0863 is located directly upstream of the *msrF* gene encoding for a regulator protein. Because of the genomic location and the results for MsmS it was assumed that MA0863 and MsrF also form a two-component system.

#### MA0863 interacts with regulator proteins MsrG/F/C

In order to test whether MA0863 is also able to interact with the regulator MsrF and the other two regulators MsrG and MsrC, the BACTH system was used. Aerobic coexpression of MA0863\_O216K and MsrF resulted in a positive color reaction (Fig. 5.18). As a cross-regulation between the systems of kinases and regulator proteins was suggested, also the coexpression of MA0863-O216K with the regulators MsrG and MsrF were tested and revealed a positive interaction (Fig. 5.18). The color reaction of MA0863\_O216k with MsrF was less strong, as the transformation efficiency of this combination was only very small. As a second negative control (beside the combination of empty vectors) MsrG was cotransformed with the truncated MsmS\_GAF2 variant.



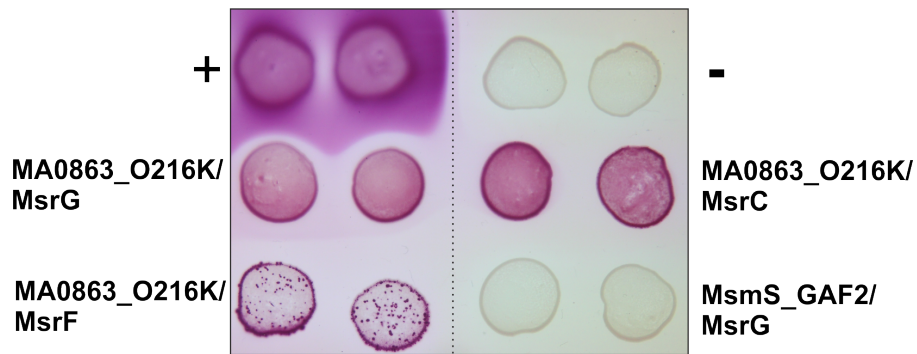


**Figure 5.18 Bacterial two-hybrid analysis of MA0863 with Msr regulator proteins.** Full-length MA0863-O216K (p25N) was cotransformed with *msrG* (pUT18C), *msrE*, *msrC* (pUT18) into BTH101 and incubated at 30 °C for 40 h under aerobic conditions. Positive control: pUT18-zip + pKT25-zip (leucine zipper), negative control: pUT18 + p25N (empty vectors), second negative control: pUT18-*msmS*-GAF2 + p25N-*msrG*. (modified from [29])

## 6 Discussion

### 6.1 Establishment of an improved method for heme protein production in *E. coli*

Production of MsmS\_sGAF2 with heme reconstitution after protein production led to a mixture of 5- and 6-coordinated heme species. As the reconstitution can lead to an incorrect incorporation into the protein a new method for the production of heme proteins was established. Determination of the protein yield comparing three different incorporation methods revealed the highest amount of produced protein per culture volume using the EcN strain. Together with a heme saturation of 74% when adding heme to the growth medium, EcN was shown to be a suitable expression strain for heme proteins of different types and from different species. This result was also supported by protein production of other types of heme proteins from *P. aeruginosa* and *D. shibae*. UV/vis and RR spectroscopy revealed that the incorporation of heme during protein production most likely represents the native heme coordination. All in all, using EcN for recombinant heme protein production results in a higher protein yield with sufficient heme saturation from a smaller culture volume. Unfortunately, the usage of the strain is limited to expression systems lacking the T7 promoter. Integration of the  $\lambda$ DE3 prophage and homolog recombination of the T7-RNA polymerase gene under a lacUV5 promoter into the EcN chromosome were not successful. The low recombination efficiency might be due to the size of the DNA fragment (~4 kb) which has to be introduced. Due to time restrictions these experiments should be repeated in the future.

### 6.2 MsmS and MA0863 - two structural similar proteins

The sensor proteins MsmS and MA0863 share a high homology as mentioned in chapter 5.3. *In silico* analysis of both proteins revealed a similar domain structure but no further homologs in *M. acetivorans*. Both kinases contain several PAS and GAF domains and a C-terminal histidine-like kinase domain (Fig. 6.1). A third kinase encoded nearby the *msr* genes, MA4377 (Fig. 1.6), possesses a considerably different domain structure, representing a membrane bound hybrid sensor kinase (CHASE4/HAMP/PAS/H\_ATPase/RES-REC/RES-REC) and can therefore not be directly compared with MsmS and MA0863. The architecture of the domains is unique for these two proteins in *M. acetivorans*. Differences in the predicted domain structure at the N-terminus (one or two PAS domains) might be due to slight sequence differences and the used prediction algorithms. For MsmS it was already postulated to be a heme-based redox sensor [95]. Due to the similar domain structure first

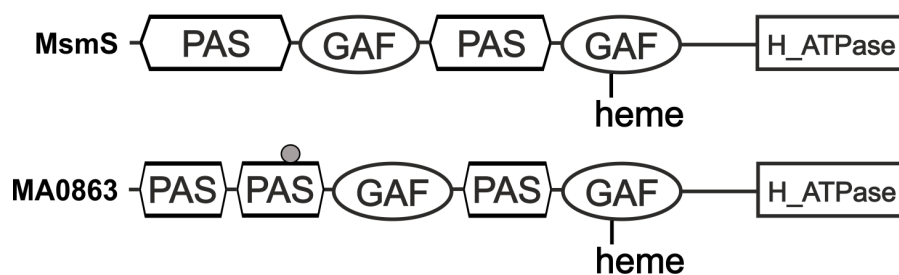


**Figure 6.1 Predicted domain structures of MsmS and MA0863.** Both proteins have a high sequence and structural similarity. In the second PAS domain of MA0863 an amber UAG codon for pyrrolysine is present. (modified from [29])

experiments with MA0863\_sGAF2 revealed also the presence of a heme cofactor covalently bound to Cys<sub>620</sub> (master thesis, K. Kwiatkowski). The cysteine residue for covalent binding as well as the putative heme iron ligand residues are conserved in MsmS and MA0863. In contrast to MsmS, MA0863 contains an in frame amber UAG codon, encoding for the amino acid pyrrolysine in the second GAF domain. At the same position in MsmS a lysine codon is located. Translation of the UAG codon was verified by MS/MS analysis, identifying peptides beyond the amber codon [106]. Both proteins are encoded in the vicinity of regulator proteins known to activate the expression of corrinoid/methyltransferase fusion proteins serving similar function and both proteins have a very similar sequence and domain structure. Due to this it raises the questions whether MsmS and MA0863 sense different signals or complement each other or whether they interact with the closely encoded regulator proteins in a 1:1 protein:protein interaction manner or a cross-interaction between the proteins.

### 6.3 MsmS and MA0863 contain a covalent bound heme cofactor - effecting the redox potential

For the truncated sGAF2 variants of both kinases a covalent bound heme cofactor via Cys<sub>656</sub> and Cys<sub>620</sub>, respectively, was identified (Master thesis, K. Kwiatkowski) [95]. Acidified butanone extraction and pyridine-hemochrome assays of the full-length proteins of MsmS and MA0863\_O216K, verified the presence of a covalently bound heme cofactor for both proteins. Non-covalently bound b-type heme shows a pyridine-hemochromogen maximum at 556 nm, whereas double covalently bound c-type hemes depict a pyridine-hemochromogen at 550 nm [9]. With a peak at 553 nm for MsmS and MA0863\_O216K it was shown that in both proteins the heme cofactor is covalently linked via one of the vinyl groups to one cysteine residue. Covalent binding of the heme cofactors occurred independent of the heme incorporation method (during protein production or heme reconstitution), the redox state of the protein or heme, or whether the protein was purified from *E. coli* or *M. acetivorans* [95] indicating an autocatalytic reaction of the proteins to covalently bind the heme molecule. Almost all known heme-based sensors possess a non-covalently bound type-b heme. Only

a few examples with covalently bound c-type heme are described in the literature, e.g., DcrA from *Desulfovibrio vulgaris* contains a cytochrome c-like fold [164] and GSU0582 from *Geobacter sulfurreducens* with a periplasmic PAS-fold domain [117]. The low abundance of heme-based sensors with covalently bound heme raises the question why in some sensors heme is covalently attached. One assumption for c-type hemes was a stabilization effect of the covalent linkage to the heme molecule inside the protein to prevent the loss of the cofactor [157, 158]. Newer studies revealed further possible roles for the covalent binding [7]. One hypothesis is the covalent attachment of the heme correlating with a lower heme to residue ratio inside monoheme proteins [7]. UV/vis spectroscopy revealed the ability of the heme cofactors in MsmS and MA0863 to bind imidazole [94, 95] (Master thesis, K. Kwiatkowski) [94]. Therefore, the heme pocket has to be large enough to enable imidazole to bind to the heme cofactor. Such a large heme pocket indicates a low heme to residue ratio. Therefore, covalent attachment might stabilize the heme cofactor inside the binding pocket. Furthermore, a redox activity of the heme cofactors in MsmS and MA0863 was shown. The cytochrome *cd1* nitrite reductase from *Thiosphaera pantotropha* undergoes a ligand switch from histidine-histidine to histidine-methionine upon reduction [155]. Along with this switch a conformational change occurs inside the protein probably leading to the loss of non-covalently bound heme. UV/vis spectra of MsmS and MA0863\_O216K demonstrated for the variants C656A and C620A (with non-covalently bound heme), respectively, neither release of heme, significant differences for heme iron coordination nor influence on autophosphorylation activity. Interestingly, the double variants MsmS\_sGAF2\_C656A/H702G and MsmS\_sGAF2\_C656A/H708G resulted in broader Soret bands than the single variants indicating indeed a stabilization effect of the covalent attachment on the heme and that free heme might be present in the sample. However, the heme still stuck strong enough to the protein and is not lost during protein purification. Due to the postulation of MsmS as a redox sensor, the redox potential of MsmS\_sGAF2 was determined with -95 mV and -75 mV for the oxidation and reduction reactions, respectively [95]. Comparing these data with the midpoint redox potentials of MsmS\_sGAF2\_C656A revealed a reduction of the redox potential by approximately 30 mV with loss of the covalent linkage (Tab. 6.1). Determination of the redox potential of MA0863\_sGAF2 and MA0863\_sGAF2\_C620A failed due to an instability of the protein during the measurements. In *M. acetivorans*, which is an obligate anaerobic organism, the redox potential inside the cell can be defined by the redox potential of hydrogen ( $E^{\circ} = -420$  mV), and the heterodisulfide CoM-S-S-CoB ( $E^{\circ} = -143$  mV) as part of methanogenesis [148]. Therefore, MsmS is most likely present in its reduced form under physiological conditions. As a redox sensor the redox potential is a crucial threshold. Hence, the increase of the redox potential due to the covalent attachment of the heme cofactor might be an important factor for sensing a specific redox signal.

**Table 6.1** Redox potentials of MsmS\_sGAF2 WT and C656A variant. [95]

	MsmS_sGAF2	
	WT	C656A
$E_{ox}$	-95 mV	-111 mV
$E_{red}$	-75 mV	-123 mV
$E_{ox}/E_{red}$	-85 mV	-117 mV

## 6.4 Configuration of the heme cofactor in MsmS and MA0863 is most likely a HS species

UV/vis spectroscopy and RR spectroscopy were performed to get more insights into the heme configuration of MA0863 and MsmS. RR spectroscopy of MsmS\_sGAF2 revealed mostly a 6c low-spin heme for the Fe(III) complex and for the Fe(II) complex a mix of high-spin (HS) and 6c low-spin (6cLS) heme. Interestingly, the UV/vis spectra showed a changing structure in MsmS from a 5c/6c mix to a 6-coordinated heme with each domain added to the sGAF2 variant. This suggests a dependence of the heme coordination not only on the second GAF domain but on the complete structure. In addition, investigation of the effect of oxygen during growth and purification showed that regardless of the growth conditions, anaerobic purification led to an increased amount of HS species in the Fe(II) complex. Recent RR spectra of MA0863\_sGAF2 measured with samples prepared by a current Master student revealed the same results as for MsmS\_sGAF2. Whereas the Fe(III) complex was present mostly as a 6cLS species, the Fe(II) complex was present as a mix of 5cHS and 6cLS heme species (Master thesis, T. Bauer). RR measurements of full-length MA0863 performed in this study revealed a 6-coordinated heme for MA0863\_O216K for the Fe(III) and Fe(II) complex. However, for MsmS a prevailing HS species was observed in the Fe(II) complex comparable to the result of anaerobically purified MsmS\_sGAF2. All in all, these results indicate a native heme state as HS for the Fe(II) and LS for the Fe(III) complex as the conditions of the full-length MsmS and anaerobically purified MsmS\_sGAF2 is most closely to the conditions of protein synthesis in the anaerobic archaeon *M. acetivorans* [76]. These results are similar to the heme state of the horseradish peroxidase HRP-C, present as a mixture of 6cHS and 5cHS forms [55]. Nevertheless, it is unknown whether the distal (sixth) ligand is an amino acid residue or a small molecule.

## 6.5 Putative heme coordinating ligands in MsmS

In order to identify the axial ligands of the heme iron in MsmS, UV/vis spectroscopy was performed. Truncated sGAF2 and full-length variants were constructed containing mutations of putative ligands. For MsmS some variants have already been analyzed in former studies (Master thesis, C. Twittenhoff) [94]. Since these variants were produced with heme

reconstitution which might result in a non-native heme incorporation, they were once again produced using the new method with EcN to verify the results. For further analysis of the axial ligand also new variants of MsmS\_sGAF2 were constructed and interesting amino acid exchanges were introduced into full-length MsmS. UV/vis spectroscopy revealed a significant difference between the wild-type sGAF2 and variant M645A, which is located at the distal site of the heme molecule (Fig. 6.2, green). The Fe(III) complex showed a broader Soret band than for the wild-type. In addition the Fe(II) complex of M645A was present as a 6-coordinated low-spin heme instead of the 5c- and 6c- heme species mix of wild-type sGAF2. Due to no effect of the pH value on the M645A variant it was postulated that this residue not directly coordinates the heme iron but has an impact on other nearby located residues [94]. The histidine residue 646, also located at the distal site (Fig. 6.2, green) did not show an impact on the coordination structure of heme. At the proximal site of the heme molecule the histidine residues 702 and 704 are located (Fig. 6.2, green). The variant sGAF2\_H702G resulted in the strongest differences in the spectral behaviour, indicating an involvement in coordination of the heme at the proximal site. However, His<sub>704</sub> has no impact on the coordination structure. The sGAF2\_H702G variant revealed two distinct Q-bands for the Fe(II) complex representing a 6-coordinated heme iron. Also former UV/vis and RR spectroscopic analysis of this variant produced with heme reconstitution revealed a large difference to the wild-type (Master thesis, C. Twittenhoff), strongly suggesting the His<sub>702</sub> as a putative proximal ligand in MsmS. The switch from a 5c/6c heme mix to a 6-coordinated Fe(II) complex comparing wild-type and H702G variant was not observed for full-length MsmS as the full-length wild-type is not present as a mixture of heme species. However, the full-length H702G variants showed strong shifts of the Soret band and Q-bands in comparison to the wild-type. UV/vis spectroscopy of the variant H708G revealed a slight impact on heme iron coordination. As this residue is located in vicinity of the heme molecule (Fig. 6.2, green) it cannot function as an axial ligand. But it might play a role for stability of the protein and thereby effects the heme coordination. Two additional sGAF2

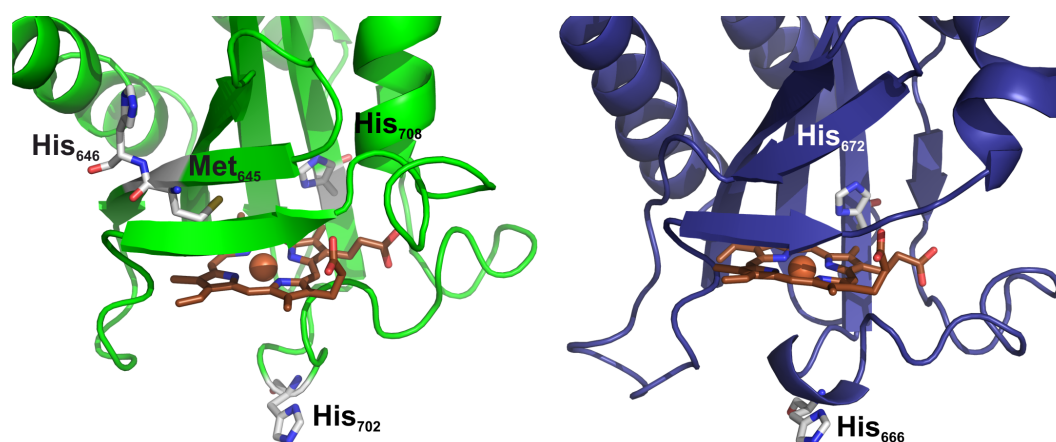


**Figure 6.2 Structural models of second GAF domains with putative heme ligands.** Model structure of MsmS\_sGAF2 (green) and MA0863\_sGAF2 (blue) with putative axial heme iron ligands. Models were constructed using PHYRE2 and PyMOL.

variants, K661G and Y665F, did not reveal any impact on the heme coordination. Some of the MsmS\_sGAF2 variants were analyzed by RR spectroscopy in a cooperation project (C. J. Querebillo, unpublished data, TU Berlin). RR measurements revealed no differences for the Fe(III) complex of the measured variants as all proteins are present as a 6c low-spin and 5c-high-spin heme. Therefore, these results imply that even when a single axial ligand is mutated, another residue might serve as a ligand. Together with the UV/vis results, a heme pocket with a flexible structure is suggested. These measurements support the results of UV/vis spectroscopy indicating His<sub>702</sub> as a putative proximal ligand. However, RR data revealed His<sub>702</sub> playing also a role as a hydrogen bond donor to another nearby located residue, like in the cytochrome c peroxidase from *Saccharomyces cerevisiae* [136]. In addition, His<sub>646</sub> was found to play a role for coordination which did not show an impact in UV/vis spectroscopy. RR spectroscopy is more precisely in analyzing heme coordination, therefore, more information of the heme coordination can be obtained by this method. Furthermore, it is assumed that the 6th ligand is not an amino acid residue but a small molecule like H<sub>2</sub>O. The binding of a small molecule might be assisted by His<sub>646</sub>.

## 6.6 Putative heme coordinating ligands in MA0863

Due to the high sequence similarity between MsmS and MA0863 the putative heme iron ligands found in MsmS are also present in MA0863. Thereby, the histidine residues His<sub>702</sub>, His<sub>704</sub> and His<sub>708</sub> in MsmS correspond to the residues His<sub>666</sub>, His<sub>668</sub> and His<sub>672</sub> in MA0863. First UV/vis measurements were performed with proteins produced with heme reconstitution. The obtained spectra revealed a strong impact of His<sub>666</sub> on the heme coordination. While the Fe(II) complex of wild-type MA0863\_sGAF2 is present as a 6-coordinated heme, variant H666G depicted a mixture of 5c and 6c heme species. His<sub>672</sub>, which is located next to the heme molecule (Fig. 6.2, blue), did show a less effect on heme coordination than His<sub>666</sub> whereas Lys<sub>625</sub> is not involved in heme coordination. Therefore, His<sub>666</sub> is suggested to be the proximal ligand (Fig. 6.2, blue). These results corresponds with the results of MsmS\_sGAF2. Also the full-length variants of His<sub>666</sub> and His<sub>672</sub> revealed distinct differences to the wild-type protein indicating both residues playing a role for the heme iron coordination. In the single variants H666G and H672G a switch between amino acid residues might occur. Therefore, the double H666G/H672Q and triple H666G/H668G/H672Q sGAF2 variants were constructed. Interestingly, the single H666G variant did show the strongest effect on heme coordination. When produced in EcN with incorporation of the heme cofactor during protein production, the yield of purified protein containing mutations of His to Gly, is much lower than for the wild-type protein. The mutations led to a more unstable protein, which is also supported by the finding that the full-length H672Q variant can be produced and purified but not the H672G variant. The histidine to glycine exchange might destabilize the protein. Therefore, it would be necessary to construct the double and triple mutant with

glutamine exchanges for all histidine residues to test whether the differences are due to a destabilized protein structure or not.

## 6.7 MA0863 is a redox sensor similar to MsmS

MA0863 was found to possess a redox dependent autophosphorylation activity. Due to its high similarity with MsmS the redox dependent activity was first attributed to the redox-active heme cofactor. Therefore, molecules like CO or DMS, which are both present during methanogenesis, were hypothesized to bind to the heme iron as putative signals. Formation of Fe(III)-DMS, Fe(II)-DMS and Fe(II)-CO complex were already shown before (Masterthesis, K. Kwiatkowski) [95] but they did not have an impact on autophosphorylation activity of MsmS or MA0863\_O216K. With a redox potential of  $\sim -85$  mV for MsmS the sensors are most likely present in their reduced form under physiological conditions. As *M. acetivorans* is an obligate anaerobic organism [32] oxygen is unlikely to be the signal for oxidation. Both redox sensors are associated to regulator proteins activating the expression of three corrinoid/methyltransferase (*mts*) fusion proteins known to play a role during methylotrophic methanogenesis [14, 95, 108]. Therefore, MA0863 was renamed in RdmS (redox dependent methyltransferase-associated Sensor). The "oxidizing" condition activating the kinases and leading to autophosphorylation might be generated by this pathway representing the redox state inside the cell. Sensing the signal further activates the expression of the *mts* genes. One candidate signal is the heterodisulfide CoM-S-S-CoB. A reduced flux through methanogenesis might lead to its accumulation when appropriate substrates get scarce.

## 6.8 Redox sensing is probably mediated by thiol/disulfide switch

Interestingly, incubation of MsmS and RdmS\_O216K with the reduced CoM-SH resulted in a decreased autophosphorylation activity but did not show an impact on the heme redox state, questioning whether the heme cofactor is sensing the redox change. Indeed kinase assays of apo-RdmS\_O216K revealed a heme-independent redox sensing, indicating a different redox sensing mechanism. Due to the results of the Ellmann's Assay and kinase assays with reducing agents specific for disulfide bonds, redox sensing is most likely mediated by redox active cysteine residues forming disulfide bonds. The oligomerization state of the kinases is not redox dependent assuming the disulfide bonds to be intracellular within one protein molecule. Interestingly, in the BACTH analysis MsmS interacts only with itself when incubated under anaerobic/reducing conditions. Unfortunately, it could not be determined whether the kinase is present in its phosphorylated or dephosphorylated form when produced in *E. coli* under aerobic or anaerobic conditions. The formation of the



disulfide bond under oxidizing conditions might result in a conformational change inside the protein leading to autophosphorylation of the kinase (Fig. 6.3). Single exchanges of the twelve present cysteine residues in RdmS did not reveal a loss of activity. This observation might indicate the presence of more than one disulfide bond in the oxidized protein. In addition, a switch between nearby located cysteine residues might occur. Five of the twelve cysteine residues of RdmS are conserved in the sequence compared to MsmS (Fig. 6.4). In addition, an alignment of RdmS, MsmS, two histidine kinases and eight PAS-domain S-box proteins from methanogenic Archaea, identified in a BLASTp search, revealed conserved cysteine residues. Cys<sub>514</sub> and Cys<sub>933</sub> of RdmS are conserved in 80% and 90% of the aligned sequences, respectively. Conserved cysteine residues in particular, are candidates for having a specific function. Currently the identity of cysteine residues involved in redox sensing is under investigation in our lab as part of a master thesis.

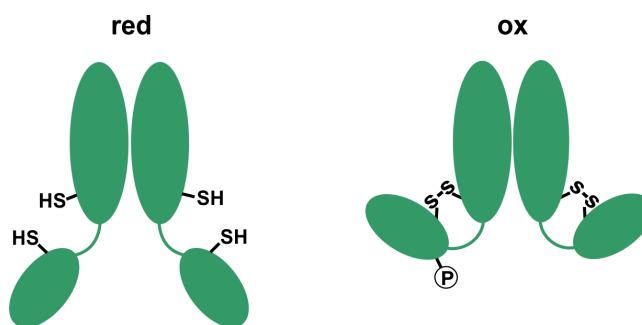


**Figure 6.3 Model for putative activation/oxidation reaction.** Under reducing conditions the cysteine residues are present as free thiol groups and the kinases are inactive. Therefore, no autophosphorylation occurs. Upon oxidation, intramolecular disulfide bonds are formed resulting in a conformational change and activation of the kinases. (modified from [94])

The thiol/disulfide switch is a common redox sensing mechanism monitoring changes of cellular redox state, oxygen or reactive oxygen species [4]. The sensor OxyR from *E. coli*, for example, is activated by the formation of an intracellular disulfide bond due to hydrogen peroxide [166]. Another example is the transcriptional regulator MsvR from *M. acetivorans*. For MsvR six cysteines residues were postulated to be involved in the formation of disulfide bonds upon oxidation by ROS. In addition, it was shown that MsvR can be reduced and thereby reactivated by the NADPH-dependent thioredoxin system of *M. acetivorans* [129]. The thioredoxin system consisting of thioredoxin reductase (TrxR) and thioredoxin (trx) is the most ubiquitous thiol-disulfide exchanges system found in all living cells [92]. It maintains the cellular redox state and reduces disulfides in certain proteins. Interestingly, a glutaredoxin-like protein was identified for *M. acetivorans*, named Methanoredoxin (MRX) [163]. MRX was postulated to utilize coenzyme M (CoM-SH) as reductant for insulin disulfide reductase activity. CoM-SH was reported to belong to the low-molecular weight thiol protective systems in prokaryotes as a putative analogous redox regulator to glutathione [135]. In this way CoM-SH may work as a thiol protectant of MsmS and RdmS after a local

redox change of the redox potential led to the formation of disulfide bonds inside the sensor kinases.

## 6.9 Heme cofactor might integrate a second signal

When the heme cofactor is not responsible for redox sensing, then which function does it have for the kinases? The covalent attachment of the heme cofactor was shown to be no artefact from the recombinant production in *E. coli* as it is also present in the protein when purified from *M. acetivorans* [95]. Due to the ability of the heme cofactors in MsmS and RdmS to bind small molecules like CO and DMS it is proposed that the kinases sense the availability of substrates belonging to methanogenesis. UV/vis spectroscopy showed the ability of the heme cofactors in RdmS and MsmS to bind these molecules. Heme irons are well known to bind external ligands. Furthermore, for MsmS a comparatively high affinity to sulfur ligands was shown [138]. For an H-NOX protein from *V. cholerae* it was postulated that the protein without the heme cofactor was still able to sense redox changes conducted by the reversible oxidation of Cys residues [98]. Mukhopadyay *et al.* suggested a dual sensor for NO and redox changes. Therefore, the kinases RdmS and MsmS are suggested to not only sense the redox state inside the cell but also the presence of alternative substrates, like DMS. In this study the autophosphorylation activities of MsmS and RdmS were only tested *in vitro* with purified proteins. *In vivo*, sensing two signals might play a role for the interaction of the kinases with the regulators. A stepwise phosphorylation of specific amino acid residues within the kinases is conceivable, which could be dependent on the presence of two signals. Sensing multiple signals can be found for several sensors [86, 132].

## 6.10 Incorporation of pyrrolysine into RdmS in *E. coli*

Not many organisms are able to synthesize the 22<sup>nd</sup> amino acid pyrrolysine and incorporate it into proteins. Coproduction of the pyrrolysine biosynthesis machinery, tRNA synthetase and tRNA<sup>Pyl</sup> with RdmS resulted in a small amount of full-length protein. As in *E. coli* the UAG amber codon is usually recognized as a stop codon, a strong protein band was observed at ~25 kDa representing the truncated protein. However, mass spectrometry identified peptides beyond the UAG codon for the low amount of full-length protein. Therefore, the protein was used for further experiments as the wild-type protein. After purification, several truncated variants were observed on the SDS-PAGE and western blot of RdmS. As these bands were also detectable via the C-terminal *StrepII*-tag, the bands likely represent degradation products of the full-length protein, implying an unstable incorporation of Pyl in comparison to the O216K variant. Mass spectrometry was unable to definitely identify pyrrolysine incorporated at position 216. Former studies using the *pyl* coexpression system have successfully shown that this method is sufficient for pyrrolysine incorporation [84].



Feeding *E. coli* with additional substrates have shown that the tRNA can also bind pyrrolysine analogues and incorporate them into a protein [118]. However, no additional substrates were added in our experiment, excluding the incorporation of an analogue molecule. To enhance the production yield of the full-length protein the expression conditions need to be improved. One possibility is to add L-lysine to the growth culture to support the production of pyrrolysine inside *E. coli*. Another option is to produce the protein under anaerobic conditions as the protein PylB (conversion of lysine to methyl-D-ornithine) belongs to the radical S-adenosylmethionine enzyme family and contains an iron-sulfur cluster [38, 124]. Hence, PylB is likely to be sensitive to oxygen. This would result in a low activity of the protein leading to limited pyrrolysine production.

## 6.11 Role of pyrrolysine in RdmS

In the family *Methanosarcinaceae* pyrrolysine was found in mono-, di- and trimethyltransferases with a specific function [112]. However, it can also be present as a "normal" amino acid residue without an additional function. In the methyltransferase MtmB, the pyrrolysine residue is located within the active center catalyzing the transfer of methyl groups from methylamines to a corrinoid protein [49]. Pyl might be recruited/retained in the genetic code due to its unique properties [70]. Pyl is the first example of an electrophilic residue which is genetically encoded. This led to the assumption that the pyrrolysine residue in RdmS also possess a specific role as the kinase is associated to the Mts-system. However, all experiments (covalent binding, heme iron coordination and autophosphorylation activity) conducted during this study with RdmS did not show any differences to the O216K variant. Nevertheless, it cannot be ruled out that pyrrolysine has additional function in RdmS like signal perception. This has to be further investigated especially with *in vivo* experiments. Constructing a RdmS deletion mutant complemented with the O216K variant would help to understand the role of the Pyl residue. In MsmS, the same position is occupied with a lysine residue. Due to the high homology between these two kinases the Pyl codon can also be retained in RdmS by neutral evolution like in the tRNA<sup>His</sup> guanylyltransferase from *M. acetivorans* [51]. The transferase is not essential for the organism and Pyl does not lead to an evolutionary disadvantage.

## 6.12 Signaltransduction by MsmS and RdmS - no typical two-component system

Both kinases lack the conserved H-box for phosphorylation as it is typically found in classical histidine kinases. For MsmS it was shown that it is probably phosphorylated on serine and tyrosine residues [94]. Thin layer chromatography of RdmS\_O216K revealed a phos-

phorylation on a tyrosine residue. For further analysis of signal transduction between the kinases and regulators, identification of the phosphorylation sites is crucial. Mass spectrometry in combination with phosphopeptide enrichment might be an option to resolve this.

Phosphorylation on serine and tyrosine is widely distributed in Eukaryotes but it can also be found in Archaea [1, 63, 109]. The only example of a bacterial sensor kinase phosphorylated on a tyrosine residue is DivL from *Caulobacter crescentus* [161]. In DivL the conserved histidine residue of the regular H-box is replaced by a tyrosine residue. In the domain of Archaea, only one kinase is described until now, which is phosphorylated at a threonine residue: ST1565 from *Sulfolobus tokadaii* [154]. For ST1565 one threonine residue was postulated to stimulate autophosphorylation and another leads to a loss of activity when exchanged. In addition it was shown that ST1565 is able to phosphorylate a forkhead-associated-domain-containing protein. Therefore, phosphotransfer from a kinase, not phosphorylated at a histidine residue, is possible. However, the regulator proteins MsrG/F/C lack a receiver domain containing the conserved aspartate phosphoacceptor residue. Thus far, a phosphotransfer typical for His-Asp phosphorylation of classical two-component systems was not observed for MsmS and RdmS. Nevertheless, BACTH analysis revealed an interaction of both kinases with all three regulators. In addition, protein-protein interaction studies of MsrG combined with truncated MsmS variants imply the requirement of the full-length kinase for the kinase/regulator interaction. Interaction between kinase and regulator might occur via one of the PAS domains. PAS domains play a role for protein-protein interactions like for the HLH/PAS dioxin receptor-Arnt transcription factor complex [82]. MsmS and RdmS do not contain a classical Dhp domain for dimerization and phosphorylation. However, BACTH analyses revealed the region for forming homodimers of MsmS as the C-terminus, the second GAF domain or H\_ATPase domain. In summary, the proteins do not form a two-component system but rather a multicomponent cross-interacting system. Cross-talk between TCS has already been reported. For example, the *E. coli* TCSs PmrAB and EnvZ-OmpR cross-interact with QseBC and ArcBA [44, 87], respectively. In *Bacillus anthracis* the TCSs HssRS and HitRS cross-regulate each other [93].

Western blot analysis of wild-type cells have revealed a dependence of MtsF bioynthesis on the presence of the kinase MsmS only when grown with DMS in the growth medium [95]. In contrast, the methyltransferase was also detectable in the absence of the kinase MsmS when no DMS was in the medium (Fig. 1.6, B & Fig. 6.5). Therefore, the kinases might negatively regulate the expression of the *mts* genes. Putting all the findings together, a hypothesis for RdmS and MsmS can be proposed: In the reduced state, the redox active cysteine residues are present as thiol groups. Under these conditions, the kinases directly interact/bind a regulator and inhibit the activation of *mts* transcription. Upon oxidation and formation of disulfide bonds, a conformational change occurs in the kinase resulting in the release of the regulator and binding to the *mts* promoter (Fig. 6.5, A). The exact role of the heme cofactor and the integration of the phosphorylation signal is currently still unknown. In or-

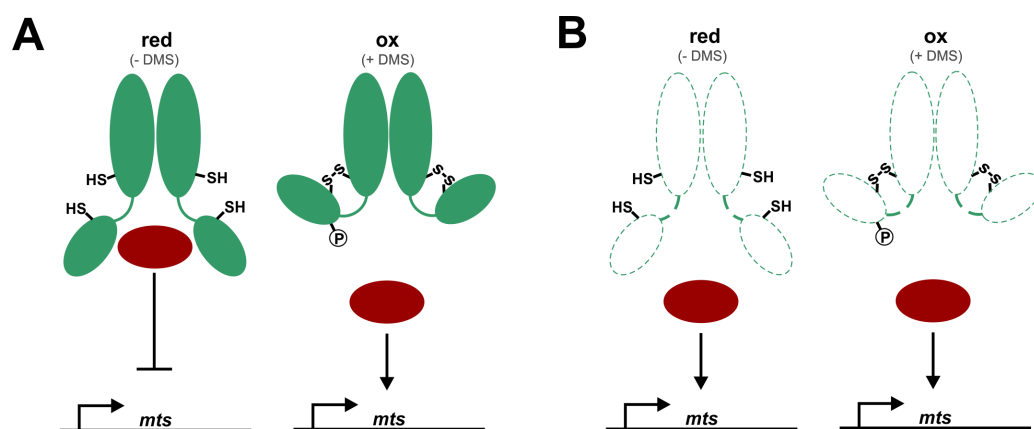


**Figure 6.5 Models for putative signal transduction cascades based on collected data.** Schematic presentation of kinases in green and regulator proteins in red. **(A)** The reduced kinase (w/o DMS) interacts with the regulator and inhibits activation of *mts* transcription. Oxidation of the redox active thiols lead to a release of the regulator which can bind to the *mts* promoter and activate expression (DMS present in growth medium). **(B)** In the absence of MsmS the regulator is free and activates transcription of *mts* genes independent of DMS presence. (modified from [94])

der to further analyze the signal transduction pathway, additional analyses of kinase deletion strains in combination with regulator deletions would be advantageous. Furthermore, other protein partners might be required for full activity of the regulators. In this regard, co-immunoprecipitation experiments are currently under way in our laboratory. Thus far, we were unable to detect any functional differences between MsmS and RdmS. Therefore, future experiments will be directed towards the specific role of the individual kinases.

### 6.13 MsmS and RdmS belong to the methylsulfide metabolism of *M. acetivorans*

The three corrinoid/methyltransferase fusion proteins MtsH/D/F were found to be regulated by the adjacent encoded transcriptional regulators MsrG/F/C, respectively [14, 108]. In the vicinity of these three regulators the genes for the three sensor kinases MsmS, RdmS and MA4377 are encoded. All current data suggest a cross-interaction of the sensor kinases with the Msr-regulators to regulate the expression of the *mts* genes. Association of the kinases to the Mts-proteins link them to the methylsulfide metabolism of *M. acetivorans*. Quantification of mRNA levels have shown that the transcription of the Mts-proteins is upregulated when grown on CO and methylated compound like DMS or MeSH with substrate preferences for single isozymes. Mutational analysis have also revealed that they are required for DMS formation when grown on CO and for growth on methylmercaptopropionate (MMPA). [14, 31, 108]. In addition, MtsF was shown to possess a  $\text{CH}_3\text{-H}_4\text{MPT:CoM}$  methyltransferase activity [31]. Taking all findings of mutational analysis and mRNA quantification together, MtsF/D/H use a broad range of substrates for methyl group transfer (Fig. 6.6). Bypass-

ing the membrane bound, energy-conserving Mtr CoM:H: 4MPT methyltransferase as well as introducing methyl groups into to oxidative and reductive branch of methylotrophic methanogenesis would be an advantage when growing on low-energy substrates, such as DMS. However, CoM:H<sub>4</sub>MPT methyltransferase activity of both Mts and Mtr at the same time is not efficient. Due to a specific condition, oxidized cofactors of methanogenesis might accumulate inside the cell resulting in an reduced activity of the MtrA-H complex and a decrease flux of methanogenesis. The cellular redox potential raises leading to an oxidation of the sensor kinases MsmS and RdmS. The kinases get activated/phosphorylated, interact with/release the regulator proteins which subsequently activate the expression of *mts* genes. The Mts proteins then can utilize the alternative low-energy substrate or bypass the Mtr CoM:H<sub>4</sub>MPT methyltransferase step. After reorganization of metabolism, the kinases are reduced by CoM-SH and Methanoredoxin and expression of *mts* genes stops.

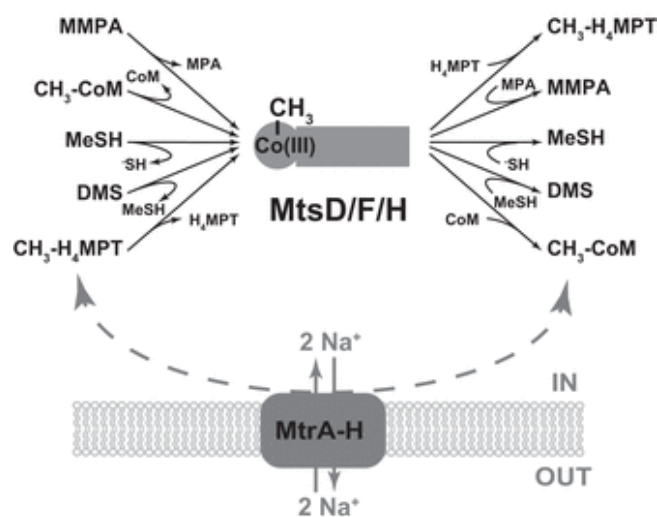


**Figure 6.6** Putative functions of MtsF/D/H in methylsulfide metabolism of *M. acetivorans*. Schematic overview of proposed substrate range of MtsF/D/H. The three proteins are assumed to be able to bypass the usual energy conserving Mtr H<sub>4</sub>MPT:CoM methyltransferase step as well as utilizing methylated compounds for introducing methyl groups into the reductive and oxidative branch of methylotrophic methanogenesis [31].

## 7 Summary

MsmS is a heme-based redox sensor kinase in *Methanosarcina acetivorans* consisting of alternating PAS and GAF domains connected to a C-terminal kinase domain. In addition to MsmS, *M. acetivorans* possesses a second kinase, MA0863 with high sequence similarity. Interestingly, MA0863 possesses an amber codon in its second GAF domain, encoding for the amino acid pyrrolysine. Thus far, no function of this residue has been resolved.

In order to examine the heme iron coordination in both proteins, an improved method for the production of heme proteins was established using the *Escherichia coli* strain Nissle 1917. This method enables the complete reconstitution of a recombinant hemoprotein during protein production, thereby resulting in a native heme coordination. Analysis of the full-length MsmS and MA0863 confirmed a covalently bound heme cofactor, which is connected to one conserved cysteine residue in each protein. In order to identify the coordinating amino acid residues of the heme iron, UV/vis spectra of different variants were measured. These studies revealed His<sub>702</sub> in MsmS and the corresponding His<sub>666</sub> in MA0863 as the proximal heme ligands.

MsmS has previously been described as a heme-based redox sensor. In order to examine whether the same is true for MA0863, redox dependent kinase assays were performed. MA0863 indeed displays redox dependent autophosphorylation activity, which is independent of heme ligands and only observed under oxidizing conditions. Interestingly, autophosphorylation was shown to be independent of the heme cofactor but rather relies on thiol oxidation. Therefore, MA0863 was renamed in RdmS (redox dependent methyltransferase-associated sensor). In order to identify the phosphorylation site of RdmS, thin layer chromatography was performed identifying a tyrosine as the putative phosphorylation site. This observation is in agreement with the lack of a so-called H-box in typical histidine kinases.

Due to their genomic localization, MsmS and RdmS were postulated to form two-component systems (TCS) with vicinal encoded regulator proteins MsrG and MsrF. Therefore, protein-protein interaction studies using the bacterial adenylate two hybrid system were performed suggesting an interaction of RdmS and MsmS with the three regulators MsrG/F/C. Due to these multiple interactions these signal transduction pathways should rather be considered multicomponent system instead of two component systems.



## 8 Zusammenfassung

MsmS ist eine Häm-basierte Redox-Sensorkinase aus *Methanosarcina acetivorans*. Sie besteht aus alternierenden PAS und GAF Domänen und einer C-terminalen Kinasedomäne. Zusätzlich zu MsmS, besitzt *M. acetivorans* eine zweite Kinase, MA0863, mit einer hohen Sequenzähnlichkeit zu MsmS. Interessanterweise enthält MA0863 ein Amber-Codon in der zweiten GAF Domäne, das für die Aminosäure Pyrrolysin kodiert. Bisher ist keine Funktion für diesen Aminosäurerest bekannt.

Um die Koordination des Hämeisens in beiden Proteinen zu untersuchen, wurde eine verbesserte Methode zur Produktion von Hämproteinen entwickelt. Für diese wurde der *Escherichia coli* Stamm Nissle 1917 verwendet, der die vollständige Rekonstitution des rekombinanten Hämproteins während der Proteinproduktion ermöglicht. Dadurch kann eine native Hämkoordination erhalten werden. Analysen von MsmS und MA0863 als Vollängen-Protein bestätigten einen kovalent gebundenen Hämkofaktor, der über einen konservierten Cysteinrest in jedem Protein gebunden ist. Um die koordinierenden Aminosäurereste zu identifizieren, wurden UV/vis Spektren verschiedener Varianten gemessen. Diese ergaben, dass H<sub>702</sub> in MsmS und das entsprechende H<sub>666</sub> in MA0863 als proximale Hämliganden dienen.

Im Vorfeld wurde MsmS als Häm-basierter Redoxsensor beschrieben. Um zu untersuchen, ob dies auch auf MA0863 zutrifft, wurden redox-abhängige Kinase-Assays durchgeführt. So konnte für MA0863 ebenfalls eine redox-abhängige Autophosphorylierungs-Aktivität festgestellt werden, die unabhängig von Hämliganden ist und nur unter oxidierenden Bedingungen auftritt. Interessanterweise konnte gezeigt werden, dass die Autophosphorylierung unabhängig vom Hämkofaktor ist, sondern auf die Oxidation von Thiolen zurückgeführt werden kann. Daher wurde MA0863 in RdmS (Redox deependent methyltransferase-associated Sensor) umbenannt. Um die Phosphorylierungsstelle in RdmS zu identifizieren, wurde eine Dünnschicht-Chromatographie durchgeführt, die Tyrosin als putative Phosphorylierungsstelle identifizierte. Diese Beobachtung steht im Einklang mit der nicht vorhandenen H-box in typischen Histidinkinasen.

Auf Grund der genomischen Lokalisation wurde für MsmS und RdmS postuliert, dass sie Zwei-Komponenten Systeme (ZWS) mit den in unmittelbarer Nähe kodierten Regulatorproteinen MsrG und MsrF bilden. Daher wurden Protein-Protein Interaktions-Analysen mittels dem Bacterial Two-Hybrid-System durchgeführt, die auf eine Interaktion von MsmS und RdmS mit den drei Regulatoren MsrG/F/C hindeuten. Infolge dieser mehrfachen Interaktionen dieser Signaltransduktionssysteme sollten sie eher als Multikomponenten System bezeichnet werden und nicht als Zwei-Komponenten System.

# References

- [1] M. Aivaliotis, B. Macek, F. Gnad, P. Reichelt, M. Mann, and D. Oesterhelt. Ser/Thr/Tyr protein phosphorylation in the archaeon *Halobacterium salinarum*—a representative of the third domain of life. *PloS one*, 4(3):e4777, 2009.
- [2] C. Albermann, N. Trachtmann, and G. A. Sprenger. A simple and reliable method to conduct and monitor expression cassette integration into the *Escherichia coli* chromosome. *Biotechnology Journal: Healthcare Nutrition Technology*, 5(1):32–38, 2010.
- [3] A. Ambrogelly, S. Palioura, and D. Söll. Natural expansion of the genetic code. *Nature Chemical Biology*, 3(1):29–35, 2007.
- [4] H. Antelmann and J. D. Helmann. Thiol-based redox switches and gene regulation. *Antioxidants & Redox Signaling*, 14(6):1049–1063, 2011.
- [5] M. K. Ashby. Distribution, structure and diversity of “bacterial” genes encoding two-component proteins in the Euryarchaeota. *Archaea*, 2(1):11–30, 2006.
- [6] F. Åslund, M. Zheng, J. Beckwith, and G. Storz. Regulation of the OxyR transcription factor by hydrogen peroxide and the cellular thiol—disulfide status. *Proceedings of the National Academy of Sciences*, 96(11):6161–6165, 1999.
- [7] P. D. Barker and S. J. Ferguson. Still a puzzle: why is haem covalently attached in c-type cytochromes? *Structure*, 7(12):R281–R290, 1999.
- [8] R. F. Beers and I. W. Sizer. A spectrophotometric method for measuring the breakdown of hydrogen peroxide by catalase. *Journal of Biological Chemistry*, 195(1):133–140, 1952.
- [9] E. A. Berry and B. L. Trumpower. Simultaneous determination of hemes a, b, and c from pyridine hemochrome spectra. *Analytical Biochemistry*, 161(1):1–15, 1987.
- [10] A. Bilaska-Wilkosz, M. Iciek, M. Górny, and D. Kowalczyk-Pachel. The role of hemo-proteins: Hemoglobin, myoglobin and neuroglobin in endogenous thiosulfate production processes. *International Journal of Molecular Sciences*, 18(6):1315, 2017.
- [11] P. Boccazzi, J. K. Zhang, and W. W. Metcalf. Generation of Dominant Selectable Markers for Resistance to Pseudomonic Acid by Cloning and Mutagenesis of the *ileS* Gene from the Archaeon *Methanosarcina barkeri* Fusaro. *Journal of Bacteriology*, 182(9):2611–2618, 2000.

- [12] G. Borrel, N. Parisot, H. M. Harris, E. Peyretailade, N. Gaci, W. Tottey, O. Bardot, K. Raymann, S. Gribaldo, P. Peyret, et al. Comparative genomics highlights the unique biology of *Methanomassiliicoccales*, a Thermoplasmatales-related seventh order of methanogenic archaea that encodes pyrrolysine. *BMC Genomics*, 15(1):679, 2014.
- [13] A. Bose, M. A. Pritchett, M. Rother, and W. W. Metcalf. Differential regulation of the three methanol methyltransferase isozymes in *Methanosarcina acetivorans* C2A. *Journal of Bacteriology*, 188(20):7274–7283, 2006.
- [14] A. Bose, G. Kulkarni, and W. W. Metcalf. Regulation of putative methyl-sulphide methyltransferases in *Methanosarcina acetivorans* C2A. *Molecular Microbiology*, 74(1):227–238, 2009.
- [15] M. Breuer, K. M. Rosso, J. Blumberger, and J. N. Butt. Multi-haem cytochromes in *Shewanella oneidensis* MR-1: structures, functions and opportunities. *Journal of the Royal Society Interface*, 12(102):20141117, 2015.
- [16] D. Burbulys, K. A. Trach, and J. A. Hoch. Initiation of sporulation in *B. subtilis* is controlled by a multicomponent phosphorelay. *Cell*, 64(3):545–552, 1991.
- [17] J. Cheung and W. A. Hendrickson. Sensor domains of two-component regulatory systems. *Current Opinion in Microbiology*, 13(2):116–123, 2010.
- [18] H. Y. Cho, H. J. Cho, Y. M. Kim, J. I. Oh, and B. S. Kang. Structural insight into the heme-based redox sensing by DosS from *Mycobacterium tuberculosis*. *Journal of Biological Chemistry*, 284(19):13057–13067, 2009.
- [19] P. J. Cock and D. E. Whitworth. Evolution of prokaryotic two-component system signaling pathways: gene fusions and fissions. *Molecular Biology and Evolution*, 24(11):2355–2357, 2007.
- [20] K. C. Costa and J. A. Leigh. Metabolic versatility in methanogens. *Current Opinion in Biotechnology*, 29:70–75, 2014.
- [21] D. A. Dalton, L. D. del Castillo, M. L. Kahn, S. L. Joyner, and J. M. Chatfield. Heterologous expression and characterization of soybean cytosolic ascorbate peroxidase. *Archives of Biochemistry and Biophysics*, 328(1):1–8, 1996.
- [22] K. A. Datsenko and B. L. Wanner. One-step inactivation of chromosomal genes in *Escherichia coli* K-12 using PCR products. *Proceedings of the National Academy of Sciences*, 97(12):6640–6645, 2000.
- [23] S. Demolli, M. M. Geist, J. E. Weigand, N. Matschiavelli, B. Suess, and M. Rother. Development of  $\beta$ -lactamase as a tool for monitoring conditional gene expression by a tetracycline-riboswitch in *Methanosarcina acetivorans*. *Archaea*, 2014, 2014.

- [24] U. Deppenmeier, V. Müller, and G. Gottschalk. Pathways of energy conservation in methanogenic archaea. *Archives of Microbiology*, 165(3):149–163, 1996.
- [25] U. Deppenmeier, A. Johann, T. Hartsch, R. Merkl, R. A. Schmitz, R. Martinez-Arias, A. Henne, A. Wiezer, S. Bäumer, C. Jacobi, et al. The genome of *Methanosarcina mazei*: evidence for lateral gene transfer between bacteria and archaea. *Journal of Molecular Microbiology and Biotechnology*, 4(4):453–461, 2002.
- [26] C. Ehlers, K. Weidenbach, K. Veit, U. Deppenmeier, W. W. Metcalf, and R. A. Schmitz. Development of genetic methods and construction of a chromosomal glnK 1 mutant in *Methanosarcina mazei* strain Gö1. *Molecular Genetics and Genomics*, 273(4):290–298, 2005.
- [27] D. Esser, T. Pham, J. Reimann, S. Albers, B. Siebers, and P. Wright. Change of carbon source causes dramatic effects in the phospho-proteome of the archaeon *Sulfolobus solfataricus*. *Journal of Proteome Research*, 11(10):4823–4833, 2012.
- [28] R. C. Fahey. Novel thiols of prokaryotes. *Annual Reviews in Microbiology*, 55(1):333–356, 2001.
- [29] K. Fiege and N. Frankenberg-Dinkel. Thiol-based redox sensing in the methyltransferase associated sensor kinase Rdms in *Methanosarcina acetivorans*. *Environmental Microbiology*, 2019, in press.
- [30] K. Fiege, C. J. Querebillo, P. Hildebrandt, and N. Frankenberg-Dinkel. Improved Method for the Incorporation of Heme Cofactors into Recombinant Proteins Using *Escherichia coli* Nissle 1917. *Biochemistry*, 57(19):2747–2755, 2018.
- [31] H. Fu and W. W. Metcalf. The genetic basis for metabolism of methylated sulfur compounds in *Methanosarcina*. *Journal of Bacteriology*, 197(8):1515–1524, 2015.
- [32] J. E. Galagan, C. Nusbaum, A. Roy, M. G. Endrizzi, P. Macdonald, W. FitzHugh, S. Calvo, R. Engels, S. Smirnov, D. Atnoor, et al. The genome of *M. acetivorans* reveals extensive metabolic and physiological diversity. *Genome Research*, 12(4):532–542, 2002.
- [33] M. Y. Galperin. A census of membrane-bound and intracellular signal transduction proteins in bacteria: bacterial IQ, extroverts and introverts. *BMC Microbiology*, 5(1):35, 2005.
- [34] M. Y. Galperin. Diversity of structure and function of response regulator output domains. *Current Opinion in Microbiology*, 13(2):150–159, 2010.

- [35] M. Y. Galperin, K. S. Makarova, Y. I. Wolf, and E. V. Koonin. Phyletic distribution and lineage-specific domain architectures of archaeal two-component signal transduction systems. *Journal of Bacteriology*, 200(7):e00681–17, 2018.
- [36] R. Gao and A. M. Stock. Biological insights from structures of two-component proteins. *Annual Review of Microbiology*, 63:133–154, 2009.
- [37] M. A. Gaston, R. Jiang, and J. A. Krzycki. Functional context, biosynthesis, and genetic encoding of pyrrolysine. *Current Opinion in Microbiology*, 14(3):342–349, 2011.
- [38] M. A. Gaston, L. Zhang, K. B. Green-Church, and J. A. Krzycki. The complete biosynthesis of the genetically encoded amino acid pyrrolysine from lysine. *Nature*, 471(7340):647, 2011.
- [39] S. C. Gill and P. H. Von Hippel. Calculation of protein extinction coefficients from amino acid sequence data. *Analytical Biochemistry*, 182(2):319–326, 1989.
- [40] M. A. Gilles-Gonzalez, G. S. Ditta, and D. R. Helinski. A haemoprotein with kinase activity encoded by the oxygen sensor of *Rhizobium meliloti*. *Nature*, 350(6314):170, 1991.
- [41] H. M. Girvan and A. W. Munro. Heme sensor proteins. *Journal of Biological Chemistry*, 288(19):13194–13203, 2013.
- [42] S. G. Grant, J. Jessee, F. R. Bloom, and D. Hanahan. Differential plasmid rescue from transgenic mouse DNAs into *Escherichia coli* methylation-restriction mutants. *Proceedings of the National Academy of Sciences*, 87(12):4645–4649, 1990.
- [43] L. Grozdanov, C. Raasch, J. Schulze, U. Sonnenborn, G. Gottschalk, J. Hacker, and U. Dobrindt. Analysis of the genome structure of the nonpathogenic probiotic *Escherichia coli* strain Nissle 1917. *Journal of Bacteriology*, 186(16):5432–5441, 2004.
- [44] K. R. Guckes, M. Kostakioti, E. J. Breland, A. P. Gu, C. L. Shaffer, C. R. Martinez, S. J. Hultgren, and M. Hadjifrangiskou. Strong cross-system interactions drive the activation of the QseB response regulator in the absence of its cognate sensor. *Proceedings of the National Academy of Sciences*, 110(41):16592–16597, 2013.
- [45] A. M. Guss, M. Rother, J. K. Zhang, G. Kulkkarni, and W. W. Metcalf. New methods for tightly regulated gene expression and highly efficient chromosomal integration of cloned genes for *Methanosarcina* species. *Archaea*, 2(3):193–203, 2008.
- [46] S. K. Hanks. Genomic analysis of the eukaryotic protein kinase superfamily: a perspective. *Genome Biology*, 4(5):111, 2003.

- [47] S. K. Hanks, A. M. Quinn, and T. Hunter. The protein kinase family: conserved features and deduced phylogeny of the catalytic domains. *Science*, 241(4861):42–52, 1988.
- [48] L. Hannibal, R. Somasundaram, J. Tejero, A. Wilson, and D. J. Stuehr. Influence of heme-thiolate in shaping the catalytic properties of a bacterial nitric oxide synthase. *Journal of Biological Chemistry*, 286(45):39224–39235, 2011.
- [49] B. Hao, W. Gong, T. K. Ferguson, C. M. James, J. A. Krzycki, and M. K. Chan. A new UAG-encoded residue in the structure of a methanogen methyltransferase. *Science*, 296(5572):1462–1466, 2002.
- [50] B. Hao, C. Isaza, J. Arndt, M. Soltis, and M. K. Chan. Structure-based mechanism of O<sub>2</sub> sensing and ligand discrimination by the FixL heme domain of *Bradyrhizobium japonicum*. *Biochemistry*, 41(43):12952–12958, 2002.
- [51] I. U. Heinemann, P. O’Donoghue, C. Madinger, J. Benner, L. Randau, C. J. Noren, and D. Söll. The appearance of pyrrolysine in tRNA<sup>His</sup> guanylyltransferase by neutral evolution. *Proceedings of the National Academy of Sciences*, 106(50):21103–21108, 2009.
- [52] S. Hill, S. Austin, T. Eydmann, T. Jones, and R. Dixon. *Azotobacter vinelandii* NifL is a flavoprotein that modulates transcriptional activation of nitrogen-fixation genes via a redox-sensitive switch. *Proceedings of the National Academy of Sciences*, 93(5):2143–2148, 1996.
- [53] J. A. Hoch. Two-component and phosphorelay signal transduction. *Current Opinion in Microbiology*, 3(2):165–170, 2000.
- [54] S. Hou, R. W. Larsen, D. Boudko, C. W. Riley, E. Karatan, M. Zimmer, G. W. Ordal, and M. Alam. Myoglobin-like aerotaxis transducers in Archaea and Bacteria. *Nature*, 403(6769):540, 2000.
- [55] B. D. Howes, J. N. Rodriguez-Lopez, A. T. Smith, and G. Smulevich. Mutation of distal residues of horseradish peroxidase: influence on substrate binding and cavity properties. *Biochemistry*, 36(6):1532–1543, 1997.
- [56] Z. J. Huang, I. Edery, and M. Rosbash. PAS is a dimerization domain common to *Drosophila* period and several transcription factors. *Nature*, 364(6434):259, 1993.
- [57] T. N. Huynh, L.-L. Chen, and V. Stewart. Sensor-response regulator interactions in a cross-regulated signal transduction network. *Microbiology*, 161(7):1504–1515, 2015.
- [58] F. Jacob-Dubuisson, A. Mechaly, J.-M. Betton, and R. Antoine. Structural insights into the signalling mechanisms of two-component systems. *Nature Reviews Microbiology*, 16:585–593, 2018.

- [59] D. C. Johnson, D. R. Dean, A. D. Smith, and M. K. Johnson. Structure, function, and formation of biological iron-sulfur clusters. *Annual Review of Biochemistry*, 74:247–281, 2005.
- [60] G. Karimova, J. Pidoux, A. Ullmann, and D. Ladant. A bacterial two-hybrid system based on a reconstituted signal transduction pathway. *Proceedings of the National Academy of Sciences*, 95(10):5752–5756, 1998.
- [61] G. Karimova, A. Ullmann, and D. Ladant. Protein-protein interaction between *Bacillus stearothermophilus* tyrosyl-tRNA synthetase subdomains revealed by a bacterial two-hybrid system. *Journal of Molecular Microbiology and Biotechnology*, 3(1):73–82, 2001.
- [62] G. Karimova, N. Dautin, and D. Ladant. Interaction network among *Escherichia coli* membrane proteins involved in cell division as revealed by bacterial two-hybrid analysis. *Journal of Bacteriology*, 187(7):2233–2243, 2005.
- [63] P. J. Kennelly. Protein Ser/Thr/Tyr phosphorylation in the *Archaea*. *Journal of Biological Chemistry*, 289(14):9480–9487, 2014.
- [64] D.-J. Kim and S. Forst. Genomic analysis of the histidine kinase family in bacteria and archaea. *Microbiology*, 147(5):1197–1212, 2001.
- [65] C. Klomsiri, P. A. Karplus, and L. B. Poole. Cysteine-based redox switches in enzymes. *Antioxidants & Redox Signaling*, 14(6):1065–1077, 2011.
- [66] S. Klumpp and J. Krieglstein. Phosphorylation and dephosphorylation of histidine residues in proteins. *European Journal of Biochemistry*, 269(4):1067–1071, 2002.
- [67] P. R. A. Kohler and W. W. Metcalf. Genetic manipulation of *Methanosarcina* spp. *Frontiers in Microbiology*, 3:259, 2012.
- [68] K. K. Koretke, A. N. Lupas, P. V. Warren, M. Rosenberg, and J. R. Brown. Evolution of two-component signal transduction. *Molecular Biology and Evolution*, 17(12):1956–1970, 2000.
- [69] T. Krell. Exploring the (almost) unknown: archaeal two-component systems. *Journal of Bacteriology*, 200(7):e00774–17, 2018.
- [70] J. A. Krzycki. Function of genetically encoded pyrrolysine in corrinoid-dependent methylamine methyltransferases. *Current Opinion in Chemical Biology*, 8(5):484–491, 2004.
- [71] A. Künkel, J. A. Vorholt, R. K. Thauer, and R. Hedderich. An *Escherichia coli* hydrogenase-3-type hydrogenase in methanogenic archaea. *European Journal of Biochemistry*, 252(3):467–476, 1998.

- [72] H. Kurokawa, D.-S. Lee, M. Watanabe, I. Sagami, B. Mikami, C. Raman, and T. Shimizu. A redox-controlled molecular switch revealed by the crystal structure of a bacterial heme PAS sensor. *Journal of Biological Chemistry*, 279(19):20186–20193, 2004.
- [73] I. B. Lansky, G. S. Lukat-Rodgers, D. Block, K. R. Rodgers, M. Ratliff, and A. Wilks. The cytoplasmic heme-binding protein (PhuS) from the heme uptake system of *Pseudomonas aeruginosa* is an intracellular heme-trafficking protein to the  $\delta$ -regioselective heme oxygenase. *Journal of Biological Chemistry*, 281(19):13625–13662, 2006.
- [74] J. A. Leigh, S.-V. Albers, H. Atomi, and T. Allers. Model organisms for genetics in the domain *Archaea*: methanogens, halophiles, *Thermococcales* and *Sulfolobales*. *FEMS Microbiology Reviews*, 35(4):577–608, 2011.
- [75] C. J. Leonard, L. Aravind, and E. V. Koonin. Novel families of putative protein kinases in bacteria and archaea: evolution of the “eukaryotic” protein kinase superfamily. *Genome Research*, 8(10):1038–1047, 1998.
- [76] D. J. Lessner and J. G. Ferry. The archaeon *Methanosarcina acetivorans* contains a protein disulfide reductase with an iron-sulfur cluster. *Journal of Bacteriology*, 189(20):7475–7484, 2007.
- [77] D. J. Lessner, L. Li, Q. Li, T. Rejtar, V. P. Andreev, M. Reichlen, K. Hill, J. J. Moran, B. L. Karger, and J. G. Ferry. An unconventional pathway for reduction of CO<sub>2</sub> to methane in CO-grown *Methanosarcina acetivorans* revealed by proteomics. *Proceedings of the National Academy of Sciences*, 103(47):17921–17926, 2006.
- [78] M. Lewis. The *lac* repressor. *Comptes Rendus Biologies*, 328(6):521–548, 2005.
- [79] J. Li, X. Zheng, X. Guo, L. Qi, and X. Dong. Characterization of an archaeal two-component system that regulates methanogenesis in *Methanosaeta harundinacea*. *PLoS one*, 9(4):e95502, 2014.
- [80] J. M. Li, H. Umanoff, R. Proenca, C. S. Russell, and S. D. Cosloy. Cloning of the *Escherichia coli* K-12 *hemB* gene. *Journal of Bacteriology*, 170(2):1021–1025, 1988.
- [81] T. Li, H. L. Bonkovsky, and J.-t. Guo. Structural analysis of heme proteins: implications for design and prediction. *BMC Structural Biology*, 11(1):13, 2011.
- [82] M. Lindebros, L. Poellinger, and M. Whitelaw. Protein-protein interaction via PAS domains: role of the PAS domain in positive and negative regulation of the bHLH/PAS dioxin receptor-Arnt transcription factor complex. *The EMBO Journal*, 14(14):3528–3539, 1995.



- [83] R. Lodinová-Žaadniková, H. Tlaskalová-Hogenová, and U. Sonnenborn. Local and serum antibody response in full-term and premature infants after artificial colonization of the intestine with *E. coli* strain Nissle 1917 (Mutaflor®). *Pediatric Allergy and Immunology*, 3(1):43–48, 1992.
- [84] D. G. Longstaff, R. C. Larue, J. E. Faust, A. Mahapatra, L. Zhang, K. B. Green-Church, and J. A. Krzycki. A natural genetic code expansion cassette enables transmissible biosynthesis and genetic encoding of pyrrolysine. *Proceedings of the National Academy of Sciences*, 104(3):1021–1026, 2007.
- [85] H. K. Ly, T. Utesch, I. Díaz-Moreno, J. M. García-Heredia, M. A. De La Rosa, and P. Hildebrandt. Perturbation of the redox site structure of cytochrome c variants upon tyrosine nitration. *The Journal of Physical Chemistry B*, 116(19):5694–5702, 2012.
- [86] T. H. Mann, W. S. Childers, J. A. Blair, M. R. Eckart, and L. Shapiro. A cell cycle kinase with tandem sensory PAS domains integrates cell fate cues. *Nature Communications*, 7: 11454, 2016.
- [87] M. Matsubara, S.-i. Kitaoka, S.-i. Takeda, and T. Mizuno. Tuning of the porin expression under anaerobic growth conditions by His-to-Asp cross-phosphorelay through both the EnvZ-osmosensor and ArcB-anaerosensor in *Escherichia coli*. *Genes to Cells*, 5 (7):555–569, 2000.
- [88] A. C. McCarver and D. J. Lessner. Molecular characterization of the thioredoxin system from *Methanosarcina acetivorans*. *The FEBS Journal*, 281(20):4598–4611, 2014.
- [89] W. W. Metcalf, J. K. Zhang, E. Apolinario, K. R. Sowers, and R. S. Wolfe. A genetic system for Archaea of the genus *Methanosarcina*: liposome-mediated transformation and construction of shuttle vectors. *Proceedings of the National Academy of Sciences*, 94 (6):2626–2631, 1997.
- [90] W. W. Metcalf, J. K. Zhang, and R. S. Wolfe. An Anaerobic, Intrachamber Incubator for Growth of *Methanosarcina* spp. on Methanol-Containing Solid Media. *Applied and Environmental Microbiology*, 64(2):768–770, 1998.
- [91] C. L. Metcalfe, O. Daltrop, S. J. Ferguson, and E. L. Raven. Tuning the formation of a covalent haem–protein link by selection of reductive or oxidative conditions as exemplified by ascorbate peroxidase. *Biochemical Journal*, 408(3):355–361, 2007.
- [92] Y. Meyer, B. B. Buchanan, F. Vignols, and J.-P. Reichheld. Thioredoxins and glutaredoxins: unifying elements in redox biology. *Annual Review of Genetics*, 43:335–367, 2009.

- [93] L. A. Mike, J. E. Choby, P. R. Brinkman, L. Q. Olive, B. F. Dutter, S. J. Ivan, C. M. Gibbs, G. A. Sulikowski, D. L. Stauff, and E. P. Skaar. Two-component system cross-regulation integrates *Bacillus anthracis* response to heme and cell envelope stress. *PLoS Pathogens*, 10(3):e1004044, 2014.
- [94] B. Molitor. *A heme-based redox sensor in the methanogenic archaeon Methanosarcina acetivorans*. PhD thesis, Ruhr-University Bochum, 2013.
- [95] B. Molitor, M. Stassen, A. Modi, S. F. El-Mashtoly, C. Laurich, W. Lubitz, J. H. Dawson, M. Rother, and N. Frankenberg-Dinkel. A heme-based redox sensor in the methanogenic archaeon *Methanosarcina acetivorans*. *Journal Biological Chemistry*, 288(25):18458–18472, 2013.
- [96] E. K. Monson, G. S. Ditta, and D. R. Helinski. The oxygen sensor protein, FixL, of *Rhizobium meliloti* role of histidine residues in heme binding, phosphorylation, and signal transduction. *Journal of Biological Chemistry*, 270(10):5243–5250, 1995.
- [97] J. J. Moran, C. H. House, J. M. Vrentas, and K. H. Freeman. Methyl sulfide production by a novel carbon monoxide metabolism in *Methanosarcina acetivorans*. *Applied and Environmental Microbiology*, 74(2):540–542, 2008.
- [98] R. Mukhopadhyay, N. Sudasinghe, T. Schaub, and E. T. Yukl. Heme-Independent Redox Sensing by the Heme-Nitric Oxide/Oxygen Binding Protein (H-NOX) from *Vibrio cholerae*. *Journal of Biological Chemistry*, 291(34):17547–17556, 2016.
- [99] A. W. Munro and J. G. Lindsay. Bacterial cytochromes P-450. *Molecular Microbiology*, 20(6):1115–1125, 1996.
- [100] M. G. Murray and W. F. Thompson. Rapid isolation of high molecular weight plant DNA. *Nucleic Acids Research*, 8(19):4321–4326, 1980.
- [101] T. Najnin, K. Siddiqui, N. Elkaid, G. Kornfeld, P. Curmi, R. Cavicchioli, et al. Characterization of a temperature-responsive two component regulatory system from the Antarctic archaeon, *Methanococcoides burtonii*. *Scientific Reports*, 6:24278, 2016.
- [102] O. Namy, Y. Zhou, S. Gundllapalli, C. R. Polycarpo, A. Denise, J.-P. Rousset, D. Söll, and A. Ambrogelly. Adding pyrrolysine to the *Escherichia coli* genetic code. *FEBS Letters*, 581(27):5282–5288, 2007.
- [103] D. D. Nayak and W. W. Metcalf. Cas9-mediated genome editing in the methanogenic archaeon *Methanosarcina acetivorans*. *Proceedings of the National Academy of Sciences*, 114(11):2976–2981, 2017.
- [104] A. Nissle. Die antagonistische Behandlung chronischer Darmstörungen mit Colibakterien. *Medizinische Klinik*, 2:29–30, 1918.

- [105] U. A. Ochsner, Z. Johnson, and M. L. Vasil. Genetics and regulation of two distinct haem-uptake systems, *phu* and *has*, in *Pseudomonas aeruginosa*. *Microbiology*, 146(1):185–198, 2000.
- [106] P. O’Donoghue, L. Prat, M. Kucklick, J. G. Schäfer, K. Riedel, J. Rinehart, D. Söll, and I. U. Heinemann. Reducing the genetic code induces massive rearrangement of the proteome. *Proceedings of the National Academy of Sciences*, 111(48):17206–17211, 2014.
- [107] E. Oelgeschläger and M. Rother. Carbon monoxide-dependent energy metabolism in anaerobic bacteria and archaea. *Archives of Microbiology*, 190(3):257–269, 2008.
- [108] E. Oelgeschläger and M. Rother. In vivo role of three fused corrinoid/methyl transfer proteins in *Methanosarcina acetivorans*. *Molecular Microbiology*, 72(5):1260–1272, 2009.
- [109] L. Parca, B. Ariano, A. Cabibbo, M. Paoletti, A. Tamburrini, A. Palmeri, G. Ausiello, and M. Helmer-Citterich. Kinome-wide identification of phosphorylation networks in eukaryotic proteomes. *Bioinformatics*, 2018.
- [110] J. S. Parkinson. Signal transduction schemes of bacteria. *Cell*, 73(5):857–871, 1993.
- [111] J. S. Parkinson and E. C. Kofoed. Communication modules in bacterial signaling proteins. *Annual Review of Genetics*, 26(1):71–112, 1992.
- [112] L. Paul, D. J. Ferguson, and J. A. Krzycki. The trimethylamine methyltransferase gene and multiple dimethylamine methyltransferase genes of *Methanosarcina barkeri* contain in-frame and read-through amber codons. *Journal of Bacteriology*, 182(9):2520–2529, 2000.
- [113] J.-L. Pellequer, K. A. Wager-Smith, S. A. Kay, and E. D. Getzoff. Photoactive yellow protein: a structural prototype for the three-dimensional fold of the PAS domain superfamily. *Proceedings of the National Academy of Sciences*, 95(11):5884–5890, 1998.
- [114] E. Pérez-Rueda and J. Collado-Vides. The repertoire of DNA-binding transcriptional regulators in *Escherichia coli* K-12. *Nucleic Acids Research*, 28(8):1838–1847, 2000.
- [115] J. Perry, K. Koteva, and G. Wright. Receptor domains of two-component signal transduction systems. *Molecular BioSystems*, 7(5):1388–1398, 2011.
- [116] L. Plate and M. A. Marletta. Nitric oxide-sensing H-NOX proteins govern bacterial communal behavior. *Trends in Biochemical Sciences*, 38(11):566–575, 2013.
- [117] P. Pokkuluri, M. Pessanha, Y. Londer, S. Wood, N. Duke, R. Wilton, T. Catarino, C. Salgueiro, and M. Schiffer. Structures and solution properties of two novel periplasmic sensor domains with c-type heme from chemotaxis proteins of *Geobacter sulfurreducens*: implications for signal transduction. *Journal of Molecular Biology*, 377(5):1498–1517, 2008.

- [118] C. R. Polycarpo, S. Herring, A. Bérubé, J. L. Wood, D. Söll, and A. Ambrogelly. Pyrrolysine analogues as substrates for pyrrolysyl-tRNA synthetase. *FEBS Letters*, 580(28-29): 6695–6700, 2006.
- [119] C. P. Ponting and L. Aravind. PAS: a multifunctional domain family comes to light. *Current Biology*, 7(11):R674–R677, 1997.
- [120] L. B. Poole. The basics of thiols and cysteines in redox biology and chemistry. *Free Radical Biology and Medicine*, 80:148–157, 2015.
- [121] L. Prat, I. U. Heinemann, H. R. Aerni, J. Rinehart, P. O’Donoghue, and D. Söll. Carbon source-dependent expansion of the genetic code in bacteria. *Proceedings of the National Academy of Sciences*, 109(51):21070–21075, 2012.
- [122] M. S. Price, L. Y. Chao, and M. A. Marletta. *Shewanella oneidensis* MR-1 H-NOX regulation of a histidine kinase by nitric oxide. *Biochemistry*, 46(48):13677–13683, 2007.
- [123] M. A. Pritchett, J. K. Zhang, and W. W. Metcalf. Development of a markerless genetic exchange method for *Methanosarcina acetivorans* C2A and its use in construction of new genetic tools for methanogenic archaea. *Applied and Environmental Microbiology*, 70(3): 1425–1433, 2004.
- [124] F. Quitterer, A. List, W. Eisenreich, A. Bacher, and M. Groll. Crystal structure of methylornithine synthase (PylB): insights into the pyrrolysine biosynthesis. *Angewandte Chemie International Edition*, 51(6):1339–1342, 2012.
- [125] D. S. Rehder and C. R. Borges. Cysteine sulfenic acid as an intermediate in disulfide bond formation and nonenzymatic protein folding. *Biochemistry*, 49(35):7748–7755, 2010.
- [126] N. C. Rockwell and J. C. Lagarias. The structure of phytochrome: a picture is worth a thousand spectra. *The Plant Cell*, 18(1):4–14, 2006.
- [127] M. Rother and W. W. Metcalf. Anaerobic growth of *Methanosarcina acetivorans* C2A on carbon monoxide: an unusual way of life for a methanogenic archaeon. *Proceedings of the National Academy of Sciences*, 101(48):16929–16934, 2004.
- [128] G. E. Schaller, S.-H. Shiu, and J. P. Armitage. Two-component systems and their co-option for eukaryotic signal transduction. *Current Biology*, 21(9):R320–R330, 2011.
- [129] R. Sheehan, A. C. McCarver, C. E. Isom, E. A. Karr, and D. J. Lessner. The *Methanosarcina acetivorans* thioredoxin system activates DNA binding of the redox-sensitive transcriptional regulator MsvR. *Journal of Industrial Microbiology & Biotechnology*, 42(6):965–969, 2015.

- [130] D. Shelver, R. L. Kerby, Y. He, and G. P. Roberts. CooA, a CO-sensing transcription factor from *Rhodospirillum rubrum*, is a CO-binding heme protein. *Proceedings of the National Academy of Sciences*, 94(21):11216–11220, 1997.
- [131] T. Shimizu, D. Huang, F. Yan, M. Stranova, M. Bartosova, V. Fojtikova, and M. Martínková. Gaseous O<sub>2</sub>, NO, and CO in signal transduction: structure and function relationships of heme-based gas sensors and heme-redox sensors. *Chemical Reviews*, 115(13):6491–6533, 2015.
- [132] H. Silva-Jiménez, Á. Ortega, C. García-Fontana, J. L. Ramos, and T. Krell. Multiple signals modulate the activity of the complex sensor kinase TodS. *Microbial Biotechnology*, 8(1):103–115, 2015.
- [133] S. Sivaramakrishnan and P. R. Ortiz de Montellano. The DosS-DosT/DosR Mycobacterial Sensor System. *Biosensors*, 3(3):259–282, 2013.
- [134] S. C. Smith, P. J. Kennelly, and M. Potts. Protein-tyrosine phosphorylation in the *Archaea*. *Journal of Bacteriology*, 179(7):2418–2420, 1997.
- [135] S. G. Smith and P. E. Rouvière. Purification and characterization of the reduced-nicotinamide-dependent 2, 2'-dithiodiethanesulfonate reductase from methanobacterium thermoautotrophicum delta h. *Journal of Bacteriology*, 172(11):6435–6441, 1990.
- [136] G. Smulevich, J. M. Mauro, L. A. Fishel, A. M. English, J. Kraut, and T. G. Spiro. Heme pocket interactions in cytochrome c peroxidase studied by site-directed mutagenesis and resonance Raman spectroscopy. *Biochemistry*, 27(15):5477–5485, 1988.
- [137] U. Sonnenborn and J. Schulze. The non-pathogenic *Escherichia coli* strain Nissle 1917—features of a versatile probiotic. *Microbial Ecology in Health and Disease*, 21(3-4):122–158, 2009.
- [138] M. Sono, S. Sun, A. Modi, M. S. Hargrove, B. Molitor, N. Frankenberg-Dinkel, and J. H. Dawson. Spectroscopic evidence supporting neutral thiol ligation to ferrous heme iron. *JBIC Journal of Biological Inorganic Chemistry*, 23(7):1085–1092, 2018.
- [139] K. R. Sowers, S. F. Baron, and J. G. Ferry. *Methanosarcina acetivorans* sp. nov., an acetotrophic methane-producing bacterium isolated from marine sediments. *Applied and Environmental Microbiology*, 47(5):971–978, 1984.
- [140] A. M. Stock, V. L. Robinson, and P. N. Goudreau. Two-component signal transduction. *Annual Review of Biochemistry*, 69(1):183–215, 2000.
- [141] J. B. Stock, A. M. Stock, and J. M. Mottonen. Signal transduction in bacteria. *Nature*, 344(6265):395, 1990.

- [142] J. B. Stock, P. Park, M. G. Surette, and M. Levit. Two-component signal transduction systems: structure-function relationships and mechanisms of catalysis. In *Two-component signal transduction*, pages 25–51. American Society of Microbiology, 1995.
- [143] F. W. Studier and B. A. Moffatt. Use of bacteriophage T7 RNA polymerase to direct selective high-level expression of cloned genes. *Journal of Molecular Biology*, 189(1):113–130, 1986.
- [144] J. Sudhamsu, M. Kabir, M. V. Airola, B. A. Patel, S.-R. Yeh, D. L. Rousseau, and B. R. Crane. Co-expression of ferredoxin allows for complete heme incorporation into recombinant proteins produced in *E. coli*. *Protein Expression and Purification*, 73(1):78–82, 2010.
- [145] D. Susanti, J. H. Wong, W. H. Vensel, U. Loganathan, R. DeSantis, R. A. Schmitz, M. Balsera, B. B. Buchanan, and B. Mukhopadhyay. Thioredoxin targets fundamental processes in a methane-producing archaeon, *Methanocaldococcus jannaschii*. *Proceedings of the National Academy of Sciences*, 111(7):2608–2613, 2014.
- [146] B. L. Taylor and I. B. Zhulin. PAS domains: internal sensors of oxygen, redox potential, and light. *Microbiology and Molecular Biology Reviews*, 63(2):479–506, 1999.
- [147] F. W. Teale. Cleavage of the Haem-protein Link by Acid Methylethylketone. *Biochimica et Biophysica Acta*, 35:543, 1959.
- [148] M. Tietze, A. Beuchle, I. Lamla, N. Orth, M. Dehler, G. Greiner, and U. Beifuss. Redox potentials of methanophenazine and CoB-S-S-CoM, factors involved in electron transport in methanogenic archaea. *Chembiochem*, 4(4):333–335, 2003.
- [149] L. E. Ulrich, E. V. Koonin, and I. B. Zhulin. One-component systems dominate signal transduction in prokaryotes. *Trends in Microbiology*, 13(2):52–56, 2005.
- [150] C. L. Varnado and D. C. Goodwin. System for the expression of recombinant hemo-proteins in *Escherichia coli*. *Protein Expression and Purification*, 35(1):76–83, 2004.
- [151] M. Vaupel and R. K. Thauer. Two F420-reducing hydrogenases in *Methanosarcina barkeri*. *Archives of Microbiology*, 169(3):201–205, 1998.
- [152] V. R. Vepachedu and J. G. Ferry. Role of the fused corrinoid/methyl transfer protein CmtA during CO-dependent growth of *Methanosarcina acetivorans*. *Journal of Bacteriology*, 194(16):4161–4168, 2012.
- [153] J. Vieira and J. Messing. The pUC plasmids, an M13mp7-derived system for insertion mutagenesis and sequencing with synthetic universal primers. *Gene*, 19(3):259–268, 1982.

- [154] B. Wang, S. Yang, L. Zhang, and Z.-G. He. Archaeal eukaryote-like serine/threonine protein kinase interacts with and phosphorylates a forkhead-associated-domain-containing protein. *Journal of Bacteriology*, 192(7):1956–1964, 2010.
- [155] P. A. Williams, V. Fülöp, E. F. Garman, N. F. Saunders, S. J. Ferguson, and J. Hajdu. Haem-ligand switching during catalysis in crystals of a nitrogen-cycle enzyme. *Nature*, 389(6649):406, 1997.
- [156] C. R. Woese and G. E. Fox. Phylogenetic structure of the prokaryotic domain: the primary kingdoms. *Proceedings of the National Academy of Sciences*, 74(11):5088–5090, 1977.
- [157] P. M. Wood. Why do c-type cytochromes exist? *FEBS Letters*, 164(2):223–226, 1983.
- [158] P. M. Wood. Why do c-type cytochromes exist?—Reprise. *Biochimica et Biophysica Acta (BBA)-Bioenergetics*, 1058(1):5–7, 1991.
- [159] S. I. Woodard and H. A. Dailey. Regulation of heme biosynthesis in *Escherichia coli*. *Archives of Biochemistry and Biophysics*, 316(1):110–115, 1995.
- [160] J. J. Woodward, N. I. Martin, and M. A. Marletta. An *Escherichia coli* expression-based method for heme substitution. *Nature Methods*, 4(1):43, 2007.
- [161] J. Wu, N. Ohta, J.-L. Zhao, and A. Newton. A novel bacterial tyrosine kinase essential for cell division and differentiation. *Proceedings of the National Academy of Sciences*, 96(23):13068–13073, 1999.
- [162] C. Yanisch-Perron, J. Vieira, and J. Messing. Improved M13 phage cloning vectors and host strains: nucleotide sequences of the M13mpl8 and pUC19 vectors. *Gene*, 33(1):103–119, 1985.
- [163] D. Yenugudhati, D. Prakash, A. K. Kumar, R. S. S. Kumar, N. H. Yennawar, H. P. Yennawar, and J. G. Ferry. Structural and biochemical characterizations of methanoredoxin from *Methanosarcina acetivorans*, a glutaredoxin-like enzyme with coenzyme M-dependent protein disulfide reductase activity. *Biochemistry*, 55(2):313–321, 2015.
- [164] S. Yoshioka, K. Kobayashi, H. Yoshimura, T. Uchida, T. Kitagawa, and S. Aono. Biophysical properties of a c-type heme in chemotaxis signal transducer protein DcrA. *Biochemistry*, 44(46):15406–15413, 2005.
- [165] J. K. Zhang, A. K. White, H. C. Kuettner, P. Boccazzi, and W. W. Metcalf. Directed mutagenesis and plasmid-based complementation in the methanogenic archaeon *Methanosarcina acetivorans* C2A demonstrated by genetic analysis of proline biosynthesis. *Journal of Bacteriology*, 184(5):1449–1454, 2002.

## REFERENCES

---

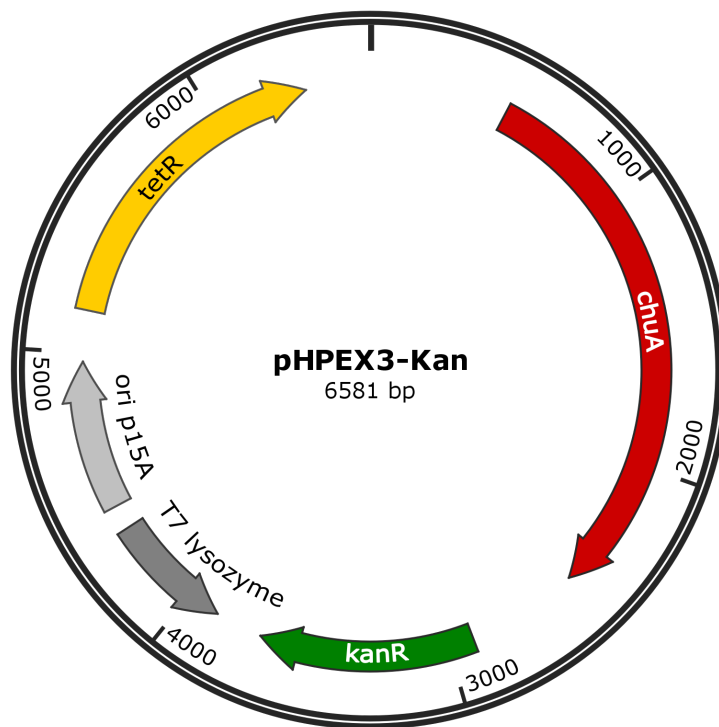
- [166] M. Zheng, F. Åslund, and G. Storz. Activation of the OxyR transcription factor by reversible disulfide bond formation. *Science*, 279(5357):1718–1722, 1998.
- [167] S. H. Zinder. Physiological ecology of methanogens. In *Methanogenesis*, pages 128–206. Springer, 1993.



# Appendix

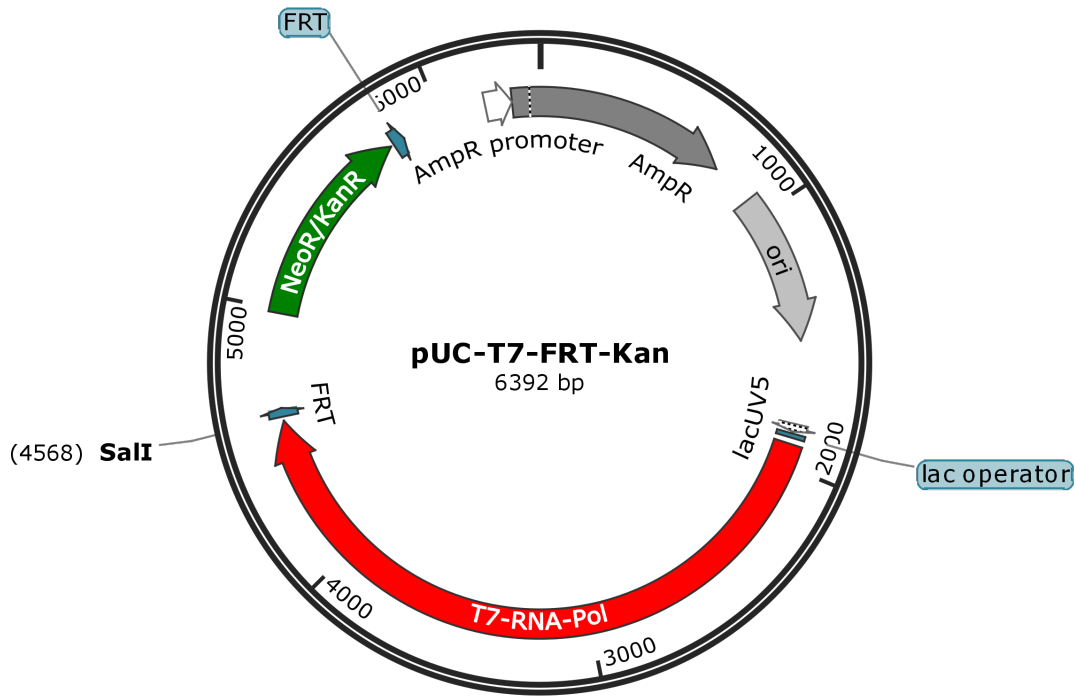
## Plasmid map of pHPEX3-Kan.

A kanamycin resistance cassette was introduced into the EcoRI restriction site of plasmid pHPEX-3 [150]. The plasmid was used for the coexpression of the *chuA* gene for heme uptake.



**Plasmid map of pUC-T7-FRT-Kan.**

The T7-RNA polymerase gene was amplified from genomic DNA of *E. coli* BL21(DE3). The lacUV5 promoter was added by PCR and the fragment of promoter, gene and Kan<sup>R</sup> cassette was cloned into the vector pYPRUB168 (pUC-Sma-only).



# Lebenslauf

## PERSÖNLICHE DATEN

Name Kerstin Fiege

## FREIWILLIGES ÖKOLOGISCHES JAHR

08/2007 - 07/2008 Biologische Station Paderborner Land

## HOCHSCHULAUSBILDUNG

09/2008 - 08/2011 Studium der Biologie, TU Braunschweig  
Abschluss: Bachelor of Science

09/2011 - 04/2014 Studium der Biologie (Mikrobiologie & Infektionsbiologie), TU Braunschweig  
Abschluss: Master of Science

## PROMOTION

09/2014 - 03/2015 Doktorandin in der Arbeitsgruppe „Physiologie der Mikroorganismen“ von Prof. Dr. Frankenberg-Dinkel an der Ruhr-Universität Bochum

Seit 04/2015 **Doktorandin in der Arbeitsgruppe „Mikrobiologie“ von Prof. Dr. Frankenberg-Dinkel an der TU Kaiserslautern**

## ZUSÄTZLICHE TÄTIGKEITEN/ QUALIFIKATIONEN

03/2009 - 01/2011 Studentische Hilfskraft, Helmholtzzentrum für Infektionsforschung, Braunschweig

06/2011 Studentische Hilfskraft, Institut für Mikrobiologie, TU Braunschweig

10/2012 Fortbildungskurs nach §15 GenTSV für Projektleiter und Biologische Sicherheitsbeauftragte

04/2013 - 07/2013 Laborpraktikum in der Arbeitsgruppe „Mikrobiologie“ von Dr. von Wachenfeldt, Mikrobiologie, Lund Universität, Schweden

09/2015 Kurs für ÄKTA System und UNICORN Kontrollsoftware

02/2016 Strahlenschutzkurs Fachkundegruppe S4.1

# Publications

**Frädrich, C.; March, A.; Fiege, K.; Hartmann, A.; Jahn, D. and Härtig, E.** (2012). The transcription factor AlsR binds and regulates the promoter of the *alsSD* operon responsible for acetoin formation in *Bacillus subtilis*. *J Bacteriol*, 194:1100–1112

**Fiege, K.; Querebillo, C.J.; Hildebrandt, P. and Frankenberg-Dinkel, N.** (2018). Improved method for the incorporation of heme cofactors into recombinant proteins using *Escherichia coli* Nissle 1917. *Biochem*, 57(19), 2747-2755

**Fiege, K. and Frankenberg-Dinkel, N.** (2019). Thiol-based redox sensing in the methyltransferase associated sensor kinase RdmS in *Methanosarcina acetivorans*. *Environ Microbiol*, in press

# Conference contributions

## Posters

**Kerstin Fiege, Christian Twittenhoff, Bastian Molitor, Jana Staffa, Christoph Laurich, Wolfgang Lubitz, Peter Hildebrandt and Nicole Frankenberg-Dinkel** (2015). Biochemical and functional analysis of heme-based sensor kinases from the methanogen *Methanosarcina acetivorans*. VAAM Annual Meeting, Marburg, Germany, Book of abstracts (BIOspektrum) p. 222 .

**Kerstin Fiege, Bastian Molitor, Kathrin Kwiatkowski, Christoph Laurich, Wolfgang Lubitz and Nicole Frankenberg-Dinkel** (2015). Biochemical and functional analysis of heme-based sensor kinases from the methanogen *Methanosarcina acetivorans*. Gordon Research Conference - Archaea, Newry, ME, USA, no book of abstracts.

**Kerstin Fiege, Bastian Molitor, Loriana Blasius, Kathrin Kwiatkowaski and Nicole Frankenberg-Dinkel** (2016). Analysis of the signal transduction by heme-based sensor kinases from the methanogen *Methanosarcina acetivorans*. VAAM Annual Meeting, Jena, Germany, Book of abstracts (BIOspektrum) p. 134 .

**Kerstin Fiege, Bastian Molitor, Christine Joy Querebillo, Christoph Laurich, Peter Hildebrandt, Wolfgang Lubitz, Ines Weidinger, Peter Hildebrandt, and Nicole Frankenberg-Dinkel** (2016). The heme-based redox sensor MsmS from *Methanosarcina acetivorans*. Gordon Research Conference - Tetrapyrroles, Newport, RI, USA, no book of abstracts.

**Kerstin Fiege, Bastian Molitor, Loriana Blasius, Christoph Laurich, Wolfgang Lubitz and Nicole Frankenberg-Dinkel** (2016). Signal transduction by the heme-based sensor kinase MsmS from *Methanosarcina acetivorans*. VAAM Special Group Meeting, 31st Symposium Mechanisms of Gene Regulation, Bad Bergzabern, Germany, no book of abstracts.

**Kerstin Fiege, Christoph Laurich, Wolfgang Lubitz and Nicole Frankenberg-Dinkel** (2018). Two heme-based sensor kinases and their role in putative two-component systems from *Methanosarcina acetivorans*. VAAM Annual Meeting, Wolfsburg, Germany, Book of abstracts (BIOspektrum) p. 130 .

## Talks

**Kerstin Fiege and Nicole Frankenberg-Dinkel** (2016). Signal transduction by the heme-based sensor kinase MsmS from *Methanosarcina acetivorans*. VAAM Special Group Meeting *Archaea*, Schmitten, Germany, no book of abstracts.

**Kerstin Fiege** (2016). Signal transduction by the heme-based sensor kinase MsmS from *Methanosarcina acetivorans*. Faculty Seminar Biology, Thallichtenberg, Germany, no book of abstracts.

**Kerstin Fiege** (2017). Signal transduction by the heme-based sensor kinase MsmS from *Methanosarcina acetivorans*. Tetrapyrrole Retreat, Fulda, Germany, no book of abstracts.

**Kerstin Fiege and Nicole Frankenberg-Dinkel** (2017). Towards the function of a heme-based sensor kinase from *Methanosarcina acetivorans*. VAAM Special Group Meeting *Archaea*, Schmitten, Germany, no book of abstracts.

**Kerstin Fiege** (2018). Towards the function of redox sensing kinases from the methanogen *Methanosarcina acetivorans*. RLP Microbiology Meeting, Mainz, Germany, no book of abstracts.

**Kerstin Fiege and Nicole Frankenberg-Dinkel** (2018). Towards the function of two sensor kinases and their role in putative two-component systems from the methanogen *Methanosarcina acetivorans*. EMBO workshop "Molecular biology of Archaea: From mechanisms to ecology", Vienna, Austria, book of abstracts p. 15.